

Quantum field theory for many body systems

Prof. Karsten Held, Prof. Alessandro Toschi, Sen. Lec. Jan M. Tomczak, Dr.
Anna Kauch, and Felix Hoefenstock

Institute of Solid State Physics
Vienna University of Technology

March 12, 2024

Contents

| | | |
|----------|---|-----------|
| 3 | Many body Green function | 5 |
| 3.1 | Definition | 5 |
| 3.2 | Equation of motion | 7 |
| 3.3 | Matsubara frequencies | 9 |
| 3.4 | Green function for independent particles | 10 |
| 3.5 | Spectral representation | 11 |
| 3.6 | Analytical properties of the Green function | 12 |
| 4 | Landau Fermi Liquid Theory | 17 |
| 4.1 | Adiabatic switching on of the Coulomb interaction | 17 |
| 4.2 | Microscopic formulation of the Fermi-liquid theory | 20 |
| 4.2.1 | Green's function and finite lifetime | 20 |
| 4.2.2 | Self-energy | 21 |
| 4.2.3 | Quasiparticle spectral function | 23 |
| 5 | Feynman diagrams | 27 |
| 5.1 | Perturbation series in interaction | 27 |
| 5.1.1 | Perturbative series of the S-Matrix | 28 |
| 5.1.2 | Perturbative series of Green's function | 31 |
| 5.2 | Wick's theorem | 32 |
| 5.3 | Feynman diagrams and linked cluster theorem | 36 |
| 5.3.1 | Hartree term | 39 |
| 5.3.2 | Fock term | 41 |
| 5.3.3 | Topology | 43 |
| 5.3.4 | Feynman rules | 45 |
| 5.4 | Self-energy and Dyson equation | 46 |
| 5.5 | Skeleton diagrams | 47 |
| 6 | Linear response theory | 51 |
| 6.1 | External fields as probing tools | 51 |
| 6.2 | Linear response | 52 |
| 6.3 | Kubo-Nakano formula | 54 |
| 6.3.1 | Examples of applications of the Kubo-Nakano formula | 56 |

| | | |
|----------|---|------------|
| 6.4 | Computing the response function in QFT | 57 |
| 6.4.1 | Practical considerations | 61 |
| 6.4.2 | The static response ($i\Omega_n = 0$) | 61 |
| 6.4.3 | Feynman diagrammatic calculations of response functions | 62 |
| 6.5 | LRT for the electromagnetic field | 66 |
| 6.5.1 | Considerations on the gauge-invariance | 71 |
| 6.5.2 | Calculation of the generalized conductivity for the non-interacting case | 73 |
| 6.6 | Optical Conductivity | 74 |
| 7 | Random phase approximation (RPA) | 81 |
| 7.1 | Derivation of the RPA in the context of screening | 81 |
| 7.2 | Diagrammatic representation | 83 |
| 7.3 | RPA for the electron-gas | 85 |
| 7.3.1 | Evaluation of χ^0 | 86 |
| 7.3.2 | Eigenmodes encoded in χ^{RPA} excitations | 86 |
| 7.3.3 | Properties of the plasmon | 88 |
| 7.3.4 | The excitation spectrum of the electron-gas within RPA | 88 |
| 7.3.5 | Static screening at long wavelengths | 89 |
| 7.3.6 | Beyond the long wavelength limit: Friedel oscillation | 90 |
| 7.4 | The GW approach | 92 |
| 7.4.1 | Screened Hartree term | 93 |
| 7.4.2 | Screened Fock term | 94 |
| A | Time-evolution of perturbed states | 101 |
| B | Explicit relation between 2P-Greens' functions and linear response functions | 103 |

Chapter 3

Many body Green function

In this chapter, we introduce the many-body Green function, first as a propagator as a function of time and then as a function of energy (frequency) where it is directly related to a physical observable: the photoemission spectrum. We also learn about its spectral representation and its analytic properties. The many-body Green function is the central object of quantum field theory.

3.1 Definition

In the quantum theory lecture, we follow the time evolution of a single particle and calculated its wave function or, alternatively, its propagator. For a many body system with $\mathcal{O}(10^{23})$ electrons per cm^3 in a solid such a propagator for all particles from time t to t' would be ($\hbar \equiv 1$):

$$U(\vec{r}'_{10^{23}}, \dots, \vec{r}'_1, t'; \vec{r}_{10^{23}}, \dots, \vec{r}_1, t) = \langle \vec{r}'_{10^{23}}, \dots, \vec{r}'_1 | e^{-iH(t'-t)} | \vec{r}_{10^{23}}, \dots, \vec{r}_1 \rangle. \quad (3.1)$$

This propagator of all particles is way *too complicated* (we cannot calculate it), and also *useless* (even if we knew it, it would contain too much irrelevant information; we would first need to reduce the amount of information to something we can handle/we are interested in).

Let us consider instead the **propagation of a single extra particle** through the many body system. That is we start with the many body system in its ground state (or one state of a thermal ensemble) add a particle at time t , let it propagate to t' , and remove a particle at time t' .

Definition: This can be described by the **causal¹ Green function**

$$G_C(\vec{r}', t'; \vec{r}, t) \equiv -i \langle \psi(\vec{r}', t') \psi^\dagger(\vec{r}, t) \rangle \Theta(t' - t) \underbrace{\pm}_{\text{for fermions/bosons}} i \langle \psi^\dagger(\vec{r}, t) \psi(\vec{r}', t') \rangle \Theta(t - t'). \quad (3.2)$$

Here, $\psi(\vec{r}, t)$ ($\psi^\dagger(\vec{r}, t)$) is the annihilation (creation) operator for a particle in second quantization at position \vec{r} in the Heisenberg picture, connected to the same operator in the Schrödinger picture as

¹It is called causal because the perturbation (adding/removing a particle) is before the response of the system (measured by removing/adding a particle). This is more transparent in linear response theory, where the causal Green function describes that the action such as a switching on a magnetic field is before the response such as a magnetization of the system. Sometimes it is also called the time-ordered Green function.

$\psi(\vec{r}, t) \equiv e^{iHt}\psi(\vec{r})e^{-iHt}$ ($\psi^\dagger(\vec{r}, t) \equiv e^{iHt}\psi^\dagger(\vec{r})e^{-iHt}$); and $\Theta(t)$ denotes the Heaviside step function. The expectation value is with respect to the ground state (GS) for $T = 0$ or a thermal ensemble² for $T > 0$ ($\beta = 1/(k_B T)$), i.e.:

$$\langle \dots \rangle \equiv \langle \text{GS} | \dots | \text{GS} \rangle \text{ for } T = 0; \quad \langle \dots \rangle \equiv \frac{\text{Tr} \dots e^{-\beta H}}{\text{Tr} e^{-\beta H}} \text{ for } T > 0. \quad (3.3)$$

In the Schrödinger picture Eq. (3.2) becomes for $T = 0$:

$$\begin{aligned} G_C(\vec{r}', t'; \vec{r}, t) &= -i \langle \text{GS} | e^{iHt'} \psi(\vec{r}') e^{iH(t-t')} \psi^\dagger(\vec{r}) e^{-iHt} | \text{GS} \rangle \Theta(t' - t) \\ &\quad \pm i \langle \text{GS} | e^{iHt} \psi^\dagger(\vec{r}) e^{iH(t'-t)} \psi(\vec{r}') e^{-iHt'} | \text{GS} \rangle \Theta(t - t') \end{aligned} \quad (3.4)$$

That is, we have the following [physical interpretation](#) (see fish picture in the lecture notes):

$t' > t$ Starting point is the many body ground state which we propagate until time t . At time t we add a particle to the system (creation operator). We let the many-body system with now one additional particle propagate until time t' . At time t' , we remove a particle (which need not be the same since the particles are indistinguishable). Finally we take the amplitude to end up in the ground state again (we take the overlap with $\langle \text{GS} | e^{iHt'}$, i.e., the time propagated ground state).

$t > t'$ If the times are reversed, we have essentially the same, except for that we now add a hole (remove a particle). That is at time t' we remove a particle from the system. We then let the many body system with one particle less propagate until the (now later) time t , when we add a particle (remove a hole).

For a canonical or grand canonical ensemble we have the same picture with all states (properly weighted by $e^{-\beta H}$) instead of only the ground state.

For a more compact notation, we define the [Wick time ordering operator](#) \mathcal{T} , which orders the subsequent Heisenberg operators according to time, so that the operator with the earliest time is right-most, then comes the one with the second earliest time etc. until the left-most operator with the latest time. For every two Fermionic operators that are exchanged this way, we collect a minus sign. For our causal Green function that gives us the compact notation:

$$\begin{aligned} G_C(\vec{r}', t'; \vec{r}, t) &= -i \langle \mathcal{T} \psi(\vec{r}', t') \psi^\dagger(\vec{r}, t) \rangle \\ &\stackrel{\text{def. } \mathcal{T}}{\equiv} -i \langle \psi(\vec{r}', t') \psi^\dagger(\vec{r}, t) \rangle \Theta(t' - t) \pm i \langle \psi^\dagger(\vec{r}, t) \psi(\vec{r}', t') \rangle \Theta(t - t'). \end{aligned} \quad (3.5)$$

For finite temperatures $T > 0$, the [temperature Green function](#) (GF) is often most suitable (hence this one has no subscript in the following). It can be obtained from the causal GF through a so-called Wick rotation $t \rightarrow -i\tau$, see Fig. 3.1, which is an analytical continuation in the complex plane.

²In case of a grand canonical ensemble (instead of a canonical one) we would have $H - \mu N$ (N : particle number operator) in all exponents. To make life simpler and to have a single notation for both ensembles, we absorb μ in the Hamiltonian in the following. That is possible since the zero of energy is arbitrary. We shift it such that $\mu = 0$, which requires shifting the Hamiltonian energies correspondingly.

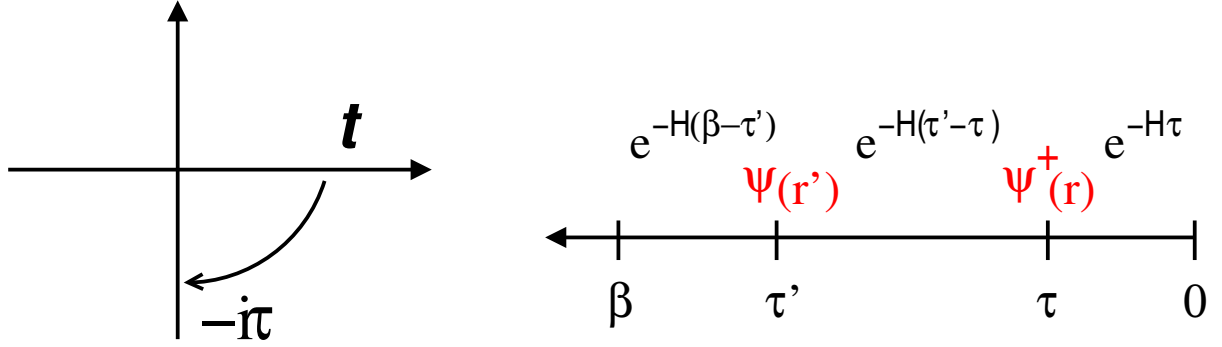


Figure 3.1: Left: Wick rotation from real time t to imaginary time τ . Right: Time evolution in imaginary time in the interval $[0, \beta]$ [Eq. (3.6)].

Definition: temperature Green function

$$\begin{aligned}
 G(\vec{r}', \tau'; \vec{r}, \tau) &\equiv -iG_C(\vec{r}', t' = -i\tau'; \vec{r}, t = -i\tau) \\
 &= -\langle \underbrace{\mathcal{T} \psi(\vec{r}', t' = -i\tau') \psi^\dagger(\vec{r}, -i\tau)}_{\substack{e^{H\tau'} \psi(\vec{r}') e^{-H\tau'} \\ \equiv \psi(\vec{r}', \tau')}} \rangle \\
 &= -\text{Tr} e^{-H(\beta-\tau')} \psi(\vec{r}') e^{-H(\tau'-\tau)} \psi^\dagger(\vec{r}) e^{-H\tau} / [\text{Tr} e^{-\beta H}] \Theta(\tau' - \tau) \\
 &\quad \pm \text{Tr} e^{-H(\beta-\tau)} \psi^\dagger(\vec{r}) e^{-H(\tau-\tau')} \psi(\vec{r}') e^{-H\tau'} / [\text{Tr} e^{-\beta H}] \Theta(\tau - \tau'),
 \end{aligned} \tag{3.6}$$

where the Wick time ordering operator \mathcal{T} is now ordering imaginary times in the same way as real times before.

The advantage is that now **time** τ and **Boltzmann** β are on the same (imaginary) time axis, which is illustrated in Fig. 3.1 and often makes calculations considerably simpler. At the end of the day, if we are interested in the propagation in real time, we need to make an analytical continuation back to real time. For most physical purposes, this analytical continuation will be done in Fourier (energy/frequency) space, which directly corresponds to spectroscopic experiments.

3.2 Equation of motion

Let us consider as a starting point a quite general Hamiltonian consisting of a non-interacting (one particle) part h_0 and an interaction V which might e.g. describe electrons in a solid

$$\begin{aligned}
 H &= \int d^3r \psi^\dagger(\vec{r}) \underbrace{H_0(\vec{r})}_{\text{e.g. } -\frac{\Delta}{2m} + V_0(\vec{r})} \psi(\vec{r}) \\
 &\quad + \frac{1}{2} \int d^3r'' \int d^3r \psi^\dagger(\vec{r}'') \psi^\dagger(\vec{r}) \underbrace{V(\vec{r}'' - \vec{r})}_{\text{e.g. } \frac{e^2}{|\vec{r}'' - \vec{r}|}} \psi(\vec{r}) \psi(\vec{r}'').
 \end{aligned} \tag{3.7}$$

The Heisenberg equation for an operator $A(t)$ is given by $i\hbar \frac{dA(t)}{dt} = [A(t), H]$. We have the same for many body GF in imaginary time

$$-\frac{d\psi(\vec{r}', \tau')}{d\tau'} = [\psi(\vec{r}', \tau'), H] = e^{H\tau'} [\psi(\vec{r}'), H] e^{-H\tau'}, \quad (3.8)$$

setting $\hbar \equiv 1$. Note there is no factor “ i ” because we are in imaginary time. Similar as the Heisenberg equation, Eq. (3.8) directly follows from $\psi(\vec{r}, \tau) = e^{H\tau} \psi(\vec{r}) e^{-H\tau}$ or from $t \rightarrow -i\tau$.

Inserting H from Eq. (3.7) into the Heisenberg equation of motion (3.8), using the fermions/bosonic (upper/lower sign) commutation rules

$$[\psi(\vec{r}'), \psi^\dagger(\vec{r})]_{\pm} \equiv \psi(\vec{r}')\psi^\dagger(\vec{r}) \pm \psi^\dagger(\vec{r})\psi(\vec{r}') = \delta(\vec{r} - \vec{r}') \quad (3.9)$$

$$[\psi(\vec{r}'), \psi(\vec{r})]_{\pm} = 0 \quad (3.10)$$

$$[\psi^\dagger(\vec{r}'), \psi^\dagger(\vec{r})]_{\pm} = 0 \quad (3.11)$$

and $[A, BC] = [A, B]C + B[A, C]$, we arrive at the following form of the Heisenberg equation of motion (3.8)³

$$-\frac{d\psi(\vec{r}', \tau')}{d\tau'} = h_0(\vec{r}')\psi(\vec{r}', \tau') + \int d^3r'' \psi^\dagger(\vec{r}'', \tau') V(\vec{r}'' - \vec{r}') \psi(\vec{r}'', \tau') \psi(\vec{r}', \tau'). \quad (3.14)$$

Knowing the Heisenberg equation of motion for the annihilation operator, we can now obtain the (Heisenberg) equation of motion for the GF which was defined as

$$G(\vec{r}', \tau'; \vec{r}, \tau) = -\langle \psi(\vec{r}'\tau') \psi^\dagger(\vec{r}, \tau) \rangle \Theta(\tau' - \tau) \pm \langle \psi^\dagger(\vec{r}, \tau) \psi(\vec{r}', \tau') \rangle \Theta(\tau - \tau').$$

It reads

$$\begin{aligned} \frac{\partial G(\vec{r}', \tau'; \vec{r}, \tau)}{\partial \tau'} &= -\langle \psi(\vec{r}', \tau') \psi^\dagger(\vec{r}, \tau) \pm \psi^\dagger(\vec{r}, \tau) \psi(\vec{r}', \tau') \rangle \delta(\tau - \tau') \\ &\quad + h_0(\vec{r}') \langle \mathcal{T} \psi(\vec{r}', \tau') \psi^\dagger(\vec{r}, \tau) \rangle \\ &\quad + \int d^3r'' V(\vec{r}'' - \vec{r}') \langle \mathcal{T} \psi^\dagger(\vec{r}'', \tau') \psi(\vec{r}'', \tau') \psi(\vec{r}', \tau') \psi^\dagger(\vec{r}, \tau) \rangle. \end{aligned} \quad (3.15)$$

If we define a two-particle Green function as

$$G^{(2)}(\vec{r}_1\tau_1, \vec{r}_2\tau_2; \vec{r}_3\tau_3, \vec{r}_4\tau_4) \equiv \langle \mathcal{T} \psi(\vec{r}_1, \tau_1) \psi(\vec{r}_2, \tau_2) \psi^\dagger(\vec{r}_3, \tau_3) \psi^\dagger(\vec{r}_4, \tau_4) \rangle \quad (3.16)$$

³For Fermions, we need to replace the commutator of the equation of motion by the anticommutator of the fermionic commutation relations. This is possible since

$$[\psi(\vec{r}'), \psi^\dagger(\vec{r})\psi(\vec{r})]_{-} \equiv \psi(\vec{r}')\psi^\dagger(\vec{r})\psi(\vec{r}) - \psi^\dagger(\vec{r})\underbrace{\psi(\vec{r})\psi(\vec{r}')}_{-\psi(\vec{r}')\psi(\vec{r})} \quad (3.12)$$

$$= [\psi(\vec{r}'), \psi^\dagger(\vec{r})]_{+} \psi(\vec{r}). \quad (3.13)$$

the **equation of motion for the Green function** reads

$$\begin{aligned} \left[\frac{\partial}{\partial \tau'} + h_0(\vec{r}') \right] G(\vec{r}', \tau'; \vec{r}, \tau) &= -\delta(\vec{r} - \vec{r}') \delta(\tau - \tau') \\ &+ \lim_{\substack{\tau_2 \rightarrow \tau' \\ \tau_2 < \tau_1 < \tau'}} \int d^3 r'' V(\vec{r}'' - \vec{r}') G^{(2)}(\vec{r}'' \tau_1, \vec{r}' \tau_2; \vec{r}'' \tau', \vec{r} \tau). \end{aligned} \quad (3.17)$$

For non-interacting particles, i.e., $V(\vec{r}'' - \vec{r}') = 0$, the extra particle propagates independently of the other particles and Eq. (3.17) would be indeed the Green function of the one-particle Schrödinger equation. Hence the name *Green function*. However, with interaction it becomes more complicated since we now also have a two-particle GF on the right hand side.

One can derive a similar equation of motion as for the one-particle GF also for the two-particle GF which leads to a new differential equation (DE in τ') that also involves the three-particle GF etc. This series of DEs is also called the hierarchy of equation of motions. Since it is not a closed set of equations it does not allow the calculation of the GF. One might perform however an approximation (decoupling of the equation of motion) where one approximates

$$N\text{-particle GF} \approx (N - M)\text{-particle GF} \times M\text{-particle GF}.$$

For example, we might decouple

$$G^{(2)}(\vec{r}_1 \tau_1, \vec{r}_2 \tau_2; \vec{r}_3 \tau_3, \vec{r}_4 \tau_4) \approx G(\vec{r}_2 \tau_2; \vec{r}_3 \tau_3) G(\vec{r}_1 \tau_1; \vec{r}_4 \tau_4) - G(\vec{r}_2 \tau_2; \vec{r}_4 \tau_4) G(\vec{r}_1 \tau_1; \vec{r}_3 \tau_3)$$

which would correspond to the Hartree-Fock approximation, which we will learn later on. But there is no systematic way to do such a decoupling, which hence is typically only an uncontrolled approximation. Later we will learn a more systematic way to calculate (approximate) GFs through Feynman diagrams.

3.3 Matsubara frequencies

Let us now go from the Green function in time, where it plays the role of a propagator, to the Green function in Fourier space, i.e., the Green function as a function of frequencies or energies. If the Hamiltonian does not depend on time, i.e., if we have translational invariance in time, the GF only depends on the time difference:

$$G_k(\vec{r}', t'; \vec{r}, t) = G_k(\vec{r}', t' - t; \vec{r}, 0), \quad (3.18)$$

$$G(\vec{r}', \tau'; \vec{r}, \tau) = G_k(\vec{r}', \tau' - \tau; \vec{r}, 0). \quad (3.19)$$

The latter, i.e., the temperature GF now fulfills the following cyclic property for $0 \leq \tau \leq \beta$:

$$\begin{aligned} G(\vec{r}', \underbrace{\tau - \beta}_{\leq 0}; \vec{r}, 0) &\equiv \pm \langle \psi^\dagger(\vec{r}) \psi(\vec{r}', \tau - \beta) \rangle \\ &= \pm \text{Tr} \psi^\dagger(\vec{r}) e^{(\tau - \beta)H} \psi(\vec{r}') e^{-(\tau - \beta)H} e^{-\beta H} / \text{Tr} e^{-\beta H} \end{aligned} \quad (3.20)$$

$$\begin{aligned} &\stackrel{\text{cycl. prop. of Tr}}{=} \pm \text{Tr} e^{\tau H} \psi(\vec{r}') e^{-\tau H} \psi^\dagger(\vec{r}) e^{-\beta H} / \text{Tr} e^{-\beta H} \\ &\equiv \mp G(\vec{r}', \tau; \vec{r}, 0) \end{aligned} \quad (3.21)$$

That is shifting the time by β we get a minus sign for fermions. In other words the GF is antiperiodic in times. In contrast, the GF for bosons [lower sign in Eq. (3.21)] is periodic. Note that we showed this only for the GF from $-\beta$ to $+\beta$. Actually outside the interval the GF is defined by further antiperiodizing (periodizing) it whenever it is shifted further by β .⁴

Since the GF is antiperiodic respectively periodic in time, only discrete Fourier components are allowed, namely those that fulfill the antiperiodic respectively periodic property. That is we have the Fourier frequencies (also called Matsubara frequencies):

$$\omega_\nu = (2\nu + 1)\pi/\beta \quad \text{for fermions,} \quad (3.22)$$

$$\omega_\nu = 2\nu\pi/\beta \quad \text{for bosons,} \quad (3.23)$$

yielding the Fourier transformations

$$G(\vec{r}', \tau; \vec{r}, 0) = \frac{1}{\beta} \sum_{\nu} G(\vec{r}'; \vec{r}, i\omega_\nu) e^{-i\omega_\nu \tau}, \quad (3.24)$$

$$G(\vec{r}'; \vec{r}, i\omega_\nu) = \int_0^\beta d\tau G(\vec{r}', \tau; \vec{r}, 0) e^{i\omega_\nu \tau}. \quad (3.25)$$

This fulfills the (anti)periodicity because the Matsubara frequencies do:

$$e^{i\omega_\nu(\tau-\beta)} = \mp e^{i\omega_\nu \tau}. \quad (3.26)$$

It is no coincidence that the Matsubara frequencies $i\omega_\nu$ are also the poles of the Fermi/Bose function $1/(1 \pm e^{\pm\beta\omega})$. Indeed, as will be shown in the exercises, sums over (imaginary) Matsubara frequencies can often be transformed into (real) frequency integrals over the Fermi/Bose function.

3.4 Green function for independent particles

Now let us take a look at the arguably simplest problem: independent, i.e., non-interacting, particles $[V(\vec{r}' - \vec{r}) = 0]$. For simplicity, let us also Fourier-transform from space to momentum:

$$\psi(\vec{r}, \tau) = \frac{1}{(2\pi)^3} \int d^3k e^{i\vec{k}\vec{r}} c_{\vec{k}}(\tau) \quad \psi^\dagger(\vec{r}, \tau) = \frac{1}{(2\pi)^3} \int d^3k e^{-i\vec{k}\vec{r}} c_{\vec{k}}^\dagger(\tau) \quad (3.27)$$

This yields altogether for the GF

$$G(\vec{k}', \vec{k}, i\omega_\nu) = \int d^3r \int d^3r' \int_0^\beta d\tau e^{i\omega_\nu \tau + i\vec{k}\vec{r} - i\vec{k}'\vec{r}'} G(\vec{r}', \tau; \vec{r}, 0). \quad (3.28)$$

This is simpler, since \vec{k} is a good quantum number for a periodic crystal because of Bloch's theorem.⁵ This implies that the non-interacting Hamiltonian is diagonal in \vec{k} :

$$H_0 = \frac{1}{(2\pi)^3} \int d^3k \varepsilon_{\vec{k}} c_{\vec{k}}^\dagger c_{\vec{k}}. \quad (3.29)$$

⁴Actually outside the two intervals $[-\beta, 0]$ and $[0, \beta]$ [left and right hand side of Eq. (3.21), respectively], our definition of the GF does not work. For example, if $\tau' < -\beta$ the last two exponentials of the nominator of Eq. (3.20) get $e^{\eta H}$ with $\eta > 0$ which diverges since the Hamiltonian is usually not bound from above (for positive energies).

⁵Note that if $c_{\vec{k}}$ annihilates not a plane wave but an electron eigenstate of the one-particle Hamiltonian H_0 , we have $\langle \vec{r} | \vec{k} \rangle = \psi_{\vec{k}}(\vec{r})$, i.e., the eigenfunction corresponding to $\varepsilon_{\vec{k}}$ instead of $e^{i\vec{k}\vec{r}}$ in Eqs. (3.27) and (3.28).

As momentum is conserved, $\langle c_{\vec{k}'}(\tau)c_{\vec{k}}^\dagger \rangle = 0 \ \forall \vec{k} \neq \vec{k}'$, and we only need to consider the diagonal component of the GF $G(\vec{k}, \tau) \equiv -\langle \mathcal{T} c_{\vec{k}}(\tau)c_{\vec{k}}^\dagger \rangle$.

We can now employ the equation of motion (3.17) which for $V(\vec{r}' - \vec{r}) = 0$ becomes a simple algebraic equation in Fourier space and yields as the **non-interacting Green function**

$$G_0(\vec{k}, i\omega_\nu) = \frac{1}{i\omega_\nu - \varepsilon_{\vec{k}}} \quad (3.30)$$

Here and in the following we denote the non-interacting Green function with a subscript zero (G_0) and the interacting GF without subscript (G). Please remind that we shifted the chemical potential (and Hamiltonian) to $\mu = 0$. We can obtain the expressions with chemical potential by substituting $i\omega_\nu \rightarrow i\omega_\nu + \mu$ in, e.g., Eq. (3.30).

3.5 Spectral representation

For a better understanding of the Green function, let us assume that we have an eigenbasis $|n\rangle$ of the full Hamiltonian H , i.e., $H|n\rangle = E_n|n\rangle$. Using this eigenbasis we can rewrite the GF as

$$\begin{aligned} G(\vec{k}, i\omega_\nu) &= - \int_0^\beta d\tau e^{i\omega_\nu \tau} \text{Tr} e^{-\beta H} e^{\tau H} c_{\vec{k}} e^{-\tau H} c_{\vec{k}}^\dagger / \underbrace{\text{Tr} e^{-\beta H}}_{\equiv Z} \\ &= - \frac{1}{Z} \int_0^\beta d\tau e^{i\omega_\nu \tau} \sum_{mn} e^{-\beta E_m} e^{\tau(E_m - E_n)} \langle m | c_{\vec{k}} | n \rangle \langle n | c_{\vec{k}}^\dagger | m \rangle \\ &= - \frac{1}{Z} \sum_{mn} e^{-\beta E_m} \frac{e^{(i\omega_\nu + E_m - E_n)\beta} - 1}{i\omega_\nu + E_m - E_n} \langle m | c_{\vec{k}} | n \rangle \langle n | c_{\vec{k}}^\dagger | m \rangle \\ &\equiv \int d\omega' \frac{A(\vec{k}, \omega')}{i\omega_\nu - \omega'}. \end{aligned} \quad (3.31)$$

with the **spectral function** $A(\vec{k}, \omega)$ defined as

$$A(\vec{k}, \omega) \equiv \frac{1}{Z} (1 \pm e^{-\beta\omega}) \sum_{mn} e^{-\beta E_m} \underbrace{\langle m | c_{\vec{k}} | n \rangle \langle n | c_{\vec{k}}^\dagger | m \rangle}_{\langle m | \psi_{\vec{r}'} | n \rangle \langle n | \psi_{\vec{r}}^\dagger | m \rangle \text{ in } \vec{r} \text{ basis}} \delta(\omega - (E_n - E_m)). \quad (3.32)$$

Note that $|n\rangle$ has one more particle than $|m\rangle$. Integrating the spectral function over all frequencies we get:

$$\int_{-\infty}^{\infty} d\omega A(\vec{k}, \omega) = 1, \quad (3.33)$$

which can be proven using (3.32) and the commutation relations of the c operators (we do not show the proof here).

For $T = 0$ and $\omega > 0$ this simplifies to

$$A(\vec{k}, \omega) = \sum_n |\langle n | c_{\vec{k}}^\dagger | \text{GS} \rangle|^2 \delta(\omega - (E_n - E_{\text{GS}})). \quad (3.34)$$

That is the spectral function counts (sums) all states n that can be reached from the ground state (GS) by adding a particle ($c_{\vec{k}}^\dagger$) with momentum \vec{k} [first term] and for which energy conservation is fulfilled, i.e., $E_n - E_{\text{GS}} = \omega$ [second term].

For non-interacting particles, Eq. (3.30) implies $A(\vec{k}, \omega) = \delta(\omega - \epsilon_{\vec{k}})$. Indeed we obtain the same from Eq. (3.34) when we remind ourselves that: (i) the eigenstates $|n\rangle$ are Slater determinants where for the ground state with N particles the lowest N states are occupied (up to the Fermi level $E_F \equiv 0$; $E_{\text{GS}} = \sum_{\vec{k}|\epsilon_{\vec{k}} < E_F} \epsilon_{\vec{k}}$); and (ii) $\omega > 0$ implies $\epsilon_{\vec{k}} > 0$, i.e., it is not occupied so that $|\langle n|c_{\vec{k}}^\dagger|\text{GS}\rangle|^2 = 1$.

For $T = 0$ and $\omega < 0$ E_n and E_m exchange their roles (E_n can now be restricted to the ground state energy and $E_m > E_n$) and we analogously get

$$A(\vec{k}, \omega) = \sum_m |\langle m|c_{\vec{k}}|\text{GS}\rangle|^2 \delta(\omega - (E_{\text{GS}} - E_m)). \quad (3.35)$$

This also gives us a **physical interpretation** of the spectral function: It is the amplitude to add particle at $\omega > 0$ or remove a particle at $\omega < 0$ with given momentum \vec{k} to the ground state of the system (or the thermal ensemble thereof). The energy of the solid increases by $|\omega|$. For $\omega < 0$ this process can be realized experimentally by **angular-resolved photoemission spectroscopy (ARPES)**.⁶ Here a photon with energy ω_{ph} and momentum \vec{k}_{ph} kicks out an electron from the solid to the vacuum where it has the free energy ω_f and momentum \vec{k}_f . Energy and momentum conservation imply that, see Fig. 3.2,

$$\begin{array}{ccc} \text{before} & & \text{after} \\ E_{\text{GS}} + \omega_{ph} & = & E_m + \omega_f \quad \text{or} \quad \omega = E_{\text{GS}} - E_m = \omega_f - \omega_{ph} < 0 \end{array} \quad (3.36)$$

$$\vec{k} = \vec{k}_f - \vec{k}_{ph}. \quad (3.37)$$

Note that this describes a process changing the particle number, $N \rightarrow N - 1$.

The inverse process ($\omega > 0$, $N \rightarrow N + 1$) is experimentally realized by inverse photoemission spectroscopy (adding an electron, emitting a photon), which is however not very efficient, or x-ray absorption spectroscopy (XAS) where the photon kicks out a tightly bound core electron but not to the vacuum as in ARPES but to a state above the Fermi level in the solid. That is we have effectively added one electron to the unoccupied states above the Fermi level. However, there is also a core hole which Coulomb interacts with the electrons, making this process somewhat more complicated. For these reasons our experimental knowledge of the occupied electronic states is much better than the unoccupied ones. Most other experiments are related to the two-particle Green function or response function which we will discuss later in the lecture.

3.6 Analytical properties of the Green function

Given Eq. (3.31), the analytical continuation appears simple, just substituting $i\omega_\nu$ by ω . However special care needs to be taken for the poles in the Green function.

⁶This direct relation between spectral function and ARPES is valid under some approximations: one has (i) to assume a sudden kick-out so that the outgoing electron is not interacting with further electrons [e.g., kicking out further (Auger)electrons] and (ii) neglect possible matrix elements (the electromagnetic field of the photon in general interacts more strongly with some states than with others).

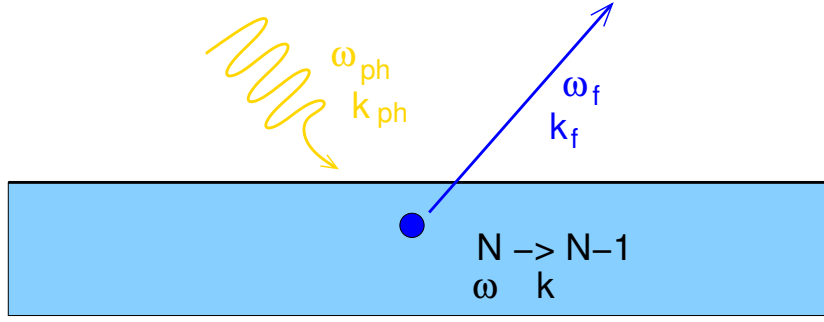


Figure 3.2: ARPES: An incoming phonon with frequency ω_{ph} and momentum \vec{k}_{ph} kicks out an electrons with ω_f and \vec{k}_f ; particle, energy and momentum conservation imply that the solid state system goes from $N \rightarrow N - 1$ electrons, and changes its energy by $\omega = \omega_{ph} - \omega_f$ and its momentum by $\vec{k} = \vec{k}_{ph} - \vec{k}_f$. This corresponds, on the theoretical side, to the spectral function $A(\vec{k}, \omega)$.

Let us to this end first consider an auxiliary calculation, the Fourier transform of the Θ function, which is a bit tricky and we have to introduce an (infinitesimal) factor $\delta > 0$ for making the integral convergent:

$$\int_{-\infty}^{\infty} dt \Theta(t) e^{i(\omega + i\delta)t} = \left. \frac{e^{i(\omega + i\delta)t}}{i(\omega + i\delta)} \right|_0^{\infty} = i \frac{1}{\omega + i\delta} \quad (3.38)$$

$$= i \frac{\omega - i\delta}{\omega^2 + \delta^2} \xrightarrow{\delta \rightarrow 0} i \frac{1}{\omega} + \pi \delta(\omega). \quad (3.39)$$

Before turning to the causal GF let us consider first two additional Green functions that are commonly used, the retarded (R) and advanced (A) GF. They are defined as

$$G_R(\vec{r}', t'; \vec{r}, 0) \equiv -i \left(\langle \psi(\vec{r}', t') \psi^\dagger(\vec{r}, 0) \rangle \pm \langle \psi^\dagger(\vec{r}, 0) \psi(\vec{r}', t') \rangle \right) \Theta(t') \quad (3.40)$$

$$G_A(\vec{r}', t'; \vec{r}, 0) \equiv +i \left(\langle \psi(\vec{r}', t') \psi^\dagger(\vec{r}, 0) \rangle \pm \langle \psi^\dagger(\vec{r}, 0) \psi(\vec{r}', t') \rangle \right) \Theta(-t'). \quad (3.41)$$

where the \pm sign refers to fermions/bosons. According to our considerations for the Fourier transform of the $\Theta(t)$ function, the Fourier transform for the retarded GF becomes

$$G_R(\vec{k}, \omega) = \int d\omega' \frac{A(\vec{k}, \omega')}{\omega - \omega' + i\delta}, \quad (3.42)$$

$$G_A(\vec{k}, \omega) = \int d\omega' \frac{A(\vec{k}, \omega')}{\omega - \omega' - i\delta} \quad (3.43)$$

with an infinitesimal small δ . That for the advanced GF can be derived analogously to Eq. (3.39).

For the causal GF, which has a $\Theta(t)$ if first adding a particle (corresponding to $\omega > 0$) and a $\Theta(-t)$ if first removing a particle (corresponding to $\omega < 0$), we have a mixture

$$G_C(\vec{k}, \omega) = \int d\omega' \frac{A(\vec{k}, \omega')}{\omega - \omega' + i\delta \text{sgn}(\omega)}. \quad (3.44)$$

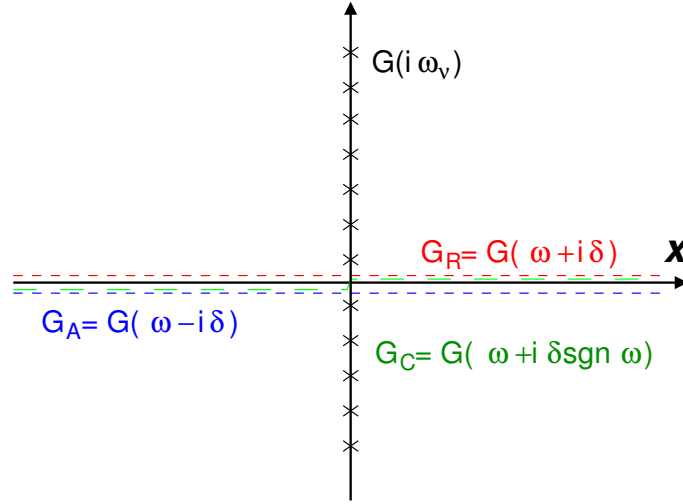


Figure 3.3: Illustration of the Green function in the complex plane.

All of these GFs can be united into a **single GF in the complex ω plane**, see Fig. 3.3,

$$G(\vec{k}, \omega) = \int d\omega' \frac{A(\vec{k}, \omega')}{\omega - \omega'}. \quad (3.45)$$

That is the Green function has its poles on the real axis at $\omega = E_n - E_m$.⁷ Away from the real axis this GF is analytical in the upper (lower) complex plane. Hence knowing the GF on a line such as the retarded GF above the real axis (the advanced GF below) is sufficient to get the GF everywhere in the upper (lower) complex plane, as is knowing the temperature GF at the Matsubara frequencies [where instead of a line we have an accumulation point at $+\infty$ ($-\infty$)]. In practice, one typically calculates the many-body calculations in Matsubara frequencies yielding $G(\vec{k}, i\omega_\nu)$, and at the end employs an analytical continuation to obtain the GF $G(\vec{k}, \omega)$ and spectral function $A(\vec{k}, \omega)$ for real frequencies. For an analytical calculation one can substitute $i\omega_\nu \rightarrow \omega$, for a numerical calculation one can employ the maximum entropy method or a Padé fit.

Since the GF is an analytic function, its real and imaginary part are not independent. This is expressed by the **Kramers-Kronig relations**. These can be derived by using the formula of Weierstrass for an analytic function $F(x)$

$$\int dx F(x) \frac{1}{x \pm i\delta} = \mathcal{P} \int dx F(x) \frac{1}{x} \mp i\pi F(0), \quad (3.46)$$

Here \mathcal{P} denotes the principle value of the integral, and the formula can be understood as half a residue, see Fig. 3.4. Employing Eq. (3.46) for

$$G_R(\vec{k}, \omega) = \int d\omega' \frac{A(\vec{k}, \omega')}{\omega - \omega' + i\delta} \quad (3.47)$$

⁷The number of poles increases exponentially with system size and becomes a continuum of poles in the thermodynamic limit.

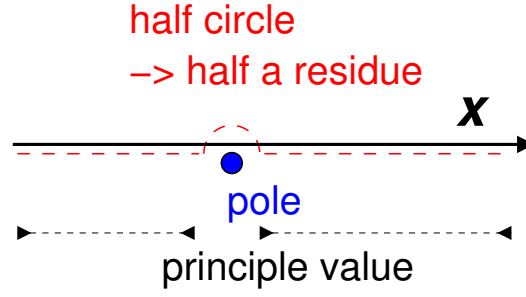


Figure 3.4: The Weierstrass formula, Eq. (3.46), decomposes the integration above the pole (red dashed lines and arc) into the principle value (black dashed lines) and half a circle (red dashed arc) corresponding to half a residue.

requires the imaginary part of the left side of Eq. (3.47) to be equal to that of the right side calculated through Eq. (3.46), i.e., (now with left and right sides exchanged)

$$A(\vec{k}, \omega) = -\frac{1}{\pi} \text{Im} G_R(\vec{k}, \omega'). \quad (3.48)$$

Substituting $A(\vec{k}, \omega)$ in Eq. (3.47) and now comparing the real part of the left and right side yields the **Kramers-Kronig relation**

$$\text{Re} G_R(\vec{k}, \omega) = -\frac{1}{\pi} \mathcal{P} \int d\omega' \frac{\text{Im} G_R(\vec{k}, \omega')}{\omega - \omega'} \quad (3.49)$$

Extending this Kramers-Kronig relation to the full GF by an analytic continuation yields the **second Kramers-Kronig relation**

$$\text{Im} G_R(\vec{k}, \omega) = \frac{1}{\pi} \mathcal{P} \int d\omega' \frac{\text{Re} G_R(\vec{k}, \omega')}{\omega - \omega'}. \quad (3.50)$$

Chapter 4

Landau Fermi Liquid Theory

The Landau Fermi liquid theory originates from the observation that many electronic properties of metals can be described by treating electrons as a gas of non-interacting particles. This is true also in many cases when electrons inside a given material are actually strongly interacting. Indeed the Coulomb interaction is comparable to their kinetic energy ($\sim 1-10\text{eV}$). But features like linear specific heat capacity ($C_V \propto T$), a well-defined Fermi surface and temperature-independent paramagnetic behavior can be described as though the electrons were independent. Although there are other applications of Landau Fermi-liquid theory such as liquid ^3He and neutron stars (see [5] Chapter 6), it is more interesting for us to investigate the properties of metals. Landau's approach was to consider a non-interacting fermionic gas (such as liquid ^3He) and turn the Coulomb interaction *adiabatically* on. If the probability of scattering between the fermions is low, the lifetime of the resulting excited states is long enough to treat them as though they were stable particles (since they have a finite lifetime, we call them *quasi-particles*). Their quantum numbers – spin and charge – are conserved. Even in cases when Coulomb interaction is strong, the excitations of the electronic systems still behave as independent quasi-particles, with charge and spin of the electrons, but with renormalized mass m^* .

4.1 Adiabatic switching on of the Coulomb interaction

We start with a system of non-interacting electrons at $T = 0$. In the ground state every one-particle state with one-particle energy below the Fermi energy ε_F is occupied and every state above is unoccupied. We add an electron with energy $\varepsilon_1 \geq \varepsilon_F$ and allow it to interact (scatter) with another electron with energy ε_2 . Since only states below Fermi energy are occupied, $\varepsilon_2 \leq \varepsilon_F$. After the scattering event (see Fig.4.1) we end up with two states with energies ε_3 and ε_4 . Due to energy conservation we have

$$\varepsilon_1 + \varepsilon_2 = \varepsilon_3 + \varepsilon_4. \quad (4.1)$$

The scattered electrons must have energies $\varepsilon_3, \varepsilon_4 \geq \varepsilon_F$, because all other states below the Fermi energy are occupied. First, we assume $\varepsilon_1 = \varepsilon_F$. Then (4.1) leads to

$$\varepsilon_2 = \underbrace{\varepsilon_3}_{\geq \varepsilon_F} + \underbrace{\varepsilon_4}_{\geq \varepsilon_F} - \varepsilon_F \Rightarrow \varepsilon_2 \geq \varepsilon_F. \quad (4.2)$$

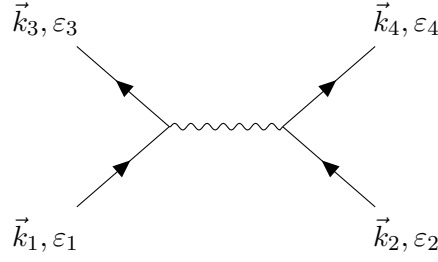
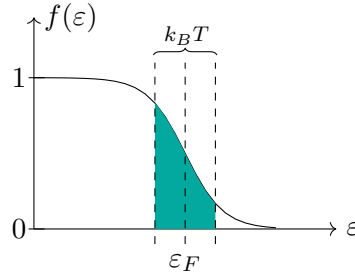


Figure 4.1: Feynman diagram for scattering of two electrons

Figure 4.2: Fermi-Dirac distribution function. For $T > 0$, there are some unoccupied states below ε_F and occupied states above ε_F in the energy window $\sim k_B T$.

But since $\varepsilon_2 \leq \varepsilon_F$ this can only be fulfilled if $\varepsilon_2 = \varepsilon_F$ and that finally leads to $2\varepsilon_F = \varepsilon_3 + \varepsilon_4$. With $\varepsilon_3, \varepsilon_4 \geq \varepsilon_F$ the only possibility is $\varepsilon_3 = \varepsilon_4 = \varepsilon_F$. Therefore the scattering occurs only on the Fermi surface. Due to momentum conservation there are not enough states at the Fermi energy that could result from such scattering and consequently there is no phase space for scattering, i.e. the lifetime τ of the states on the Fermi surface is infinite

$$\tau \rightarrow \infty \Rightarrow \frac{1}{\tau} \rightarrow 0,$$

where the *scattering rate* $\frac{1}{\tau}$ gives the probability of scattering, which is proportional to the available phase space volume.

Let us now assume¹ $\varepsilon_1 > \varepsilon_F$ which will give for the energies after the scattering the following restriction: $\varepsilon_3 \in [\varepsilon_F, \varepsilon_1]$ and $\varepsilon_4 \in [\varepsilon_F, \varepsilon_1 - (\varepsilon_3 - \varepsilon_F)]$. Then the energy conservation (4.1) gives us

$$\varepsilon_2 = \varepsilon_3 + \varepsilon_4 - \varepsilon_1 \leq \varepsilon_F, \quad (4.3)$$

from which we can estimate the phase space volume for that scattering² and the scattering rate to be $\frac{1}{\tau} \sim (\varepsilon_1 - \varepsilon_F)^2$. For finite temperature $T > 0$ not every state below the Fermi-energy is occupied and the scattering rate increases. The occupation changes from a step function into the Fermi-Dirac distribution (see Fig.4.2):

¹Both cases that are implicit included in the relation " \geq " are then covered.

²The derivation is part of the exercises.

| | Fermi gas | adiabatic switching of the Coulomb interaction | Fermi liquid |
|---|------------------------------------|---|--|
| ① | non-interacting electrons | | non-interacting <i>quasi-particles</i> |
| ② | strongly interacting electrons | | weakly interacting <i>quasi-particles</i> |
| ③ | ε_k | | $\tilde{\varepsilon}_k$ |
| ④ | $\varepsilon_{k'} - \varepsilon_k$ | | $\tilde{\varepsilon}_{k'} - \tilde{\varepsilon}_k$ |
| ⑤ | m | | m^* |
| ⑥ | $\tau = \infty$ | | $\tau < \infty$ |

Figure 4.3: Comparison of Fermi gas and Fermi liquid theory and their properties. ①: Starting point with no Coulomb interaction ②: Conclusion after switching on the Coulomb interaction ③: One-particle energies ④: Excitation energies ⑤: Mass. ⑥: Lifetime.

$$f(\varepsilon) = \frac{1}{e^{(\varepsilon_i - \mu)/k_B T} + 1}. \quad (4.4)$$

The resulting scattering rate is given by

$$\frac{1}{\tau} \sim a(\varepsilon_1 - \varepsilon_F)^2 + b(k_B T)^2, \quad (4.5)$$

which we give here without proof ³ (a and b are positive constants that depend on the lattice).

In the above reasoning we did not make assumptions about the strength of the Coulomb interaction between the electrons. We did however make use of the assumption that we still have a Fermi surface that at $T = 0$ divides the states into occupied and unoccupied, and that we can still number the states by the same quantum numbers (momentum, spin). Landau proposed that if we turn the interaction adiabatically on, we can achieve one-to-one correspondence between excited states of the non-interacting and interacting Fermi gas. We do not need to know the ground state of the interacting system – it is enough that it "evolved" from the ground state of the non-interacting system upon adiabatic switching on of the Coulomb interaction. This approach will only be valid if the new ground state remains stable and the system does not undergo a phase transition. Mathematically speaking: the perturbation series for the free energy of that system must converge – under this condition, one can prove the exactness of Landau's Fermi liquid theory, which was done by Nozieres [12]. Landau called the excited states of the interacting system *quasi-particles*. Their energies $\tilde{\varepsilon}_k$ and mass m^* are renormalized with respect to the electrons in the Fermi gas (see Fig.4.3), hence the name: Fermi liquid.

The quasi-particles have a finite lifetime that decreases with distance from the Fermi energy and temperature (as in (4.5)). Many properties of metals depend on the states that lie at or very

³Proof is part of the exercise class.

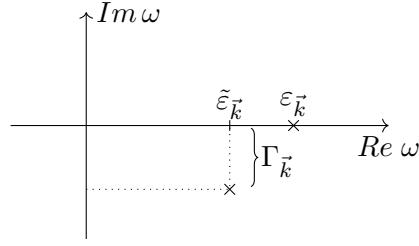


Figure 4.4: Poles of the non-interacting Green's function and the quasi-particle Green's function.

near the Fermi energy. The fact that at low temperatures and at Fermi energy the quasi-particle lifetimes become almost infinite explains why metals at low temperature are well described by the Fermi liquid theory. The specific heat is, like in the gas of independent electrons, linearly proportional to temperature $C_V = \gamma T$, with the coefficient γ proportional not to the mass of the electron m , but to the renormalized mass m^* . For elemental metals, like Cu, Na, Au, m^* is 2-10 times bigger than m , but for some intermetallic compounds $m^* \approx 1000m$. These compounds are for this reason called heavy fermions (e.g. CeCu₆, CeAl₃, UBe₁₃).

4.2 Microscopic formulation of the Fermi-liquid theory

Having started with the phenomenological formulation of the Fermi liquid theory and with phase space arguments, let us continue with quantitative description of Fermi liquids.

4.2.1 Green's function and finite lifetime

In the previous chapter we have learnt that the Green's function for independent electrons is given by (3.30)

$$G_0(\vec{k}, \omega) = \frac{1}{\omega - \varepsilon_{\vec{k}}}. \quad (4.6)$$

This Green's function has a pole on the real frequency axis at $\omega = \varepsilon_{\vec{k}}$ (see Fig. 4.4). In the time domain (for simplicity let us for a moment take $T = 0$) the retarded Green's function represents free propagation in time:

$$G_0^R(\vec{k}, t) = -i\Theta(t)e^{-i\varepsilon_{\vec{k}}t}. \quad (4.7)$$

Before we formally introduce the effects of the interaction into the Green's function, let us use the phenomenological information about the Fermi liquid to construct a Green's function of a quasi-particle. Besides changing the energy $\varepsilon_{\vec{k}} \rightarrow \tilde{\varepsilon}_{\vec{k}}$, we also need to modify (4.7) with a damping term $e^{-\Gamma_{\vec{k}}t}$ to account for the finite lifetime $\tau \sim 1/\Gamma$. the quasi-particle Green's function takes the form

$$G_{QP}^R(\vec{k}, t) = -i\Theta(t)e^{-i\tilde{\varepsilon}_{\vec{k}}t}e^{-\Gamma_{\vec{k}}t} \quad (4.8)$$

and in the frequency domain

$$G_{QP}(\vec{k}, \omega) = \frac{1}{\omega - \tilde{\varepsilon}_{\vec{k}} + i\Gamma_{\vec{k}}}. \quad (4.9)$$

Note that in comparison with (4.6) we shifted the pole away from the real axis to the complex frequency plain (see Fig. 4.4).

4.2.2 Self-energy

It is convenient to contain all the effects of the interactions between electrons in one quantity that modifies the Green's function. We could take the difference between the full Green's function for the system with interactions G and the Green's function of non-interacting particles G_0 . But it is more practical to take the difference between the inverses. This way the *self-energy* Σ is defined.

SELF-ENERGY

The effects of interactions between particles are included in a quantity called self-energy Σ . It is the difference between the inverse of the Green's functions of non-interacting and interacting system

$$\underbrace{\Sigma(\vec{k}, \omega)}_{\text{self energy}} = \underbrace{G_0^{-1}(\vec{k}, \omega)}_{\text{non-interacting GF}} - \underbrace{G^{-1}(\vec{k}, \omega)}_{\text{interacting GF}}. \quad (4.10)$$

This equation can be rewritten by using (4.6):

$$G^{-1}(\vec{k}, \omega) = G_0^{-1}(\vec{k}, \omega) - \Sigma(\vec{k}, \omega) = \omega - \varepsilon_{\vec{k}} - \Sigma(\vec{k}, \omega) \quad (4.11)$$

$$\Rightarrow G(\vec{k}, \omega) = \frac{1}{\omega - \varepsilon_{\vec{k}} - \Sigma(\vec{k}, \omega)}. \quad (4.12)$$

In general the self energy is a complex function $\Sigma = \text{Re } \Sigma + i \text{Im } \Sigma$, Eq.(4.12) then reads

$$G(\vec{k}, \omega) = \frac{1}{\omega - \varepsilon_{\vec{k}} - \text{Re } \Sigma - i \text{Im } \Sigma}. \quad (4.13)$$

Comparing (4.9) and (4.13) lets us give a phenomenological interpretation to the self-energy: the real part gives the shift of the energy $\tilde{\varepsilon}_{\vec{k}} = \varepsilon_{\vec{k}} - \text{Re } \Sigma$ and the imaginary part gives the scattering rate $\Gamma_{\vec{k}} = -\text{Im } \Sigma$ (see Fig.4.4). In general the self-energy is not a constant, but a function of both momentum and frequency. In the case of a Fermi liquid we have argued from phase space restrictions that the scattering rate is given by

$$\Gamma = \frac{1}{\tau} = a(\varepsilon_1 - \varepsilon_F)^2 + b(k_B T)^2. \quad (4.14)$$

Redefining the zero of the real frequency axis to be at the Fermi energy, we have $(\varepsilon_1 - \varepsilon_F)^2 = \omega^2$ and to the lowest order in ω the imaginary part of the Fermi liquid self-energy is given by:

$$\text{Im } \Sigma = -a\omega^2 - b(k_B T)^2, \quad (4.15)$$

with $a, b > 0$. Now we would like to investigate the low ω behaviour of the real part of the self-energy. Let us Taylor expand $\varepsilon_{\vec{k}} + \text{Re } \Sigma(\vec{k}, \omega)$ near the Fermi surface (we simplify the notation by omitting the vector arrows)

$$\begin{aligned} \varepsilon_k + \text{Re } \Sigma(k, \omega) &= \varepsilon_F + \text{Re } \Sigma(k_F, 0) + \\ &\quad + (k - k_F) \left[\left. \frac{\partial \varepsilon_k}{\partial k} \right|_{k=k_F} + \left. \frac{\partial \text{Re } \Sigma(k, 0)}{\partial k} \right|_{k=k_F} \right] + \omega \left. \frac{\partial \text{Re } \Sigma(k_F, \omega)}{\partial \omega} \right|_{\omega=0} + \\ &\quad + O(\omega^2, (k - k_F)^2) \\ &\simeq \underbrace{(k - k_F) \left[\left. \frac{\partial \varepsilon_k}{\partial k} \right|_{k=k_F} + \left. \frac{\partial \text{Re } \Sigma(k, 0)}{\partial k} \right|_{k=k_F} \right]}_{\tilde{v}_F} + \underbrace{\omega \left. \frac{\partial \text{Re } \Sigma(k_F, \omega)}{\partial \omega} \right|_{\omega=0}}_{-\alpha} \end{aligned} \quad (4.16)$$

where we expanded $\varepsilon_k = \varepsilon_F + (k - k_F) \left. \frac{\partial \varepsilon_k}{\partial k} \right|_{k=k_F} + O((k - k_F)^2)$, shifted the constant terms to zero: $\varepsilon_F + \text{Re } \Sigma(k_F, 0) = 0$. We also introduced \tilde{v}_F and $\alpha = -\left. \frac{\partial \text{Re } \Sigma}{\partial \omega} \right|_{\omega=0}$ to simplify notation.

The above Taylor expansion approximates the real part of the self-energy in the vicinity of the Fermi surface. When we plug it into the Green's function (4.13), we obtain

$$\begin{aligned} G(k, \omega) &\simeq \frac{1}{\omega + \alpha \omega - (k - k_F) \tilde{v}_F - i \text{Im } \Sigma} = \frac{1}{(1 + \alpha) \omega - (k - k_F) \tilde{v}_F - i \text{Im } \Sigma} \\ &= \frac{(1 + \alpha)^{-1}}{\omega - (1 + \alpha)^{-1} (k - k_F) \tilde{v}_F - i (1 + \alpha)^{-1} \text{Im } \Sigma} \\ &\equiv \frac{Z}{\omega - \tilde{\varepsilon}_k - i Z \text{Im } \Sigma}, \end{aligned} \quad (4.17)$$

where we defined

$$Z = (1 + \alpha)^{-1} = \left[1 - \left. \frac{\partial \text{Re } \Sigma}{\partial \omega} \right|_{\omega=0} \right]^{-1}, \quad (4.18)$$

and

$$\tilde{\varepsilon}_k = Z(k - k_F) \left[\left. \frac{\partial \varepsilon_k}{\partial k} \right|_{k=k_F} + \left. \frac{\partial \text{Re } \Sigma}{\partial k} \right|_{k=k_F} \right] \equiv (k - k_F) \frac{k_F}{m^*}. \quad (4.19)$$

Such defined quantities Z and m^* are called the *Fermi liquid parameters*. The parameter Z is the *quasiparticle weight*. From $\left. \frac{\partial \text{Re } \Sigma}{\partial \omega} \right|_{\omega=0} \leq 0$ (it follows from the $\sim a\omega^2$ behaviour of $\text{Im } \Sigma$ and the Kramers-Kronig relations which hold also for the self-energy), we have $\alpha \geq 0$ and for the quasi-particle weight holds $Z \leq 1$.

The parameter m^* is the *renormalized (effective) mass*. Assuming that $\left. \frac{\partial \varepsilon_k}{\partial k} \right|_{k=k_F} = \frac{k_F}{m}$ as in the Fermi gas, we get for the effective mass the following expression

$$m^* = \frac{m}{Z} \left[1 + \frac{m}{k_F} \left. \frac{\partial \text{Re } \Sigma}{\partial k} \right|_{k=k_F} \right]^{-1} \geq m. \quad (4.20)$$

Since $m^* \geq m$, the renormalized dispersion relation $\tilde{\varepsilon}_k$ in (4.19) is flattened in comparison to ε_k (see Fig. 4.5).

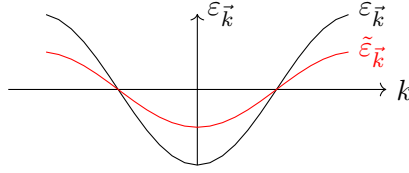


Figure 4.5: Dispersion relation of the quasi-particles $\tilde{\varepsilon}_{\vec{k}}$ compared to the dispersion relation of non-interacting electrons $\varepsilon_{\vec{k}}$

4.2.3 Quasiparticle spectral function

In Chapter 3.5 we defined the spectral function

$$A(\vec{k}, \omega) = -\frac{1}{\pi} \text{Im } G(\vec{k}, \omega). \quad (4.21)$$

The spectral function obtained for the quasi-particle Green's function from (4.17) has the following form

$$A_{QP}(\vec{k}, \omega) = \frac{Z}{\pi} \frac{Z \text{Im } \Sigma}{(\omega - \tilde{\varepsilon}_{\vec{k}})^2 + (Z \text{Im } \Sigma)^2}. \quad (4.22)$$

Integrating the above spectral function over the frequencies, we get the spectral weight Z . According to (3.33) we should however get total spectral weight of 1. In cases when the quasi-particle weight $Z < 1$, (4.17) does not describe the entire Green's function. To account for the missing spectral weight, we add a second term called *incoherent part*, which describes effects that lie beyond Fermi liquid theory. The full Green's function is therefore a sum of a *coherent*, i.e. described by Fermi liquid theory, and *incoherent* part.

$$G(\vec{k}, \omega) = \underbrace{\frac{Z}{\omega - \varepsilon_{\vec{k}} - iZ \text{Im } \Sigma}}_{\text{coherent part}} + \underbrace{(1 - Z)G'(\vec{k}, \omega)}_{\text{incoherent part}}. \quad (4.23)$$

Please note, that within Fermi liquid theory we cannot say anything about the incoherent part. Therefore, the Fermi liquid description can be used either if Z is sufficiently close to 1 or if we are interested in properties very close to the Fermi surface.

Let us recall the spectral function for non-interacting electrons: $A_0(\vec{k}, \omega) = \delta(\omega - \varepsilon_{\vec{k}})$. For a given \vec{k} , it is just a Dirac delta distribution peaked at $\omega = \varepsilon_{\vec{k}}$ (see Fig.4.6a). For the interacting system, the spectral function $A(\vec{k}, \omega)$ as a function of ω has a richer structure. We still have a peak at a shifted position $\omega = \tilde{\varepsilon}_{\vec{k}}$ and with a finite width given by $Z \text{Im } \Sigma$ (this is the quasi-particle, coherent part), but we also have weight at other frequencies (incoherent part) as illustrated in Fig.4.6b.

If we consider the quasi-particle spectral function (4.22) precisely on the Fermi surface ($\omega = 0$), $A_{QP}(\vec{k}, \omega)$ takes the form

$$A_{QP}(\vec{k}, \omega) \simeq Z \delta(\omega - \tilde{\varepsilon}_{\vec{k}}), \quad (4.24)$$

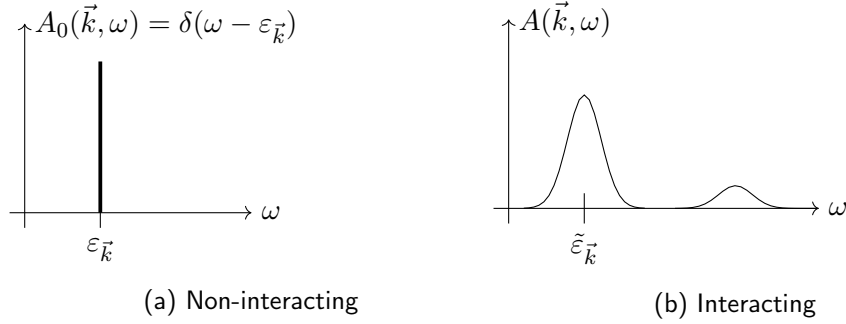
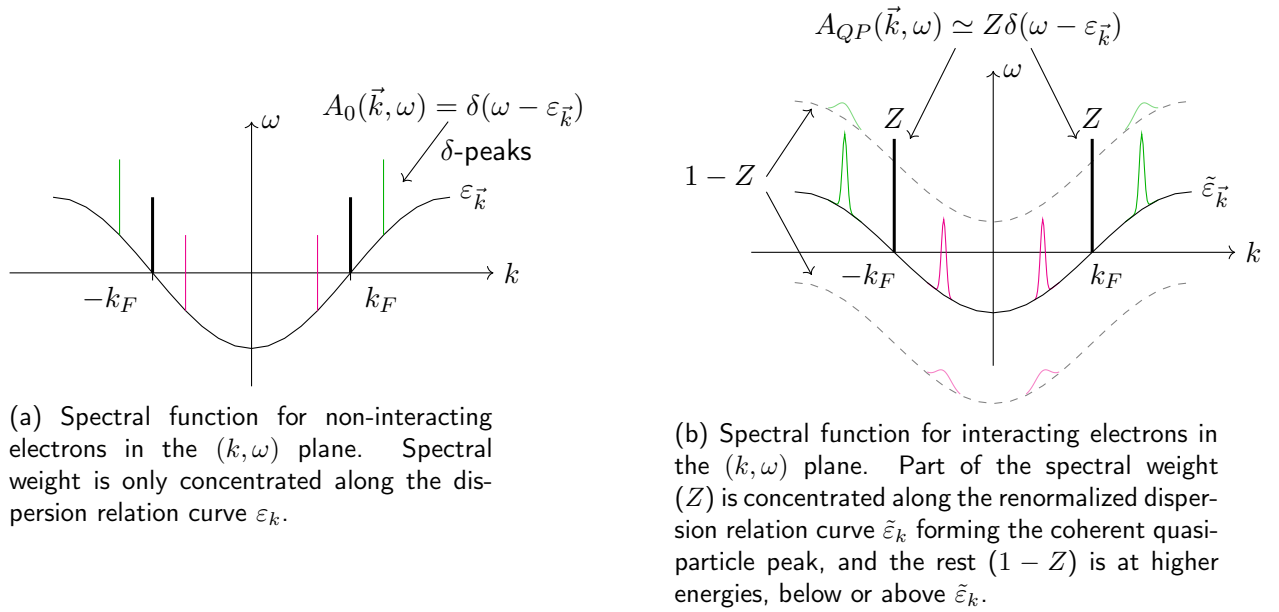


Figure 4.6: Spectral function of the non-interacting (a) and interacting (b) electrons for a given \vec{k} .



(a) Spectral function for non-interacting electrons in the (k, ω) plane. Spectral weight is only concentrated along the dispersion relation curve $\varepsilon_{\vec{k}}$.

(b) Spectral function for interacting electrons in the (k, ω) plane. Part of the spectral weight (Z) is concentrated along the renormalized dispersion relation curve $\tilde{\varepsilon}_{\vec{k}}$ forming the coherent quasi-particle peak, and the rest ($1 - Z$) is at higher energies, below or above $\tilde{\varepsilon}_{\vec{k}}$.

Figure 4.7: Comparison of the spectral functions of interacting and non-interacting electrons for selected points in the (k, ω) plane. The peaks that represent the spectral function values are to be understood as sticking out of the plane.

i.e. it consists of a δ -peak (pole of the Green's function) with a lower than 1 spectral weight Z . Away from the Fermi surface (for momenta different than k_F), the peak gets broadened in frequency, which is illustrated in Fig. 4.7b, where the spectral function is sketched for several k -points in the (k, ω) plane (for simplicity k is made one-dimensional). The broadened quasi-particle peaks lie along the renormalized dispersion curve $\tilde{\epsilon}_{\vec{k}}$, whereas the rest of the spectral weight $(1 - Z)$ lies at higher (positive and negative) frequencies.

Chapter 5

Feynman diagrams

In quantum field theory Feynman diagrams are an ingenious tool for visualizing and keeping track of an overwhelming number of mathematical expressions and for understanding the physics behind them. In this chapter we will learn how to draw them and how to work with them. For most practical problems of many-body theory it is nearly impossible to give exact solutions for interacting systems. We need perturbation theory or other methods, that are also often based on Feynman diagrams, to calculate them approximatively. There are two central objects we need to discuss in terms of perturbation theory: the S-Matrix (S for scattering) and the Green's function. The perturbative series (to all orders in the interaction) will be covered in section 5.1. In section 5.2 we will find that by evaluating Green's functions for interacting systems, there is a myriad of possibilities we need to consider. Wick's theorem will tell us how to evaluate each individual contribution. This way, at end of section 5.2 we will end up with a simplified but tedious expression of our interacting Green's function and that is exactly where Feynman diagrams come into play to help us calculating the vast amount of combinations we need to consider. In section 5.3 we will learn how to draw Feynman diagrams and how to further reduce the amount of combinations in our Green's function using, among others, the linked cluster theorem. In the last two sections, we will learn about two related methods: how to collect certain elements and combine them into a self-energy term (section 5.4) and how to even further compactify these using so-called skeleton diagrams formulated in terms of the interacting (instead of the non-interacting) Green's function (section 5.4).

5.1 Perturbation series in interaction

In section 3.4 we already calculated the Green's function

$$G_0(\vec{k}, i\omega_\nu) = \frac{1}{i\omega_\nu - \epsilon_{\vec{k}}} \quad (5.1)$$

for the non-interacting Hamiltonian

$$H_0 = \frac{1}{(2\pi)^3} \int d^3 \vec{k} \epsilon_{\vec{k}} c_{\vec{k}}^\dagger c_{\vec{k}}. \quad (5.2)$$

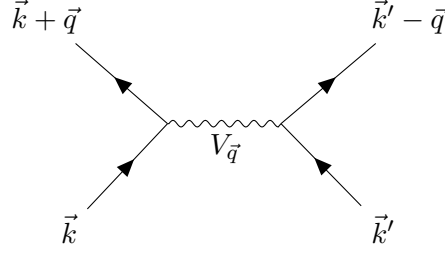


Figure 5.1: Feynman diagram for the interaction, scattering particles from momenta \vec{k} and \vec{k}' to $\vec{k} + \vec{q}$ and $\vec{k}' - \vec{q}$.

If we assume we know all the states and the energies of our non-interacting particles, the eigenstates of Eq.(5.2) are just by the occupation number states and the energy is given by simply summing up $\varepsilon_{\vec{k}} c_{\vec{k}}^\dagger c_{\vec{k}} = \varepsilon_{\vec{k}} n_{\vec{k}}$, where $n_{\vec{k}}$ is the occupation number. For interacting particles an exact solution does not, in general, exist. With an additive interacting part H_V , the Hamiltonian reads

$$H = H_0 + H_V, \quad (5.3)$$

where

$$H_V = \frac{1}{(2\pi)^9} \int d\vec{k} \int d\vec{k}' \int d^3\vec{q} c_{\vec{k}+\vec{q}}^\dagger c_{\vec{k}'-\vec{q}}^\dagger \frac{V_{\vec{q}}}{2} c_{\vec{k}'} c_{\vec{k}}. \quad (5.4)$$

On the right hand side of Eq.(5.4)¹ we have $\frac{1}{(2\pi)^9}$ which is the normalization of the three momentum integrals, then we have from right to left (or from bottom to top in Fig. 5.1) the annihilation operators for particles at \vec{k}' and \vec{k} ; the interaction $V_{\vec{q}}$ of these two particles which puts them at (scatters them to) $\vec{k} + \vec{q}$ and $\vec{k}' - \vec{q}$ with corresponding creation operators in Eq.(5.4). To avoid a double counting, as the summation \vec{k} and \vec{k}' hits each pair of electrons twice, we need to add a factor $\frac{1}{2}$. The goal of this subchapter is to express the Green's function in the perturbation series in H_V (5.4) to all orders of H_V . This will require the derivation of the perturbative series of the S-Matrix for this problem first.

5.1.1 Perturbative series of the S-Matrix

To study interacting systems we are going to use the *interaction picture* (see [10] Ch.1.3.3) where we write time dependent operators as

$$c_{\vec{k}}(\tau) = e^{+H_0\tau} c_{\vec{k}}(0) e^{-H_0\tau}, \quad (5.5)$$

note that we are working in imaginary time $\tau = it$ here. First we define

$$S(\tau_2, \tau_1) := e^{H_0\tau_2} e^{-H(\tau_2-\tau_1)} e^{-H_0\tau_1}, \quad (5.6)$$

as the so called S-matrix (scattering matrix), which is just the time propagation operator $e^{-H(\tau_2-\tau_1)}$ of the Schrödinger picture transferred to the interaction picture. Some useful properties are

¹which is just the continuous form of $F^{(2)} = \sum_{\alpha_1\alpha_2\alpha_3\alpha_4} f_{\alpha_1\alpha_2\alpha_3\alpha_4}^{(2)} a_{\alpha_1}^\dagger a_{\alpha_2}^\dagger a_{\alpha_3} a_{\alpha_4}$ (see [10] Ch.7.3.2)

1. Composition of S-matrices:

$$\begin{aligned}
S(\tau_2, \tau_3)S(\tau_3, \tau_1) &= e^{H_0\tau_2}e^{-H(\tau_2-\tau_3)}e^{-H_0\tau_3}e^{H_0\tau_3}e^{-H(\tau_3-\tau_1)}e^{-H_0\tau_1} \\
&= e^{H_0\tau_2}e^{-H(\tau_2-\tau_1)}e^{-H_0\tau_1} \\
&= S(\tau_2, \tau_1)
\end{aligned} \tag{5.7}$$

That means going from time τ_1 to τ_3 and then from τ_3 to τ_2 , is the same as just going from τ_1 to τ_2 .

2. Inverse S-matrix:

$$\begin{aligned}
S(\tau_2, \tau_1)S(\tau_1, \tau_2) &= S(\tau_2, \tau_2) \\
&= \mathbb{1}
\end{aligned} \tag{5.8}$$

from this follows

$$S^{-1}(\tau_2, \tau_1) = S(\tau_1, \tau_2) \tag{5.9}$$

So if you go from time τ_2 to τ_1 and then from τ_1 to τ_2 , we are basically going from τ_2 to τ_2 which corresponds to $\mathbb{1}$.

3. Translational symmetry in time (if H is time independent):

$$S(\tau_2, \tau_1) = S(\tau_2 + \tau_3, \tau_1 + \tau_3) \underset{\tau_3 = -\tau_1}{=} S(\tau_2 - \tau_1, 0) \equiv S(\tau_2 - \tau_1) \tag{5.10}$$

If we calculate the derivative of $S(\tau) = e^{H_0\tau}e^{-H\tau}$ with respect to imaginary time τ we obtain:

$$\frac{\partial S(\tau)}{\partial \tau} = \frac{\partial}{\partial \tau} (e^{H_0\tau}e^{-H\tau}) \tag{5.11}$$

$$= e^{H_0\tau}H_0e^{-H\tau} + e^{H_0\tau}(-H)e^{-H\tau} \tag{5.12}$$

$$= -e^{H_0\tau} \underbrace{(H - H_0)}_{H_V} e^{-H\tau} \tag{5.13}$$

$$= e^{H_0\tau}H_V \underbrace{\mathbb{1}}_{=e^{-H_0\tau}e^{+H_0\tau}} e^{-H\tau} \tag{5.14}$$

$$= - \underbrace{e^{H_0\tau}H_Ve^{-H_0\tau}}_{H_V(\tau)} \underbrace{e^{+H_0\tau}e^{-H\tau}}_{S(\tau)} \tag{5.15}$$

$$= -H_V(\tau)S(\tau). \tag{5.16}$$

The solution to that differential equation is

$$S(\tau) = \mathcal{T}e^{-\int_0^\tau d\tau' H_V(\tau')}. \tag{5.17}$$

Proof. We start by integrating (5.16) on both sides

$$\Rightarrow \int_0^\tau d\tau' \left(\frac{\partial S(\tau)}{\partial \tau} \Big|_{\tau=\tau'} \right) = - \int_0^\tau d\tau' H_V(\tau') S(\tau') \quad (5.18)$$

$$S(\tau) - S(0) = - \int_0^\tau d\tau' H_V(\tau') S(\tau') \quad (5.19)$$

$$S(\tau) = \underbrace{S(0)}_{\mathbb{1}} - \int_0^\tau d\tau' H_V(\tau') S(\tau') \quad (5.20)$$

Next, we iterate this equation by inserting S recursively. Starting with $S(\tau') = 1$ which yields

$$S(\tau') = \mathbb{1} - \int_0^{\tau'} d\tau'' H_V(\tau''). \quad (5.21)$$

In the next step of this iteration, we plug (5.21) into (5.20) and obtain

$$S(\tau) = \mathbb{1} - \int_0^\tau d\tau' H_V(\tau') \left(\mathbb{1} - \int_0^{\tau'} d\tau'' H_V(\tau'') \right) \quad (5.22)$$

$$= \mathbb{1} - \int_0^\tau d\tau' H_V(\tau') + \int_0^\tau d\tau' H_V(\tau') \int_0^{\tau'} d\tau'' H_V(\tau''). \quad (5.23)$$

If we continue this process infinitely many times we eventually get

$$S(\tau) = \sum_{n=0}^{\infty} (-1)^n \int_0^\tau d\tau_1 \int_0^{\tau_1} d\tau_2 \dots \int_0^{\tau_{n-1}} d\tau_n H_V(\tau_1) H_V(\tau_2) \dots H_V(\tau_n). \quad (5.24)$$

If we integrate τ_2 to τ_1 and then τ_1 to τ we integrate over the yellow area in Fig.5.2. But we can extend that area by the blue region if we integrate τ_2 also to τ . But since in the blue region $\tau_2 > \tau_1$ we have the wrong time order of the H_V 's. We can however exchange the time-order of the H_V 's using inserting a Wick time ordering operator \mathcal{T} . Since both H_V 's have two creation and two-annihilation operators, the time-ordering operator \mathcal{T} ². The area of integration has been doubled by extending the integration boundaries, so we need to add a factor $\frac{1}{2}$. Altogether this yields

$$S(\tau) = \sum_{n=0}^{\infty} \frac{(-1)^n}{2} \int_0^\tau d\tau_1 \int_0^\tau d\tau_2 \int_0^{\tau_3} d\tau_3 \dots \int_0^{\tau_{n-1}} d\tau_n \mathcal{T} H_V(\tau_1) H_V(\tau_2) \dots H_V(\tau_n). \quad (5.25)$$

We can extend the integration of all times times to $[0, \tau]$. There are $n!$ possible orders of n times, but the Wick time ordering operator again guarantees the proper time order of the H_V 's starting with the earliest time to the right as in the original expression. Hence we obtain altogether

$$S(\tau) = \mathcal{T} \sum_{n=0}^{\infty} \frac{(-1)^n}{n!} \int_0^\tau d\tau_1 \int_0^\tau d\tau_2 \dots \int_0^\tau d\tau_n H_V(\tau_1) H_V(\tau_2) \dots H_V(\tau_n). \quad (5.26)$$

² \mathcal{T} orders all operators from right to left in ascending time, if an odd number of fermionic creation or annihilation operators needs to be exchanged multiply by (-1) .

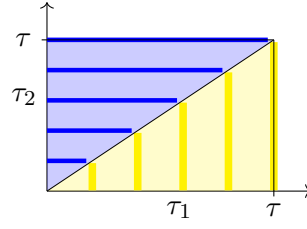


Figure 5.2: Extension of integration area.

S-matrix

Eq.(5.26) is just the Taylor series of the exponential (operator valued) function, which we can write as

$$S(\tau) = \mathcal{T} e^{-\int_0^\tau d\tau' H_V(\tau')} . \quad (5.27)$$

This perturbative series proves Eq. (5.17). It is also called the *Dyson series*, not to be confused with the *Dyson equation* from Chapter 4.

□

5.1.2 Perturbative series of Green's function

Now that we derived the perturbative series of the S-Matrix we continue by using our results to derive the Green's function of Eq.(5.4)³. We have to consider the two cases when $\tau > 0$ and $\tau < 0$. For $\tau > 0$

$$G(\vec{k}, \tau > 0) \equiv -\langle c_{\vec{k}}^H(\tau) c_{\vec{k}}^\dagger(0) \rangle. \quad (5.28)$$

To calculate the expectation value we, in principle, have to consider the cases when $T > 0$ and $T = 0$ (see (3.3))

$$\langle c_{\vec{k}}^H(\tau) c_{\vec{k}}^\dagger(0) \rangle = \begin{cases} \text{Tr} \frac{e^{-\beta H}}{Z} c_{\vec{k}}^H(\tau) c_{\vec{k}}^\dagger(0) & T > 0 \\ \langle GS | c_{\vec{k}}^H(\tau) c_{\vec{k}}^\dagger(0) | GS \rangle & T = 0 \end{cases}. \quad (5.29)$$

³The annihilation operator shall be marked in this chapter with an H for Heisenberg picture, i.e., $c_{\vec{k}}^H(\tau)$. This $c_{\vec{k}}^H(\tau)$ enters in the definition of the Green's function, not $c_{\vec{k}}(\tau)$ of the interaction picture. Note that $c_{\vec{k}}^\dagger(0)$ is independent of the Heisenberg or interaction (or Schrödinger) picture.

However, the case $T = 0$ can also be obtained from the former taking the limit $T \rightarrow 0$, Hence let us here only consider the case $T > 0$. For the Green's function we get

$$G(\vec{k}, \tau > 0) = -\frac{1}{Z} \text{Tr} \underbrace{e^{-\beta H}}_{e^{-\beta H_0} S(\beta)} \underbrace{e^{H\tau}}_{S^{-1}(\tau) e^{H_0 \tau}} c_{\vec{k}}(0) \underbrace{e^{-H\tau}}_{e^{-H_0 \tau} S(\tau)} c_{\vec{k}}^\dagger(0) \quad (5.30)$$

$$= -\frac{1}{Z} \text{Tr} e^{-\beta H_0} \underbrace{S(\beta) S^{-1}(\tau)}_{S(\beta, \tau)} \underbrace{e^{H_0 \tau} c_{\vec{k}}(0) e^{-H_0 \tau}}_{c_{\vec{k}}(\tau)} S(\tau) c_{\vec{k}}^\dagger(0) \quad (5.31)$$

$$= -\frac{\text{Tr} e^{-\beta H_0} \mathcal{T} c_{\vec{k}}(\tau) c_{\vec{k}}^\dagger(0) S(\beta)}{\text{Tr} e^{-\beta H_0} S(\beta)}. \quad (5.32)$$

As the interaction part, H_V , of the Hamiltonian involves an even number of creation and annihilation operators, the S -Matrix $S(\tau)$ can be commuted with the annihilation operator in the interaction representation, without incurring a minus sign, when the time-ordering operator is present. The above holds (without proof) for $\tau < 0$. Altogether this can be rewritten as

$$G(\vec{k}, \tau) = -\frac{\langle \mathcal{T} c_{\vec{k}}(\tau) c_{\vec{k}}^\dagger(0) S(\beta) \rangle_0}{\langle S(\beta) \rangle_0}, \quad (5.33)$$

where $\langle \dots \rangle_0$ now denotes the *non-interacting* thermal expectation value

$$\langle \dots \rangle_0 = \frac{\text{Tr} e^{-\beta H_0} \dots}{\text{Tr} e^{-\beta H_0}}. \quad (5.34)$$

Next, we make use of our derived series of the S -Matrix (5.26) and insert that into (5.33) to derive the perturbative series of the Green's function

$$G(\vec{k}, \tau) = -\frac{1}{\langle S(\beta) \rangle_0} \sum_{n=0}^{\infty} \frac{(-1)^n}{n!} \int_0^\beta d\tau_1 \dots \int_0^\beta d\tau_n \times \langle \mathcal{T} c_{\vec{k}}(\tau) c_{\vec{k}}^\dagger(0) H_V(\tau_1) \dots H_V(\tau_n) \rangle_0. \quad (5.35)$$

Each term is now much simpler, since we have simplified the interacting problem to a sum of non-interacting problems. The price we pay is that we now have to calculate a whole sum, and the remainder of this chapter will deal on how to evaluate this sum.

5.2 Wick's theorem

A relation we need to prove before we proceed with Wick's theorem is

$$c_{\vec{k}}^\dagger(\tau) = e^{H_0 \tau} c_{\vec{k}}^\dagger(0) e^{-H_0 \tau} = e^{\epsilon_{\vec{k}} \tau} c_{\vec{k}}^\dagger, \quad (5.36)$$

which holds because the time-propagation in Eq.(5.36) is with respect to the non-interacting Hamiltonian.

Proof. We prove the operator identity Eq.(5.36) in a complete basis set, the occupation number basis $\{|n_{\vec{k}_1} n_{\vec{k}_2}, \dots\rangle = \dots (c_{\vec{k}_2}^\dagger)^{n_{\vec{k}_2}} (c_{\vec{k}_1}^\dagger)^{n_{\vec{k}_1}} |0\rangle\}$. Acting with $c_k^\dagger(\tau)$ on such a basis state yields

$$c_k^\dagger(\tau) |n_{\vec{k}_1} n_{\vec{k}_2} \dots n_{\vec{k}} \dots\rangle \equiv e^{H_0\tau} c_k^\dagger e^{-H_0\tau} |n_{\vec{k}_1} n_{\vec{k}_2} \dots n_{\vec{k}} \dots\rangle \quad (5.37)$$

$$= e^{H_0\tau} c_k^\dagger e^{-\tau \sum_{k_i} \epsilon_{k_i} n_{k_i}} |n_{\vec{k}_1} n_{\vec{k}_2} \dots n_{\vec{k}} \dots\rangle \quad (5.38)$$

$$= e^{H_0\tau} e^{-\tau \sum_{k_i} \epsilon_{k_i} n_{k_i}} c_k^\dagger |n_{\vec{k}_1} n_{\vec{k}_2} \dots n_{\vec{k}} \dots\rangle \quad (5.39)$$

$$= e^{H_0\tau} e^{-\tau \sum_{k_i} \epsilon_{k_i} n_{k_i}} \sqrt{n_k + 1} |n_{\vec{k}_1} n_{\vec{k}_2} \dots (n_{\vec{k}} + 1) \dots\rangle \quad (5.40)$$

$$= e^{\tau \sum_{k_i} \epsilon_{k_i} n_{k_i} + \epsilon_k \tau} e^{-\tau \sum_{k_i} \epsilon_{k_i} n_{k_i}} \sqrt{n_k + 1} |n_{\vec{k}_1} n_{\vec{k}_2} \dots (n_{\vec{k}} + 1) \dots\rangle \quad (5.41)$$

$$= e^{\tau \epsilon_k} \sqrt{n_k + 1} |n_{\vec{k}_1} n_{\vec{k}_2} \dots (n_{\vec{k}} + 1) \dots\rangle \quad (5.42)$$

$$= e^{\epsilon_k \tau} c_k^\dagger |n_{\vec{k}_1} n_{\vec{k}_2} \dots n_{\vec{k}} \dots\rangle. \quad (5.43)$$

As the occupation number basis constitutes a full basis of the Fock space this proves Eq.(5.36). \square

A corresponding relation holds for the annihilation operator:

$$c_k(\tau) = e^{-\epsilon_k \tau} c_k. \quad (5.44)$$

Therefore, the time-evolution of the creation and annihilation operators in the interaction picture and the non-interacting eigenbasis are just numbers. With that in mind we may now proceed. Before stating the result for (5.35) we start with a simpler example for understanding Wick's theorem. In Eq.. 5.35, we need to calculate expectation values such as

$$\left\langle \mathcal{T} c_{\vec{k}_1}(\tau_1) c_{\vec{k}_2}(\tau_2) c_{\vec{k}'_1}^\dagger(\tau'_1) c_{\vec{k}'_2}^\dagger(\tau'_2) \right\rangle_0 \quad (5.45)$$

with $k_1 \neq k_2$. Without restriction of generality we can take the trace in the occupation number basis. Here $c_{\vec{k}'_1}^\dagger(\tau'_1)$, adds a particle with momentum \vec{k}'_1 and multiplies a factor $e^{\epsilon_{\vec{k}'_1} \tau'_1}$. That is, we get another occupation number state with one electron more. At the end, we however have to come back to the original occupation number state of the trace. This means any particle at momentum \vec{k}'_1 added, also needs to be removed by an annihilation operator. We have two possibilities how to combine the annihilation and creation operators

$$\left\langle \mathcal{T} c_{\vec{k}_1}(\tau_1) c_{\vec{k}_2}(\tau_2) c_{\vec{k}'_1}^\dagger(\tau'_1) c_{\vec{k}'_2}^\dagger(\tau'_2) \right\rangle_0$$

This becomes for the red contribution assuming⁴ $\vec{k}'_1 = \vec{k}_1 \neq \vec{k}_2 = \vec{k}'_2$

$$\begin{aligned}
 &= \left\langle \mathcal{T} c_{\vec{k}_1}(\tau_1) c_{\vec{k}_2}(\tau_2) c_{\vec{k}'_1}^\dagger(\tau'_1) c_{\vec{k}'_2}^\dagger(\tau'_2) \right\rangle_0 \\
 &= \mp \left\langle \mathcal{T} c_{\vec{k}_1}(\tau_1) c_{\vec{k}'_1}^\dagger(\tau'_1) c_{\vec{k}_2}(\tau_2) c_{\vec{k}'_2}^\dagger(\tau'_2) \right\rangle_0 \\
 &= \mp \delta_{\vec{k}_1 \vec{k}'_1} \delta_{\vec{k}_2 \vec{k}'_2} \left\langle \mathcal{T} c_{\vec{k}_1}(\tau_1) c_{\vec{k}_1}^\dagger(\tau'_1) c_{\vec{k}_2}(\tau_2) c_{\vec{k}_2}^\dagger(\tau'_2) \right\rangle_0;
 \end{aligned}$$

Here, we can simply exchange two fermionic/bosonic operators if $\vec{k}_1 \neq \vec{k}_2$ as the Wick time ordering operator will anyway arrange them back. But we need one exchange less or more, hence the minus sign for fermions. For the blue contribution assuming $\vec{k}'_2 = \vec{k}_1 \neq \vec{k}_2 = \vec{k}'_1$, we get

$$\begin{aligned}
 &= \left\langle \mathcal{T} c_{\vec{k}_1}(\tau_1) c_{\vec{k}_2}(\tau_2) c_{\vec{k}'_1}^\dagger(\tau'_1) c_{\vec{k}'_2}^\dagger(\tau'_2) \right\rangle_0 \\
 &= + \left\langle \mathcal{T} c_{\vec{k}_2}(\tau_2) c_{\vec{k}'_1}^\dagger(\tau'_1) c_{\vec{k}_1}(\tau_1) c_{\vec{k}'_2}^\dagger(\tau'_2) \right\rangle_0 \\
 &= + \delta_{\vec{k}'_1 \vec{k}_2} \delta_{\vec{k}_1 \vec{k}'_2} \left\langle \mathcal{T} c_{\vec{k}_2}(\tau_2) c_{\vec{k}_2}^\dagger(\tau'_1) c_{\vec{k}_1}(\tau_1) c_{\vec{k}_1}^\dagger(\tau'_2) \right\rangle_0.
 \end{aligned}$$

Altogether (5.45) is the sum of both contributions

$$\begin{aligned}
 \left\langle \mathcal{T} c_{\vec{k}_1}(\tau_1) c_{\vec{k}_2}(\tau_2) c_{\vec{k}'_1}^\dagger(\tau'_1) c_{\vec{k}'_2}^\dagger(\tau'_2) \right\rangle_0 &= \mp \delta_{\vec{k}_1 \vec{k}'_1} \delta_{\vec{k}_2 \vec{k}'_2} \left\langle \mathcal{T} c_{\vec{k}_1}(\tau_1) c_{\vec{k}_1}^\dagger(\tau'_1) c_{\vec{k}_2}(\tau_2) c_{\vec{k}_2}^\dagger(\tau'_2) \right\rangle_0 \\
 &\quad + \delta_{\vec{k}'_1 \vec{k}_2} \delta_{\vec{k}_1 \vec{k}'_2} \left\langle \mathcal{T} c_{\vec{k}_2}(\tau_2) c_{\vec{k}_2}^\dagger(\tau'_1) c_{\vec{k}_1}(\tau_1) c_{\vec{k}_1}^\dagger(\tau'_2) \right\rangle_0. \quad (5.46)
 \end{aligned}$$

We can rewrite this in terms of Green's functions

$$\begin{aligned}
 \left\langle \mathcal{T} c_{\vec{k}_1}(\tau_1) c_{\vec{k}_2}(\tau_2) c_{\vec{k}'_1}^\dagger(\tau'_1) c_{\vec{k}'_2}^\dagger(\tau'_2) \right\rangle_0 &= \mp \delta_{\vec{k}_1 \vec{k}'_1} \delta_{\vec{k}_2 \vec{k}'_2} \left\langle \mathcal{T} c_{\vec{k}_1}(\tau_1) c_{\vec{k}_1}^\dagger(\tau'_1) \right\rangle_0 \left\langle \mathcal{T} c_{\vec{k}_2}(\tau_2) c_{\vec{k}_2}^\dagger(\tau'_2) \right\rangle_0 \\
 &\quad + \delta_{\vec{k}'_1 \vec{k}_2} \delta_{\vec{k}_1 \vec{k}'_2} \left\langle \mathcal{T} c_{\vec{k}_2}(\tau_2) c_{\vec{k}_2}^\dagger(\tau'_1) \right\rangle_0 \left\langle \mathcal{T} c_{\vec{k}_1}(\tau_1) c_{\vec{k}_1}^\dagger(\tau'_2) \right\rangle_0 \quad (5.47)
 \end{aligned}$$

$$\begin{aligned}
 &= \delta_{\vec{k}_1 \vec{k}'_1} \delta_{\vec{k}_2 \vec{k}'_2} G_0(\vec{k}_1, \tau_1 - \tau'_1) G_0(\vec{k}_2, \tau_2 - \tau'_2) \\
 &\quad + \delta_{\vec{k}_1 \vec{k}'_2} \delta_{\vec{k}_2 \vec{k}'_1} G_0(\vec{k}_2, \tau_2 - \tau'_1) G_0(\vec{k}_1, \tau_1 - \tau'_2), \quad (5.48)
 \end{aligned}$$

where we have used $\left\langle A_{\vec{k}} B_{\vec{k}'} \right\rangle_0 = \left\langle A_{\vec{k}} \right\rangle_0 \left\langle B_{\vec{k}'} \right\rangle_0$ as the occupations for different momenta $\vec{k}' \neq \vec{k}$ are completely unrelated (uncorrelated) for the non-interacting problem, and further the

⁴The case $\vec{k}'_1 = \vec{k}_1 = \vec{k}_2 = \vec{k}'_2$ is of measure zero for the momentum integration; it can also be proven explicitly but requires a bit more work, as the (anti)commutator then yields a 1, which compensates for the (two) Green's function terms we get at the end.

WICK's THEOREM

In general Wick's theorem means there are $n!$ combinations (contractions) of how to pair n creation and n annihilation operators

$$\left\langle \mathcal{T} c_{\vec{k}_1}(\tau_1) c_{\vec{k}_2}(\tau_2) \dots c_{\vec{k}_1'}^\dagger(\tau_1') c_{\vec{k}_2'}^\dagger(\tau_2') \dots \right\rangle_0 \quad (5.49)$$

$$= \delta_{\vec{k}_1 \vec{k}_1'} \delta_{\vec{k}_2 \vec{k}_2'} \dots G_0(\vec{k}_1, \tau_1 - \tau_1') G_0(\vec{k}_2, \tau_2 - \tau_2') \dots \\ + \delta_{\vec{k}_1 \vec{k}_2'} \delta_{\vec{k}_2 \vec{k}_1'} \dots G_0(\vec{k}_2, \tau_2 - \tau_1') G_0(\vec{k}_1, \tau_1 - \tau_2') \dots \quad (5.50)$$

We need to consider all the possible contractions and each contraction can be written as a non-interacting Green's function $G_0(k_i, \tau_i - \tau_i') = \langle \dots \rangle_0$ which is the main statement of Wick's theorem. Using fermionic operators we need to be careful with the sign since we get a plus for an even or a minus for an odd number of exchanges. Plugging (5.4) into (5.35) yields

$$G(\vec{k}, \tau) = -\frac{1}{\langle S(\beta) \rangle_0} \sum_{n=0}^{\infty} \frac{(-1)^n}{n!} \frac{1}{(2\pi)^9} \int d^3 \vec{k}' \int d^3 \vec{k}'' \int d^3 \vec{q} \int_0^\beta d\tau_1 \dots \int_0^\beta d\tau_n \times \\ \times \left\langle \mathcal{T} c_{\vec{k}}(\tau) c_{\vec{k}}^\dagger(0) H_V(\tau_1) \dots c_{\vec{k}''+\vec{q}}^\dagger(\tau_n) c_{\vec{k}'-\vec{q}}^\dagger(\tau_n) \frac{V_{\vec{q}}}{2} c_{\vec{k}'}(\tau_n) c_{\vec{k}''}(\tau_n) \right\rangle_0. \quad (5.51)$$

Of course we also need to consider here the contractions of the $H_V(\tau_1) \dots$ terms which need to be expressed in terms of creation and annihilation operators, too, are not shown. Although (5.51) is a simplified expression, but it is still quite tedious to calculate. In the next chapter we will introduce the famous Feynman diagrams which will help us to visualize, to keep track and to calculate such a huge number of contractions.

Before doing that, let us just show how the time-dependencies of the interacting Hamiltonian transfers to that of the creation and annihilation operators in Eq. 5.52. In the Schrödinger picture the interacting Hamiltonian can be written as

$$H_V(\tau_1) = e^{H_0 \tau_1} H_V e^{-H_0 \tau_1}. \quad (5.52)$$

This has to agree with

$$H_V(\tau_1) = \frac{1}{(2\pi)^9} \int d\vec{k} \int d\vec{k}' \int d^3\vec{q} c_{\vec{k}+\vec{q}}^\dagger(\tau_1) c_{\vec{k}'-\vec{q}}^\dagger(\tau_1) \frac{V_{\vec{q}}}{2} c_{\vec{k}'}(\tau_1) c_{\vec{k}}(\tau_1) \quad (5.53)$$

$$= \frac{1}{(2\pi)^9} \frac{V_{\vec{q}}}{2} \int d\vec{k} \int d\vec{k}' \int d^3\vec{q} c_{\vec{k}+\vec{q}}^\dagger(\tau_1) c_{\vec{k}'-\vec{q}}^\dagger(\tau_1) c_{\vec{k}'}(\tau_1) c_{\vec{k}}(\tau_1) \quad (5.54)$$

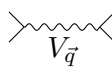
$$= \frac{1}{(2\pi)^9} \frac{V_{\vec{q}}}{2} \int d\vec{k} \int d\vec{k}' \int d^3\vec{q} \times \quad (5.55)$$

$$\times e^{H_0\tau_1} c_{\vec{k}+\vec{q}}^\dagger \underbrace{e^{-H_0\tau_1} e^{H_0\tau_1}}_{\mathbb{1}} c_{\vec{k}'-\vec{q}}^\dagger \underbrace{e^{-H_0\tau_1} e^{H_0\tau_1}}_{\mathbb{1}} c_{\vec{k}'} \underbrace{e^{-H_0\tau_1} e^{H_0\tau_1}}_{\mathbb{1}} c_{\vec{k}} e^{-H_0\tau_1}$$

$$= e^{H_0\tau_1} \underbrace{\frac{1}{(2\pi)^9} \frac{V_{\vec{q}}}{2} \int d\vec{k} \int d\vec{k}' \int d^3\vec{q} c_{\vec{k}+\vec{q}}^\dagger c_{\vec{k}'-\vec{q}}^\dagger c_{\vec{k}'} c_{\vec{k}}}_{H_V} e^{-H_0\tau_1} \quad (5.56)$$

$$= e^{H_0\tau_1} H_V e^{-H_0\tau_1}. \quad (5.57)$$

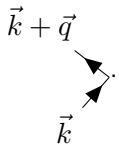
5.3 Feynman diagrams and linked cluster theorem

In Chapter 4 we already used a Feynman diagram to visualize the scattering near the fermi surface and at the beginning of this chapter we used it in Fig.5.1 to visualize Eq.(5.4). Now we are ready to study Feynman diagrams in more detail and will learn a powerful technique to keep track of the huge number of contractions of Eq.(5.52). Let us begin with the basics. The term $V(\vec{q})$ corresponds to the diagram  and describes the interaction between two particles. We can consider it as a boson

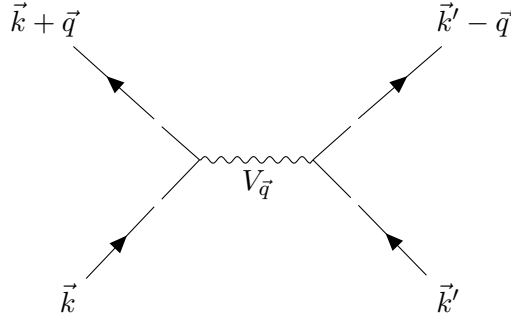
of the electromagnetic interaction (i.e. a photon). However in solid state physics, we can consider the Coulomb interaction to be instantaneous. That is we do not need to consider the boson propagation here. The two *legs* at each end of the wiggled line denotes that the interaction has two incoming and two outgoing particles. The Green's function $G(\vec{k}, \tau - \tau')$ corresponds to $c_{\vec{k}}^\dagger(\tau) \xrightarrow{\vec{k}} c_{\vec{k}}(\tau')$ and

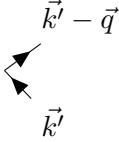
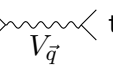
describes in general the propagation of a fermionic or bosonic particle if $\tau' > \tau$ and a hole if $\tau' < \tau$. In our case we read it as creating a particle with momentum \vec{k} at time τ and annihilating it at a later time τ' (vice versa for a hole). Note that the arrow always points from the creation operator ($c_{\vec{k}}^\dagger$) towards the annihilation operator ($c_{\vec{k}}$). Some books specify the evolution in time by reading the diagram from left to right, we do not do so here.

Let us once again have a look at Fig.5.1 and compare it with Fig.5.3 where we have illustrated the *legs* as well. We may now interpret the propagator on the left as the contribution of $c_{\vec{k}+\vec{q}}^\dagger(\tau') c_{\vec{k}}(\tau) \rightarrow$



The momentum q transferred needs to be compensated on the right hand side, i.e.,

Figure 5.3: Feynman diagram of particles with momenta \vec{k} and \vec{k}'

the term $c_{\vec{k}'-\vec{q}}^\dagger(\tau')c_{\vec{k}'}(\tau) \rightarrow$ . The term $V(\vec{q}) \rightarrow$  tells us that this exchange of momentum occurred via the Coulomb interaction with momentum transfer \vec{q} . So if we collect the contributions we get

$$c_{\vec{k}+\vec{q}}^\dagger(\tau')c_{\vec{k}}(\tau)\frac{V(\vec{q})}{2}c_{\vec{k}'-\vec{q}}^\dagger(\tau')c_{\vec{k}'}(\tau) = c_{\vec{k}+\vec{q}}^\dagger(\tau')c_{\vec{k}'-\vec{q}}^\dagger(\tau')\frac{V(\vec{q})}{2}c_{\vec{k}}(\tau)c_{\vec{k}'}(\tau). \quad (5.58)$$

The equality is true because of the commutation relation of the operators (assuming $\vec{k} \neq \vec{k}' - \vec{q}$). Let us now consider the first order term in the numerator of (5.35)

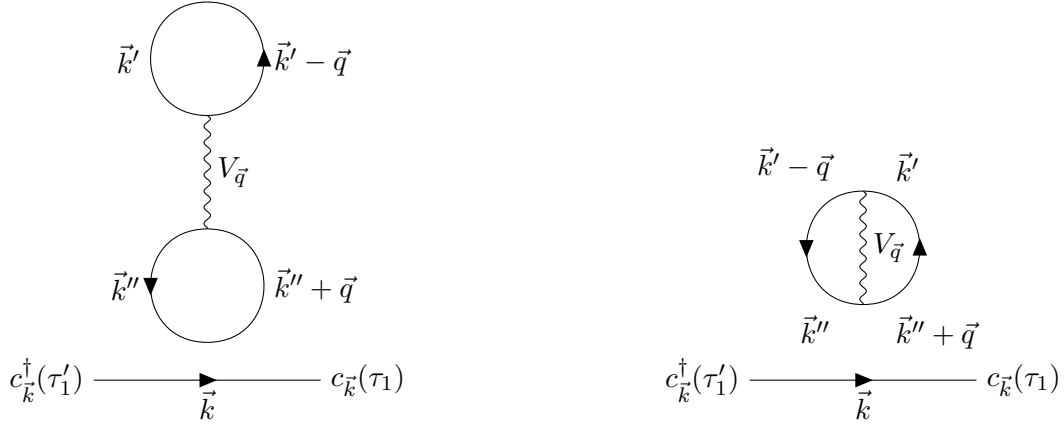
$$\begin{aligned} & (-1) \frac{1}{(2\pi)^9} \underbrace{\int d^3\vec{k}' \int d^3\vec{k}'' \int d^3\vec{q} \int_0^\beta d\tau (-1)^1}_{\text{from } S(\beta) = \mathcal{T} e^{-\int_0^\beta d\tau H_V(\tau)}} \times \\ & \times \left\langle \mathcal{T} c_{\vec{k}}(\tau_1) c_{\vec{k}}^\dagger(\tau_1') c_{\vec{k}''+\vec{q}}^\dagger(\tau) c_{\vec{k}'-\vec{q}}^\dagger(\tau) \frac{V_{\vec{q}}}{2} c_{\vec{k}'}(\tau) c_{\vec{k}''}(\tau) \right\rangle_0 \end{aligned} \quad (5.59)$$

Wick's Theorem gives us the following contractions

$$\begin{aligned} & (-1) \frac{1}{(2\pi)^9} \int d^3\vec{k}' \int d^3\vec{k}'' \int d^3\vec{q} \int_0^\beta d\tau (-1)^1 \times \\ & \times \left\langle \mathcal{T} c_{\vec{k}}(\tau_1) c_{\vec{k}}^\dagger(\tau_1') c_{\vec{k}''+\vec{q}}^\dagger(\tau) c_{\vec{k}'-\vec{q}}^\dagger(\tau) \frac{V_{\vec{q}}}{2} c_{\vec{k}'}(\tau) c_{\vec{k}''}(\tau) \right\rangle_0. \end{aligned} \quad (5.60)$$

If we read the altogether six contractions carefully⁵, we will notice that the first contraction (the solid green line) just propagates a particle with momentum \vec{k} from time τ_1 to τ_1' . The result is just our

⁵Comment: If this is too messy for you, you can just go to Eq.(5.61), Eq.(5.68) and Eq.(5.69), where the contributions are singled out and therefore better to read.



(a) Feynman diagram of the contribution for the solid green line.

(b) Feynman diagram of the contributions for the dotted green line.

Figure 5.4: Feynman diagrams of the two green contributions of Eq.(5.61)

well known Green's function $G(\vec{k}, \tau_1 - \tau_1') \rightarrow c_k^\dagger(\tau_1) \xrightarrow{\vec{k}} c_k(\tau_1)$. The other terms of the green

contraction are all at the same time, they are entirely internal in H_V . This means, diagrammatically (see Fig.5.4a), if we connect the Green's function lines with interaction lines the contractions from H_V are connected and there are no incoming or outgoing momenta. As we can further see, the two H_V contractions are disconnected from the first contraction which yields, as already discussed, $G(\vec{k}, \tau_1 - \tau_1')$. For the dotted green line we get again the disconnected Green's function $G(\vec{k}, \tau_1 - \tau_1')$:

$c_k^\dagger(\tau_1) \xrightarrow{\vec{k}} c_k(\tau_1)$ and together with the remaining terms the contraction of Fig.5.4b. Since the green contractions are the only terms that are disconnected, because they are the only one where $c_k^\dagger(\tau_1)c_k(\tau_1')$ is isolated from the term that comes from $H_V(\tau)$, we can write the green contribution as

$$\begin{aligned}
 & \left\langle \mathcal{T} c_{\vec{k}}(\tau_1) c_{\vec{k}}^\dagger(\tau_1') \right\rangle_0 = \left\langle \mathcal{T} c_{\vec{k}}(\tau_1) c_{\vec{k}}^\dagger(\tau_1') \right\rangle_0 + \left\langle \mathcal{T} c_{\vec{k}''+\vec{q}}^\dagger(\tau) c_{\vec{k}'-\vec{q}}^\dagger(\tau) \frac{V_{\vec{q}}}{2} c_{\vec{k}'}(\tau) c_{\vec{k}''}(\tau) \right\rangle_0 = \\
 & = \left\langle \mathcal{T} c_{\vec{k}}(\tau_1) c_{\vec{k}}^\dagger(\tau_1') \right\rangle_0 \left\langle \mathcal{T} c_{\vec{k}''+\vec{q}}^\dagger(\tau) c_{\vec{k}'-\vec{q}}^\dagger(\tau) \frac{V_{\vec{q}}}{2} c_{\vec{k}'}(\tau) c_{\vec{k}''}(\tau) \right\rangle_0
 \end{aligned} \tag{5.61}$$

where we used $\langle A_{\vec{k}} B_{\vec{k}'} \rangle_0 = \langle A_{\vec{k}} \rangle_0 \langle B_{\vec{k}'} \rangle_0$. The second term is equal to the first order expectation value of the denominator of (5.35) and as a result they cancel. Diagrammatically that means that only connected contributions remain if we consider nominator and denominator together. We can

visualize this cancellation as follows

$$G = \frac{\begin{array}{c} \text{---} + \frac{1}{2} \text{---} \text{---} \text{---} + \text{---} \text{---} \text{---} + \dots + \frac{1}{2} \text{---} \text{---} \text{---} + \frac{1}{2} \text{---} \text{---} \text{---} + \dots \end{array}}{1 + \frac{1}{2} \text{---} \text{---} \text{---} + \frac{1}{2} \text{---} \text{---} \text{---} + \dots} \quad (5.62)$$

$$= \frac{\left(\text{---} + \text{---} \text{---} \text{---} + \text{---} \text{---} \text{---} + \dots \right) \left(1 + \frac{1}{2} \text{---} \text{---} \text{---} + \frac{1}{2} \text{---} \text{---} \text{---} + \dots \right)}{1 + \frac{1}{2} \text{---} \text{---} \text{---} + \frac{1}{2} \text{---} \text{---} \text{---} + \dots} \quad (5.63)$$

$$= \text{---} + \text{---} \text{---} \text{---} + \text{---} \text{---} \text{---} + \dots \quad (5.64)$$

Please note that the factor inside the second parentheses of (5.63) can only be extracted if we also consider higher order terms in the interaction (which we have not analyzed here). The fact that only the connected parts survive and with a weight factor of one is called the **Linked cluster theorem**. It has only been illustrated here, but can be proven in general⁶. The other two (first order) terms of Eq.(5.64), the red and blue ones, are the so called *Hartree* and *Fock* terms. These are the (connected) red and blue contractions of Eq.(5.59) and will be evaluated in the next two sections.

5.3.1 Hartree term

For the evaluation of the Hartree term

$$(-1) \frac{1}{(2\pi)^9} \int d^3 \vec{k}' \int d^3 \vec{k}'' \int d^3 \vec{q} \int_0^\beta d\tau (-1)^1 \times$$

$$\times \left\langle \mathcal{T} c_{\vec{k}}(\tau_1) c_{\vec{k}}^\dagger(\tau_1') c_{\vec{k}''+\vec{q}}^\dagger(\tau) c_{\vec{k}'-\vec{q}}^\dagger(\tau) \frac{V_{\vec{q}}}{2} c_{\vec{k}'}(\tau) c_{\vec{k}''}(\tau) \right\rangle_0. \quad (5.65)$$

we can draw the diagram Fig.5.5. Because of momentum conservation and the fact that the dotted

⁶in this course we will do this in the exercises.

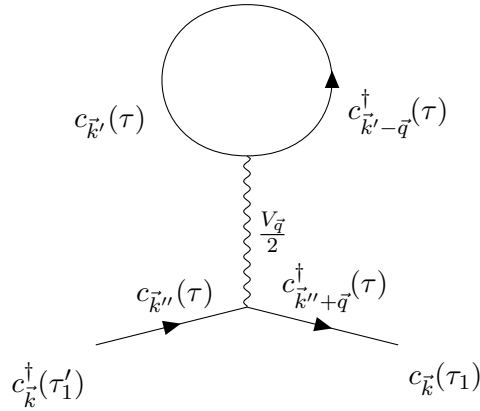


Figure 5.5: Hartree term: We start (compare with Eq.(5.65); let us consider for the physical interpretation $\tau'_1 < \tau < \tau_1$) by creating a particle with momentum \vec{k} at the left. At the interaction (wiggled line) this particle will be scattered from \vec{k}'' to $\vec{k}'' + \vec{q}$ described by an annihilation operator $c_{\vec{k}''}(\tau)$ and a creation operator $c_{\vec{k}''+\vec{q}}^\dagger(\tau)$. The interaction couples this particle to another particle scattering from \vec{k}' ($c_{\vec{k}'}(\tau)$) to $\vec{k}' - \vec{q}$ ($c_{\vec{k}'-\vec{q}}^\dagger(\tau)$). This gives us for the diagram an internal line (Green's function) that occurs at the same time, i.e. $c_{\vec{k}'-\vec{q}}^\dagger(\tau)$ and $c_{\vec{k}'}(\tau)$; and since the Green's function is diagonal in momentum: $\vec{k}' = \vec{k}' - \vec{q} \Rightarrow \vec{q} = 0$. For the last term, the term with the latest time, we connected $c_{\vec{k}}(\tau_1)$ with $c_{\vec{k}''+\vec{q}}^\dagger(\tau) \Rightarrow \vec{k}'' = \vec{k}$. If we compare the solid term carefully with the dotted term, we realize that both terms are equal, if we exchange $\vec{k}' \leftrightarrow \vec{k}''$. This means that we have the same diagram; mathematically this manifests itself in a factor 2.

This gives us the diagram illustrated in Fig.5.6. Momentum conservation and the correspondence of

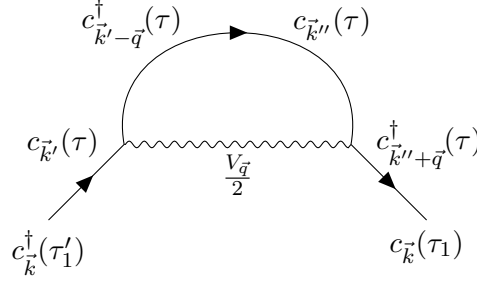


Figure 5.6: Fock term: We start (assuming $\tau'_1 < \tau < \tau_1$ as in Fig.5.5) at the left creating a particle with momentum \vec{k} . At the interaction (wiggled line) this particle will be scattered from \vec{k}' to $\vec{k}' - \vec{q}$ described by an $c_{\vec{k}'}(\tau)$ and a creation operator $c_{\vec{k}'-\vec{q}}^\dagger(\tau)$. The interaction couples this particle to another particle scattering from \vec{k}'' ($c_{\vec{k}''}(\tau)$) to $\vec{k}'' + \vec{q}$ ($c_{\vec{k}''+\vec{q}}^\dagger(\tau)$). This gives us for the diagram an internal line (Green's function) that occurs at the same time, i.e., $c_{\vec{k}'-\vec{q}}^\dagger(\tau)$ and $c_{\vec{k}''}(\tau)$ at time 0^- . Thus $\vec{k}'' = \vec{k}' - \vec{q}$. For the last term we connected $c_{\vec{k}''+\vec{q}}^\dagger(\tau)$ with $c_{\vec{k}}(\tau_1)$, which gives $\vec{k}'' + \vec{q} = \vec{k}$. This diagram gives the same contribution as when we exchange $\vec{k}' \leftrightarrow \vec{k}''$ and $\vec{q} \leftrightarrow -\vec{q}$ and therefore we get again an additional factor of 2, corresponding to the solid and dashed blue lines in (5.69).

the dotted with the solid term in Eq.(5.61) gives

$$\begin{aligned}
 &= \int_0^\beta d\tau \int \frac{d^3\vec{q}}{(2\pi)^3} 2 \times \\
 &\quad \times \frac{V_{\vec{q}}}{2} \left\langle \mathcal{T} c_{\vec{k}}(\tau_1) c_{\vec{k}}^\dagger(\tau) \right\rangle_0 \left\langle \mathcal{T} c_{\vec{k}+\vec{q}}(\tau) c_{\vec{k}+\vec{q}}^\dagger(\tau) \right\rangle_0 \left\langle \mathcal{T} c_{\vec{k}}(\tau) c_{\vec{k}}^\dagger(\tau'_1) \right\rangle_0
 \end{aligned} \tag{5.69}$$

$$\begin{aligned}
 &= - \int_0^\beta d\tau \int \frac{d^3\vec{q}}{(2\pi)^3} V_{\vec{q}} G_0(\vec{k}, \tau_1 - \tau) \underbrace{G_0(\vec{k} + \vec{q}, \tau - \tau)}_{=G_0(\vec{k}+\vec{q}, 0^-)} G_0(\vec{k}, \tau - \tau'_1)
 \end{aligned} \tag{5.70}$$

So far we have covered the contributions of our Green's functions to first order: The Hartree and Fock term.

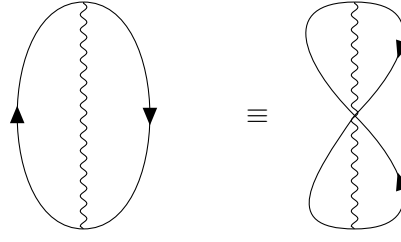


Figure 5.7: Example for topologically equivalent diagrams.

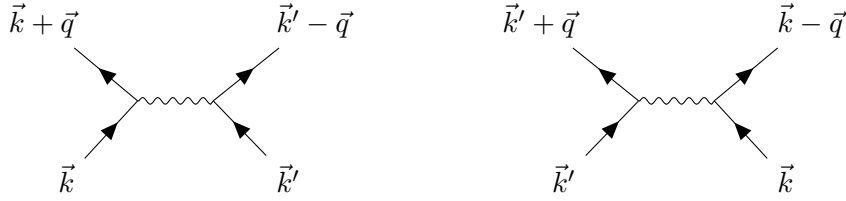


Figure 5.8: Topologically equivalent diagrams - momenta exchanged.

5.3.3 Topology

Let us get back to the equation for the Green's function we actually aim to calculate and which, with the linked cluster theorem, can be written as:

$$G(\vec{k}, \tau) = -\frac{1}{\langle S(\beta) \rangle_0} \sum_{n=0}^{\infty} \frac{(-1)^n}{n!} \int_0^\beta d\tau_1 \dots \int_0^\beta d\tau_n \times \langle \mathcal{T} c_{\vec{k}}(\tau) c_{\vec{k}}^\dagger(0) H_V(\tau_1) \dots H_V(\tau_n) \rangle_0 \quad (5.71)$$

$$= -\sum_{n=0}^{\infty} \frac{(-1)^n}{n!} \int_0^\beta d\tau_1 \dots \int_0^\beta d\tau_n \times \langle \mathcal{T} c_{\vec{k}}(\tau) c_{\vec{k}}^\dagger(0) H_V(\tau_1) \dots H_V(\tau_n) \rangle_{\text{connected}}. \quad (5.72)$$

For the Hartree and Fock term we have seen that the factor $\frac{1}{2}$ cancelled if we exchanged the *dummy* integration variable (e.g. exchanging $k \leftrightarrow k'$). This is one factor we get rid of, if we consider only *topological inequivalent* diagrams. *Topological equivalent* diagrams can be described as diagrams that can be transformed into each other by deformation (see Fig. 5.7) or transformed into each other without tearing or breaking them apart nor reconfiguring the particular connection between the interaction and the Green's function lines. Topological equivalent are also diagrams which merely differ by the naming of the internal summation indices such as $k \leftrightarrow k'$, illustrated in Fig. 5.8. For each interaction, we can exchange the left and right momenta, this factor of two cancels with the factor $\frac{1}{2}$ in the interaction, which we have introduced to start with since each interaction is counted twice. Another factor that we get rid of originates from the equivalence of exchanging the times of the different interactions (see the exchange of time in Fig. 5.9). This cancels the prefactor $\frac{1}{n!}$.

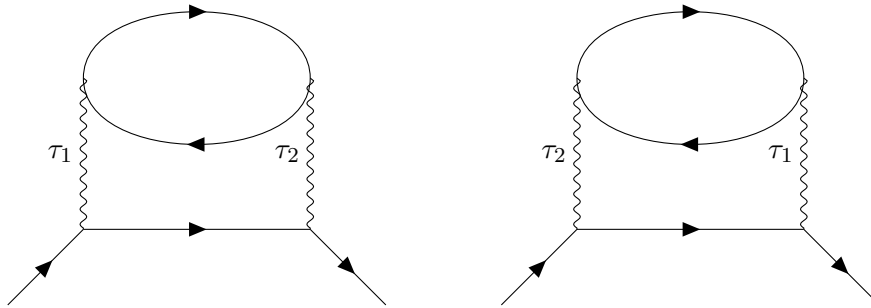


Figure 5.9: Example for topologically equivalent second order diagrams: interaction (times) exchanged).



Figure 5.10: Example for a bubble.

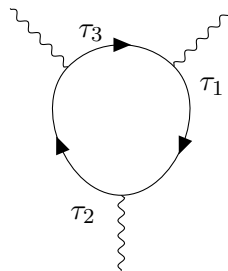


Figure 5.11: Example for a closed loop.

5.3.4 Feynman rules

Having covered the topological redundancies we are now able to gather the rules for the Feynman diagrams to draw and, eventually, to calculate the interacting Green's function $G(\vec{k}, \omega_\nu) \xrightarrow{\vec{k}}$ (notice the doubled line for the interacting Green's function as well as the representation in frequency space in this section). At the beginning of this subchapter we already discussed some basic ideas. In general, the rules can be summarized as follows:

1. Draw all topological inequivalent connected diagrams

For each order n in the interaction we draw n **wiggled (interaction) lines** $\xrightarrow{\vec{q}} V_{\vec{q}}$. Each interaction from the H_V has two annihilation and creation operator which eventually become non-interacting Green's functions. Each Feynman diagram has further an incoming and outgoing particle (a creation and annihilation operator from the definition of the Green's function that we calculate; in the last line of Eq.(5.72) the term $c_{\vec{k}}(\tau)c_{\vec{k}}^\dagger(0)$). So all together for each order n in the interaction, we get $2n + 1$ **non-interacting Green's function lines** $\xrightarrow{\vec{k}}$.

2. Mathematical evaluation

- Each $\xrightarrow{\vec{q}} V_{\vec{q}}$ gives a factor $V(\vec{q})$ or $V(\vec{q}, \omega)$ if we consider also frequency.
- Each $\xrightarrow{\vec{k}}$ gives a factor $G_0(\vec{k}, \omega_\nu) = \frac{1}{i\omega_\nu - \epsilon_{\vec{k}}}$.
- At each vertex **momentum and frequency are conserved** $\rightarrow \vec{q} \sim \begin{array}{c} \nearrow \vec{k}' \\ \searrow \vec{k} \end{array} \Rightarrow \vec{k}' = \vec{k} + \vec{q}$.
- For equal time Green's function we have to consider $\tau = 0^-$. For example, each bubble $\sim \begin{array}{c} \text{bubble} \end{array}$ gives a factor $n_0 = \frac{1}{(2\pi)^3} \int d^3k G_0(\vec{k}, 0^-)$ or $\frac{1}{(2\pi)^3} \int d^3k \frac{1}{\beta} \sum_\nu G_0(\vec{k}, i\omega_\nu) e^{-i\omega_\nu(0^-)}$ in frequency space.
- For the order n of our diagrams and the number of closed loops F (see Fig.5.11), we get further a sign $(-1)^n \cdot (\mp 1)^F$ (minus for fermions, plus for bosons). The minus sign for each closed loop F originates from the rearrangement of a loop of creation and annihilation operators (see lecture).
- We sum/integrate over each internal degree of freedom (corresponding to an internal line), therefore we get $\frac{1}{(2\pi)^3} \int d^3k, \frac{1}{\beta} \sum_{\nu=-\infty}^{\infty}$ or $\int_0^\beta d\tau$ in time representation.

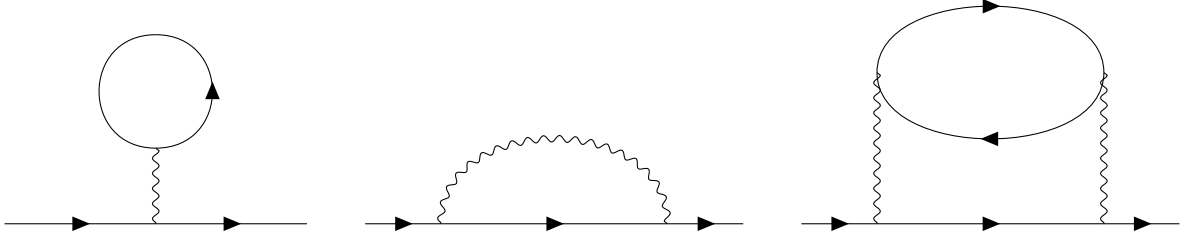


Figure 5.12: Example for irreducible diagrams.

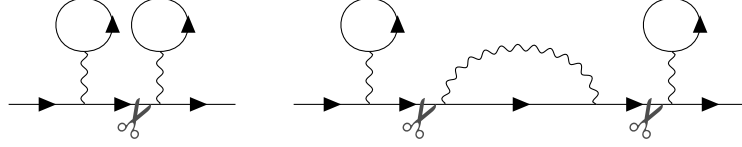


Figure 5.13: Example for reducible diagrams. The left diagram can be separated if we cut the second Green's function at the baseline. Same for the second diagram if we cut the second and/or fourth Green's function at the baseline.

We can also sum internally over all spins σ (with $\sigma = \uparrow, \downarrow$) or otherwise get an extra factor $(2s + 1)^F$. For example the Hartree term has thus a contribution in momentum-frequency space

$$(2s + 1) \left(\frac{1}{i\omega_n - \epsilon_{\vec{k}}} \right)^2 \frac{1}{(2\pi)^3} \int d^3k' \frac{1}{\beta} \sum_{n'} \frac{V(0, 0)}{i\omega_{n'} - \epsilon_{\vec{k}'}} e^{-i\omega_{n'} 0^-} \quad (5.73)$$

and the Fock term

$$(-1) \left(\frac{1}{i\omega_n - \epsilon_{\vec{k}}} \right)^2 \frac{1}{(2\pi)^3} \int d^3k' \frac{1}{\beta} \sum_{n'} \frac{V(\vec{k} - \vec{k}', \omega_n - \omega_{n'})}{i\omega_{n'} - \epsilon_{\vec{k}'}}. \quad (5.74)$$

5.4 Self-energy and Dyson equation

There is a way to further reduce the number of diagrams. To this end, let us define 1-particle irreducible diagrams as all diagrams that do not separate if we cut one Green's function line (see Fig. 5.12), and sum them up. These diagrams (without the incoming and outgoing Green's function leg) can be collected together in a quantity we discussed in the previous chapter, namely the self-energy $\Sigma(\vec{k}, \omega_\nu)$. The equivalence, we will see below. It helps us interpreting as well as simplifying our calculations due to the reduced number of diagrams. Reducible diagrams, on the other hand are diagrams that can be separated if cutting Green's function lines separates the diagram into two parts (see Fig. 5.13). From the irreducible self energy pieces, we get indeed **all** diagrams by connecting them with non-interacting Green's function lines. The resulting equation is called

the **DYSON-EQUATION**

$$\Rightarrow\Rightarrow = \rightarrow + \rightarrow \textcircled{\Sigma} \rightarrow + \rightarrow \textcircled{\Sigma} \text{ (scissor)} \textcircled{\Sigma} \rightarrow + \dots \quad (5.75)$$

$$= \rightarrow + \rightarrow \textcircled{\Sigma} \Rightarrow\Rightarrow, \quad (5.76)$$

The interacting Green's function $\Rightarrow\Rightarrow$ is also referred to as **dressed**. The scissor in Eq.(5.75) illustrates that it contains reducible diagrams. In Eq.(5.75) we see how these reducible diagrams are generated by connecting two Σ pieces by a Green's function. As we must not double count any diagram, the self-energy in turn may only contain all 1-particle irreducible diagrams. Mathematically, Eq.(5.75) can be formulated as

$$G(\vec{k}, \omega_\nu) = G_0(\vec{k}, \omega_\nu) + G_0(\vec{k}, \omega_\nu) \Sigma(\vec{k}, \omega_\nu) G(\vec{k}, \omega_\nu). \quad (5.77)$$

If we multiply this equation with $G^{-1}(\vec{k}, \omega_\nu)$ to the right and $G_0^{-1}(\vec{k}, \omega_\nu)$ to the left we get

$$\Rightarrow G_0^{-1}(\vec{k}, \omega_\nu) = G^{-1}(\vec{k}, \omega_\nu) + \Sigma(\vec{k}, \omega_\nu) \quad (5.78)$$

or written out

$$G(\vec{k}, \omega_\nu) = \frac{1}{i\omega_\nu - \epsilon_{\vec{k}} - \Sigma(\vec{k}, \omega_\nu)}, \quad (5.79)$$

which is exactly the equation we used in the previous chapter Eq.(4.12) for defining the self-energy.

5.5 Skeleton diagrams

There is one further reduction of the number of diagrams: The so called **skeleton diagrams**. We already learned the basic idea behind the 1-particle irreducible diagrams, that are contained in Σ and generate all diagrams, also reducible ones through the Dyson equation. Now we turn to diagrams where the connecting Green's function lines are the interacting (dressed) Green's functions $\Rightarrow\Rightarrow_{\vec{k}}$

instead of the non-interacting Green's function $\rightarrow_{\vec{k}}$. For the Hartree and Fock diagram this yields for the self-energy

$$\Sigma(\vec{k}, \omega_\nu) = \textcircled{\Sigma} = \text{Hartree diagram} + \text{Fock diagram} \quad (5.80)$$

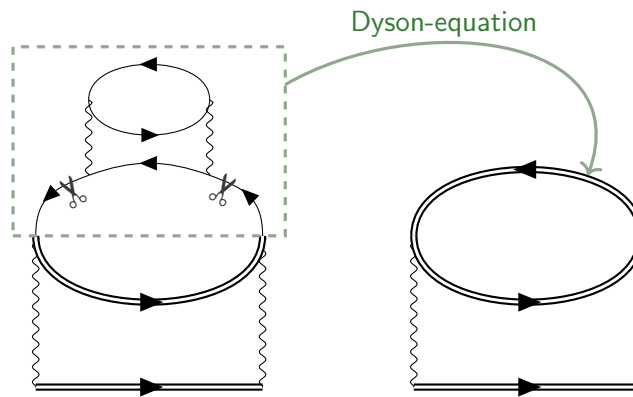
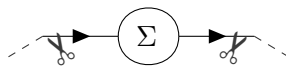


Figure 5.14: The diagram on the left transforms into the right one, when applying the Dyson-equation (see Eq.(7.23)). The Diagram on the right is called a skeleton diagram. From this and other 2-particle irreducible skeleton-diagrams, all diagrams can be generated by replacing \Rightarrow through \rightarrow using the Dyson-equation.

Let us emphasize again that the diagram for the self energy itself has no incoming or outgoing Green's function lines attached. Expanding the interacting Green's function lines by the Dyson equation we get (inserting the Hartree-Fock self-energy recursively)

$$\begin{aligned}
 \text{---} \bigcirc \Sigma \text{---} &= \text{---} \bigcirc \text{---} + \text{---} \text{---} + \text{---} \bigcirc \text{---} + \text{---} \bigcirc \text{---} \\
 &+ \text{---} \text{---} \bigcirc \text{---} + \text{---} \text{---} \text{---} + \text{---} \bigcirc \text{---} \bigcirc \text{---} + \text{---} \bigcirc \text{---} \bigcirc \text{---} + \dots \quad (5.81)
 \end{aligned}$$

Together with the Dyson-equation (7.23,5.75) which further produces 1-particle reducible diagrams for the Green's function we have drastically compactified our diagrams. These are the so called **skeleton-diagrams**. Inserting self-energies (when going from G to G) yields a piece that is connected by two Green's functions with the rest of the Feynman:  Such 2-particle reducible

diagrams must not be contained in the skeleton expansion of Σ in terms of \Rightarrow . That is the skeleton diagrams for the self-energy are just all 2-particle irreducible diagrams with \Rightarrow and \times .

Chapter 6

Linear response theory

6.1 External fields as probing tools

In this chapter we discuss the response of a many-electron system to an external field, used to *probe* the underlying physics. In particular, we will consider the regime of a *linear* response to an external perturbation – a regime, which is realized if the intensity of the applied field¹ stays small w.r.t. the characteristic scales of the system under investigation.

The “Linear Response Theory” (LRT) formalizes the way how to compute all relevant physical quantities in this kind of processes and, thus, represents a pivotal ingredient for the quantum many-body theory: It allows to directly connect the Feynman diagrammatic expressions derived in the previous chapter (Chp. 5) to the results of thermodynamic and/or spectroscopic experiments on many-electron systems.

Without loss of generality, we start by considering a many-electron system described by the following Hamiltonian

$$\hat{H} = \hat{H}_0 + \hat{H}_V, \quad (6.1)$$

which includes, as usual, a non-interacting part (\hat{H}_0) and a two-body electronic interaction (\hat{H}_V). Then, we are going to *probe* our interacting system by perturbing it with a time-dependent external field $a(t)$, treated semiclassically (i.e., as a mere time-dependent function). This field is coupled with the physical system under investigation through one of the system observables (\hat{A}). Hence, the following perturbed time-dependent Hamiltonian²

$$\hat{H}(t) = \hat{H} + \hat{V}(t) = \hat{H}_0 + \hat{H}_V + \hat{V}(t) \quad \text{with} \quad \hat{V}(t) = -\hat{A} \cdot a(t) \quad (6.2)$$

must be considered.

¹Or, more precisely, the energy scale associated to the perturbation

²In this preliminary illustration of the problem, the Schrödinger notation is used: the operator $\hat{V}(t)$ has, thus, an intrinsic time-dependence, which is entirely defined through the time-dependence of the perturbing field $a(t)$.

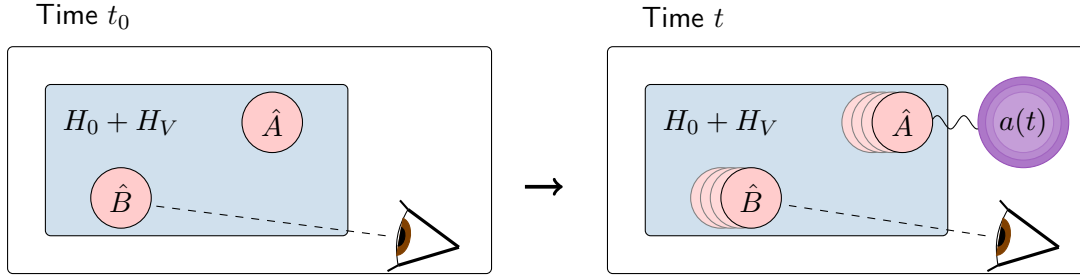


Figure 6.1: Illustration of the considered system. The field $a(t)$ is coupled via \hat{A} . We observe the response by measuring \hat{B} at time t_0 and t .

Eventually, we will extract the desired physical information by observing how the system reacts to the perturbation. In practice, this goal is achieved by measuring the change of another³ observable \hat{B} of the system induced by the external field:

$$\langle \hat{B} \rangle_{\mathcal{V}}(t) - \langle \hat{B} \rangle_{\mathcal{V}=0} \equiv \text{response of the system to the external field } a(t) \quad (6.3)$$

Evidently, for an external field $a(t)$ of arbitrary intensity and/or duration, one should expect the corresponding response of the system to be a rather complicate function of the field itself. However, as anticipated above, in this chapter we will focus exclusively on the relevant case, in which the response of the perturbed system can be assumed to be *linear* w.r.t. the field itself. As we will clarify below, this situation, which actually applies to most spectroscopy experiments on many-electron systems at equilibrium, allows to easily extract through the application of the external field direct information about the original (“unperturbed”) system described by the many-electron Hamiltonian $H = H_0 + H_V$.

Before proceeding with the illustration of the LRT in the next section⁴, a small formal remark: From now on, for the sake of readability, we will simplify the notation for the operators, i.e. $\hat{A} \rightarrow A$.

6.2 Linear response

In this section, as mentioned before, we will consider the specific, but most relevant case in which the system response is *linear* w.r.t. the external field $a(t)$.

Under this assumption, the systems response of the l.h.s. of Eq. (6.3) can be written in general as:

$$\langle B \rangle_{\mathcal{V}}(t) - \langle B \rangle_{\mathcal{V}=0} = \int_{-\infty}^{\infty} dt' \chi_{BA}(t - t') a(t'), \quad (6.4)$$

³Of course, \hat{B} may also be equal \hat{A} , and, indeed, in several cases, this situation is realized experimentally.

⁴It might be also reasonable, at this point, to recapitulate some basic concepts regarding time-evolution with perturbative terms. This had been discussed in the lecture notes of quantum mechanics II chapter 2.5 (Prof.Held) [10] or see (A) in the Appendix for a brief summary. This part might be skipped by the reader, if these concepts are well known.

where the time-dependent response function $\chi_{BA}(t-t')$ defines the so-called dynamical susceptibility of the many-electron system under consideration to the external perturbation.

The crucial point to be stressed here is the following: The linearity assumption necessarily implies that the dynamical susceptibility must be totally *independent* of the external field $a(t')$. It will depend, instead, on the two system's observables B and A involved in the specific process considered.

As a consequence, computing or measuring the response function $\chi_{BA}(t-t')$ will provide us with *intrinsic* information about the physics of the undisturbed many-electron system described by the (interacting) many-body Hamiltonian H .

Before deriving the famous *Kubo-Nakano* formula, which provides an explicit expression for the r.h.s. of Eq. (6.4) to be used in practical Feynman-diagrammatic calculations, it is important to illustrate first all the analytical properties that the response function of the LRT must obey on general ground.

The **general properties** of the response function are:

- **Causality:** Evidently, we cannot observe any response, *before* the perturbation is applied. Hence:

$$\chi(t-t') \Rightarrow \theta(t-t')\chi(t-t') \quad (6.5)$$

- **Finiteness in time:** This implies that the response cannot be fully instantaneous at any time (aka no singular δ -like term at any time):

$$|\chi(t-t')| < C \quad \forall t, t' \quad (6.6)$$

- **Fourier transform:** Most spectroscopy experiments are based on frequency measurements, providing direct information about energy rather than time. This makes the Fourier transformation extremely useful. When performing the Fourier transform, due to causality, one must restrict the integration over time to $t-t' = t > 0$ (where one can put $t' = 0$ in the case of time-translational invariant H). This restriction directly reflects onto the analytic properties of the Fourier transform χ in the complex frequency plane:

$$(6.5) \Rightarrow \chi(z) = \int_0^\infty dt e^{izt} \chi(t) \quad z \in \mathbb{C}. \quad (6.7)$$

Indeed, $\chi(z)$ is analytic in the whole upper complex plane ($z'' > 0$). We can easily verify it by substituting $z \Rightarrow z' + iz''$.⁵

$$\begin{aligned} e^{izt} &= e^{i(z'+iz'')t} = e^{iz't} e^{-z''t} \\ \Rightarrow &\lim_{z' \rightarrow \infty} e^{iz't} [\text{oscillating factor of absolute value 1}] \\ \Rightarrow &\lim_{z'' \rightarrow \infty} e^{-z''t} = 0 \\ \Rightarrow &\lim_{z \rightarrow \infty} e^{iz't} e^{-z''t} = 0. \end{aligned}$$

⁵ z' is the real-part and z'' is the imaginary-part of our complex number.

The last relation ensures the convergence of the time-integral defining $\chi(z)$ as well as of any of its derivative $\delta_{z^n} \chi(z)$, provided that $z'' > 0$, guaranteeing the analyticity of $\chi(z)$ in the upper complex plane. Hence, the corresponding value of χ on the real frequency axis must be defined as:

$$\chi(\omega) = \lim_{\delta \rightarrow 0} \chi(\omega + i\delta) = \lim_{\delta \rightarrow 0} \int_0^\infty dt e^{i(\omega + i\delta)t} \chi(t) \quad (6.8)$$

- **Kramers Kronig relation:** Similarly as for the retarded Green's function, the real and imaginary part of $\chi(\omega)$ are not independent, being linked by the following integral relation ⁶

$$\begin{aligned} \chi'(\omega) &= \frac{1}{\pi} \oint d\tilde{\omega} \frac{\chi''(\tilde{\omega})}{\tilde{\omega} - \omega} \\ \chi''(\omega) &= -\frac{1}{\pi} \oint d\tilde{\omega} \frac{\chi'(\tilde{\omega})}{\tilde{\omega} - \omega} \end{aligned} \quad (6.9)$$

6.3 Kubo-Nakano formula

In order to obtain the Kubo-Nakano formula in its general form (A.10) we derive it step by step, by starting with

$$\langle B \rangle_{\mathcal{V}=0} = \frac{1}{Z} \text{Tr}[e^{-\beta H} B] = \text{Tr}[\rho B] \quad (6.10)$$

$$\langle B \rangle_{\mathcal{V}}(t) = \text{Tr}[\rho_t B] \quad (6.11)$$

where

$$\rho = \frac{1}{Z} e^{-\beta H} = \frac{1}{Z} \sum_{\alpha} e^{-\beta E_{\alpha}} |\psi_{\alpha}\rangle \langle \psi_{\alpha}| \quad (6.12)$$

$$\rho_t = \frac{1}{Z} \sum_{\alpha} e^{-\beta E_{\alpha}} |\psi_{\alpha}(t)\rangle \langle \psi_{\alpha}(t)| \quad (6.13)$$

$$\Delta \rho = \rho_t - \rho \Leftrightarrow \rho_t = \rho + \Delta \rho. \quad (6.14)$$

Since the trace is a linear transformation we may write

$$\langle B \rangle_{\mathcal{V}}(t) - \langle B \rangle_{\mathcal{V}=0} = \text{Tr}[\rho_t B] - \text{Tr}[\rho B] = \text{Tr}[(\rho_t - \rho) B] = \text{Tr}[\Delta \rho B]. \quad (6.15)$$

Additionally we need to calculate the equation of motion for ρ_t , which we shall do in the

⁶ f represents Cauchy's principal value.

Schrödinger picture

$$\begin{aligned}
 i\hbar \frac{\partial}{\partial t} \rho_t &= \frac{i\hbar}{Z} \sum_{\alpha} e^{-\beta E_{\alpha}} \frac{\partial}{\partial t} (|\psi_{\alpha}(t)\rangle \langle \psi_{\alpha}(t)|) \\
 &= \frac{i\hbar}{Z} \sum_{\alpha} e^{-\beta E_{\alpha}} \left(\frac{\partial}{\partial t} (|\psi_{\alpha}(t)\rangle) \langle \psi_{\alpha}(t)| + |\psi_{\alpha}(t)\rangle \frac{\partial}{\partial t} (\langle \psi_{\alpha}(t)|) \right) \\
 &= \frac{1}{Z} \sum_{\alpha} e^{-\beta E_{\alpha}} \left(H_t |\psi_{\alpha}(t)\rangle \langle \psi_{\alpha}(t)| - |\psi_{\alpha}(t)\rangle \langle \psi_{\alpha}(t)| H_t \right) \\
 &= H_t \rho_t - \rho_t H_t \\
 &= [H_t, \rho_t]
 \end{aligned} \tag{6.16}$$

Similarly, we find for $\Delta\rho$, by using the result of (6.16) and substitute $\rho_t \rightarrow \rho + \Delta\rho$

$$\begin{aligned}
 i\hbar \frac{\partial}{\partial t} (\rho + \Delta\rho) &= [H_t, \rho + \Delta\rho] = [H + \mathcal{V}(t), \rho + \Delta\rho] \\
 &= (H + \mathcal{V}(t))(\rho + \Delta\rho) - (\rho + \Delta\rho)(H + \mathcal{V}(t)) \\
 &= H\rho + H\Delta\rho + \mathcal{V}(t)\rho + \mathcal{V}(t)\Delta\rho \\
 &\quad - \rho H - \rho\mathcal{V}(t) - \Delta\rho H - \Delta\rho\mathcal{V}(t) \\
 &= [H, \rho] + [H, \Delta\rho] + [\mathcal{V}(t), \rho] + [\mathcal{V}(t), \Delta\rho] \\
 &\approx [H, \Delta\rho] + [\mathcal{V}(t), \rho] = [H, \Delta\rho] - a(t)[A, \rho] \approx i\hbar \frac{\partial}{\partial t} \Delta\rho.
 \end{aligned} \tag{6.17}$$

In the last line of (6.17) we used on the right-hand side that $\frac{\partial}{\partial t}\rho = 0$ since ρ is not time-dependent and on the left-hand side that we are only considering linear terms in $\mathcal{V}(t)$, so we neglect $[\mathcal{V}(t), \Delta\rho]$.

A solution to the result of (6.17) is given by

$$\Delta\rho(t) = -\frac{1}{i\hbar} \int_{-\infty}^t e^{-i\frac{H(t-t')}{\hbar}} [A, \rho] e^{i\frac{H(t-t')}{\hbar}} a(t') dt'. \tag{6.18}$$

As one can verify that explicitly

$$i\hbar \frac{\partial}{\partial t} \Delta\rho(t) = i\hbar \left(\frac{-1}{i\hbar} \right) [A, \rho] a(t) + \left(\frac{-i}{\hbar} \right) \left[H \int_{-\infty}^t (...) - \int_{-\infty}^t (...) H \right].$$

The Kubo-Nakano formula can be derived by plugging (6.18) in (6.15) :

$$\begin{aligned}
 \langle B \rangle_{\mathcal{V}}(t) - \langle B \rangle_{\mathcal{V}=0} &= Tr[\Delta\rho B] = -\frac{1}{i\hbar} \int_{-\infty}^t dt' Tr \left[B e^{-i\frac{H(t-t')}{\hbar}} [A, \rho] e^{i\frac{H(t-t')}{\hbar}} a(t') \right] \\
 &= -\frac{1}{i\hbar} \int_{-\infty}^t dt' Tr \left[B(t) [A(t'), \rho] a(t') \right] \\
 &= -\frac{1}{i\hbar} \int_{-\infty}^t dt' Tr \left[[B(t), A(t')] \rho \right] a(t') \\
 &= -\frac{1}{i\hbar} \int_{-\infty}^t dt' \langle [B(t), A(t')] \rangle_{\mathcal{V}=0} a(t')
 \end{aligned} \tag{6.19}$$

This leads to

the KUBO-NAKANO Formula

$$\langle B \rangle_{\mathcal{V}}(t) - \langle B \rangle_{\mathcal{V}=0} = \int_{-\infty}^{+\infty} dt' \chi_{BA}(t-t') a(t') \quad (6.20)$$

$$\chi_{BA}(t-t') = -\frac{1}{i\hbar} \theta(t-t') \langle [B(t), A(t')] \rangle_{\mathcal{V}=0} \quad (6.21)$$

6.3.1 Examples of applications of the Kubo-Nakano formula

In the following, we illustrate the explicit application of Eqs. (6.3) in selected prototypical cases:

Density response:

As a first, most simple example we consider the density response of a many-electron system (i.e. $B = n(r)$) to a time- and space-dependent change of the chemical potential (i.e., $a(t) = \delta\mu(r, t) = \mu(r, t) - \mu_0$, where μ_0 is the constant chemical potential of the unperturbed systems). As the chemical potential is linearly coupled to the density operator itself, we have $A = B = n(r)$. Hence, the Eqs. (6.3) for this specific case yield:

$$\langle n(r) \rangle_{\mathcal{V}}(t) - \langle n(r) \rangle_0 = \int_{-\infty}^t dt' \int_{-\infty}^{\infty} d^d r' \chi_{nn}(r-r', t-t') \delta\mu(r', t') \quad (6.22)$$

with

$$\mathcal{V}(t) = - \int d^d r n(r) \delta\mu(r, t) \quad (6.23)$$

and

$$\chi_{nn}(r-r', t-t') = -\frac{1}{i\hbar} \theta(t-t') \langle [n(r, t), n(r', t')] \rangle_{\delta\mu=0} \quad (6.24)$$

where – we recall – the density operator in second quantization read

$$n(r, t) = \sum_{\sigma=\uparrow, \downarrow} \psi_{\sigma}^{\dagger}(r, t) \psi_{\sigma}(r, t). \quad (6.25)$$

in terms of the creation/annihilation field-operators of an electron at the position r with spin σ . The latter expression will be useful in the following to make an explicit connection with the corresponding Feynmann diagrammatic expressions.

Magnetic response:

We consider now the magnetic response of a many-electron system to an external time-/space-dependent magnetic field (i.e., $a(t) = \vec{h}(r, t)$).

This example arguably represents one of the most common situations encountered in practice. For the sake of simplicity, we assume here that the magnetic moment of the electrons reduces to its spin component only (assumption of “quenching of the orbital momentum”). The electronic magnetic moment then reads $\vec{\mu} = G\vec{S}$, where \vec{S} is the electronic spin operator and $G = -\frac{\mu_B g}{\hbar}$ (with $g \simeq 2$). Hence, we will have $B = G\vec{S}$. Considering the dipolar coupling of the magnetic moment with the external magnetic field:

$$\mathcal{V}(t) = - \int d^d r G \vec{S}(r) \cdot \vec{h}(r, t) = - \int d^d r G S_\alpha(r) h_\alpha(r, t) \quad (6.26)$$

with the index $\alpha = x, y, z$ identifying the components of the spin operator and/or of the magnetic field. Evidently, from Eq. (6.26), we can readily identify $A = G\vec{S}(r)$.

In order to write the explicit expression of the Kubo-Nakano formula for the magnetic response in a rather general case, we assume to measure the (spin) magnetic moment in a given direction $\beta = x, y, z$, which might differ from the direction (e.g., $\alpha = x, y, z$) of the applied magnetic field. Under this assumption, the corresponding (spin) magnetic susceptibility reads:

$$\chi_{S_\beta S_\alpha}(r - r', t - t') = - \frac{G^2}{i\hbar} \theta(t - t') \langle [S_\beta(r, t), S_\alpha(r', t')] \rangle_{\hbar=0}. \quad (6.27)$$

We note that while the above equation corresponds to a tensor in the general case, for isotropic and homogeneous paramagnetic systems, its tensor structure reduces to its diagonal part, i.e., $\chi_{S_\beta S_\alpha} = \chi_{\text{spin}} \delta_{\alpha\beta}$, with $\chi_{\text{spin}} = \chi_{S_x S_x} = \chi_{S_y S_y} = \chi_{S_z S_z}$.

6.4 Computing the response function in QFT

Since physical observations of many-electron systems are performed at finite temperature, in the context of the linear response theory it can be convenient to adopt the formalism mostly suited for the quantum statistical mechanical treatment of the Green's and correlations functions at thermal equilibrium. As already discussed in previous chapters, this formalism relies on a Wick rotation of the real time (t) onto the imaginary time axis ($\tau = it$), as sketched in Figure (6.2). One should always keep in mind, however, that a Wick rotation does *not* reduce to a mere substitution of $\tau = it$ in all time-dependent expressions. Indeed, such a “plain-vanilla” implementation could lead, in certain cases, to ambiguously defined or even unphysically divergent expressions. In the specific situation of interest for this Chapter, the proper way of handling the transformation of the system response between the real and the imaginary time domain – or, equivalently between real and imaginary (Matsubara) frequencies – is dictated by the general analytic properties of the response functions. As mentioned before, these directly reflect the intrinsic *retarded* nature of the physical

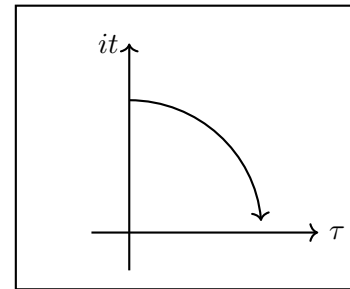


Figure 6.2: Wick rotation

response, which ensures the analyticity of the Fourier transformed susceptibility $\chi_{BA}(z)$ in the whole *upper*-complex frequency plane ($z = \omega + i\eta$ with $\eta > 0$). Not surprisingly, the most known connection between the different expressions can be naturally defined in the *upper*-half complex frequencies plane, which formally corresponds to perform a so-called “*analytic continuation*”. In particular, the previously introduced definition of the Fourier transform on the *real* frequency axis:

$$\chi_{BA}^{(R)}(\omega) = \chi_{BA}(\omega + i0^+) = i \int_0^\infty dt e^{i(\omega + i0^+)t} \langle [B(t), A(0)] \rangle_{V=0}, \quad (6.28)$$

(with $\hbar = 1$) directly corresponds, analogously as discussed in Chapter 3, to

$$\chi_{BA}^{(R)}(\omega) = \chi_{BA}(i\Omega_n = \omega + i0^+) = \int_0^\beta d\tau e^{i\Omega_n \tau} \langle \mathcal{T}_\tau B(\tau) A(0) \rangle_{V=0} \Big|_{i\Omega_n = \omega + i0^+}, \quad (6.29)$$

which provides the direct link between the Kubo-Nakano retarded response function on the real frequency domain and the one computed in the Matsubara formalism.

Beyond the straightforward analogy with the relations holding in general for the retarded Green’s functions, the correspondence between Eq. (6.28) and Eq. (6.29) can also be explicitly derived by directly comparing the associated Lehmann representations. We do not provide here the corresponding straightforward, albeit lengthy, derivation, as it can be found in several textbook. We do report below, instead, an alternative demonstration of the equivalence between the two above-mentioned equations directly expressed in the complex time domain, which has been extracted from the lecture notes⁷ by Dr. *Georg Rohringer* (University of Hamburg), whom we thank heartily for the permission of reproducing it.

The corresponding derivation (in the yellow box) is not part of the official examination topics, and it has to be understood as an additional piece of information for the interested students.

Proof. As starting point to prove the equivalence of (6.28) and (6.29), we exploit the imaginary-time integral expression of the Matsubara-frequency dependent response. Hence, we start with

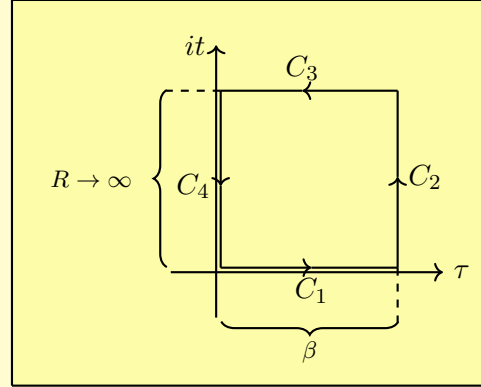
$$\oint_C dz e^{i\Omega_n z} \langle \mathcal{T}_z B(z) A(0) \rangle = 0 \quad (6.30)$$

where C is a closed path in the complex time space, being $z = \tau + it$, and $\Omega_n = \frac{2\pi n}{\beta}$ is the *bosonic* Matsubara frequency. In the following, we split that closed path into four contours alongside $C_{1,2,3,4}$:

$$(6.30) = \left(\int_{C_1} dz + \int_{C_2} dz + \int_{C_3} dz + \int_{C_4} dz \right) e^{i\Omega_n z} \langle \mathcal{T}_z B(z) A(0) \rangle, \quad (6.31)$$

⁷Link to his website: <https://www.physik.uni-hamburg.de/th1/ag-georg-rohringer/lehre.html>

as shown in the schematic picture below:



Now, we proceed by explicitly calculating those integrals:

$$C_1: \quad z = \tau \quad \tau \in [0, \beta] \quad dz = d\tau$$

$$\int_{C_1} dz e^{i\Omega_n z} \langle \mathcal{T}_z B(z) A(0) \rangle = \int_0^\beta d\tau e^{i\Omega_n \tau} \langle \mathcal{T}_\tau B(\tau) A(0) \rangle \quad (6.32)$$

That is exactly the form of (6.29).

$$C_2: \quad z = \beta + it \quad t \in [0, R) \quad R \rightarrow \infty \quad dz = i dt$$

$$\int_{C_2} dz e^{i\Omega_n z} \langle \mathcal{T}_z B(z) A(0) \rangle = \quad (6.33)$$

$$= -\frac{i}{Z} \int_0^R dt e^{i\Omega_n(\beta+it)} \text{Tr}(e^{-\beta H} e^{(\beta+it)H} B(0) e^{-(\beta+it)H} A(0)) = \quad (6.34)$$

$$= -\frac{i}{Z} \int_0^R dt \underbrace{e^{i\Omega_n \beta}}_{=1} e^{-\Omega_n t} \text{Tr}(e^{-\beta H} A(0) \underbrace{e^{itH} B(0) e^{-itH}}_{B(t)}) = \quad (6.35)$$

$$\stackrel{R \rightarrow \infty}{=} i \int_0^\infty dt e^{-\Omega_n t} \langle A(0) B(t) \rangle \quad (6.36)$$

In (6.35) we used the cyclicity of the trace. (6.36) is only analytic for $\Omega_n > 0$.

$$C_3: \quad z = \tau + iR \quad \tau \in [\beta, 0] \quad R \rightarrow \infty \quad dz = d\tau$$

$$\int_{C_3} dz e^{i\Omega_n z} \langle \mathcal{T}_z B(z) A(0) \rangle = \quad (6.37)$$

$$= \int_{\beta}^0 d\tau \underbrace{e^{i\Omega_n(\tau+iR)}}_{R \rightarrow \infty \Rightarrow 0} \langle \mathcal{T}_{(\tau+iR)} B(\tau+iR) A(0) \rangle = 0 \quad (6.38)$$

(6.38) is true for $\Omega_n > 0$.

$$C_4: \quad z = it \quad t \in (R, 0] \quad R \rightarrow \infty \quad dz = i dt$$

$$\int_{C_4} dz e^{i\Omega_n z} \langle \mathcal{T}_z B(z) A(0) \rangle = \quad (6.39)$$

$$= -\frac{i}{Z} \int_R^0 dt e^{-\Omega_n t} \text{Tr}(e^{-\beta H} e^{itH} B(0) e^{itH} A(0)) = \quad (6.40)$$

$$\stackrel{R \rightarrow \infty}{=} -i \int_0^{\infty} dt e^{-\Omega_n t} \langle B(t) A(0) \rangle \quad (6.41)$$

In (6.41) note that the trace took a sign as well as the flipping of the integration limits.

Apply results to (6.31):

$$\begin{aligned} (6.31) = & \underbrace{\int_0^{\beta} d\tau e^{i\Omega_n \tau} \langle \mathcal{T}_{\tau} B(\tau) A(0) \rangle}_{C_1} + \underbrace{i \int_0^{\infty} dt e^{-\Omega_n t} \langle A(0) B(t) \rangle}_{C_2} + \\ & + \underbrace{0}_{C_3} - \underbrace{i \int_0^{\infty} dt e^{-\Omega_n t} \langle B(t) A(0) \rangle}_{C_4} = 0 \end{aligned} \quad (6.42)$$

$$\begin{aligned} \Rightarrow & \int_0^{\beta} d\tau e^{i\Omega_n \tau} \langle \mathcal{T}_{\tau} B(\tau) A(0) \rangle = \\ & i \int_0^{\infty} dt e^{-\Omega_n t} \langle B(t) A(0) \rangle - i \int_0^{\infty} dt e^{-\Omega_n t} \langle A(0) B(t) \rangle = \end{aligned} \quad (6.43)$$

and with $\Omega_n = -i(\omega + i\delta)$ this leads to

$$\int_0^{\beta} d\tau e^{i\Omega_n \tau} \langle \mathcal{T}_{\tau} B(\tau) A(0) \rangle = i \int_0^{\infty} dt e^{i(\omega+i\delta)t} \langle [B(t), A(0)] \rangle \quad (6.44)$$



6.4.1 Practical considerations

As numerical QFT calculations are typically much more easily performed for quantities defined in imaginary time/Matsubara frequency, the procedure often adopted in practice is the following:

- (i) calculate $\chi_{BA}(\tau) = \langle \mathcal{T}_\tau B(\tau) A(0) \rangle_{V=0}$
- (ii) perform the Fourier-transformation (6.29): $\chi_{BA}(\tau) \Rightarrow \chi_{BA}(i\Omega_n)$
- (iii) perform the analytic continuation on the real frequency axis by means of the substitution: $i\Omega_n = \omega + i0^+ \Rightarrow$ (6.28)

Here, we note that the first step can be obviously skipped, if one is able to perform the QFT calculations directly in the Matsubara frequency domain. Much more importantly, we must emphasize that the last step (“*analytic continuation*”) is highly non trivial in the general case. In fact, performing the substitution in (iii) is straightforward only if one knows an analytical expression of $\chi_{BA}(i\Omega_n)$. Otherwise, if one can only numerically compute approximated values of χ_{BA} as a function of the discrete Matsubara frequencies $i\Omega_n$ or on a grid on the imaginary time axis τ , the analytic continuation becomes -formally- a mathematically ill-defined step⁸. Several *ad hoc* techniques, such as, e.g., a fit of $\chi_{BA}(i\Omega_n)$ with Padé rationale approximants or Maximum Entropy Methods (MEM), have been then developed to circumvent this issue, which indeed represents most often a quite delicate step for QFT studies at finite temperature. The usage of these approaches must be systematically checked (e.g., by comparing with limiting/known cases) and always guided by physical considerations. Under these conditions, they often yield reasonably good results, allowing for a direct comparison with the experiments.

6.4.2 The static response ($i\Omega_n = 0$)

The retarded nature of the Kubo-Nakano response functions, as well as their associated analytical properties in the upper-half-plane of complex frequencies, is reflected in the link between the analytic continuation of $\chi_{BA}(i\Omega_n)$ for $\Omega_n > 0$ to the real frequency axis $\chi_{BA}(i\Omega_n = \omega + i0^+)$, encoded in Eqs. (6.28-6.29). However, differently from the case of the one-particle *electronic* Green’s function discussed in the previous chapters, the *bosonic* nature of the Matsubara frequencies ($i\Omega_n = 2n\pi T$) of the response functions makes it possible to also compute χ_{BA} directly for a *zero* Matsubara frequency (i.e., $i\Omega_n \equiv 0$), which is -per se- a physically relevant value.

Technically, the calculation of such quantity, $\chi_{BA}(i\Omega_n=0)$, is easier w.r.t. the dynamical quantities described above, as it directly yields a physically meaningful result without the need of any delicate analytic continuation approach. However, the physics encoded in a $\Omega_n = 0$ calculation is

⁸The numerical knowledge of the values of $\chi_{BA}(i\Omega_n)$ on a finite subset of Matsubara frequencies (or even on all of them but with finite precision), and/or equivalently on a finite grid on the imaginary time axis, formally prevents to identify a *unique* analytical function on the complex upper half-plane: More than one analytical function would be actually compatible with the numerical data, which makes any numerical analytic continuation procedure intrinsically ill-posed on a strict formal level.

conceptually different from the one described by the Kubo-Nakano response functions, which is encoded -as discussed above- in all Matsubara frequencies *strictly larger* than zero ($\Omega_n > 0$), consistent with the analytical properties of a retarded dynamical response.

More specifically, setting $\Omega_n \equiv 0$ right from the beginning of a QFT calculation of a response function corresponds, physically, to compute the so-called *static* (or *isothermal*) response of the many-electron system, i.e., its response to the application of a *static, time-independent*, external field. This makes a significant difference w.r.t. the case of the Kubo-Nakano response considered so far, because now the external perturbation is always present. As a consequence, the thermal grand-canonical averages introduced in Chapter 3 must be computed considering the Hamiltonian *modified* by the presence of the static probing field. It is not surprising, then, that such a qualitative difference, which would already appear in the first steps of the derivation of the Kubo-Nakano formula (cf. Eq.(6.3)), can yield rather different final results.

In practice, this means that the zero-frequency limit of a dynamical Kubo-Nakano response, $\lim_{i\Omega_n \rightarrow 0} \chi_{BA}(i\Omega_n)$ does not necessarily correspond to its static/isothermal value $\chi_{BA}(i\Omega_n \equiv 0)$. This difference, however, should not be regarded as an artifact of the formalism, because it simply reflects the actual difference of the two physical set-ups considered for extracting (or experimentally measuring) the corresponding response function: (i) the application of a dynamical perturbation (for a relatively short time, which does not allow any thermalization of the system w.r.t. the perturbation) in the case of the Kubo-Nakano retarded response in contrast (ii) to the application of a static constant perturbation in the case of the static/isothermal response. Evidently, both pieces of information are physically relevant and can be extracted from a calculation of $\chi_{BA}(i\Omega_n)$ by following the corresponding pertinent procedure. We note, in passing, that the latter case ($i\Omega_n \equiv 0$) is the one directly linked to the static magnetic susceptibility defined in the Stat. Phys. II lecture. The interested readers can find more details about this topic in Refs. [16, 15].

6.4.3 Feynman diagrammatic calculations of response functions

Consistent to the discussion above, we will mostly work with Feynman diagrams in the imaginary time-domain. Our starting point will thus be $\chi_{BA}(r - r', \tau - \tau') = \langle \mathcal{T}_\tau B(r, \tau) A(r', \tau') \rangle_{V=0}$. Further, we assume the space- and time-translational invariance of the unperturbed system, which allows us, w.l.o.g., to set the starting time/position to zero (i.e., $r' = 0 = \tau'$).

For pedagogical reasons, we first consider the case of a non-interacting system, described by the hamiltonian $H = H_0$ ($H_V = 0$) and subsequently outline the possible Feynman diagrammatic corrections induced by the electronic interaction H_V .

Density-density response: As a first example, we start again with the simplest case of the density response of a system to a perturbation of the chemical potential, whose expression, in the imaginary time-domain, for $\tau > 0$, reads:

$$\chi_{BA}(r - r', \tau - \tau') \Rightarrow \chi_{nn}^{(0)} = \underbrace{\langle n(r, \tau) \rangle}_{B(r, \tau)} \underbrace{\langle n(0, 0) \rangle}_{A(0, 0)}_{H_0}. \quad (6.45)$$

As $n(r, \tau) = \sum_{\sigma} \psi_{\sigma}^{\dagger}(r, \tau) \psi_{\sigma}(r, \tau)$, Eq. (6.45) can be explicitly rewritten as:

$$= \sum_{\sigma \sigma'} \langle \psi_{\sigma}^{\dagger}(r, \tau) \psi_{\sigma}(r, \tau) \psi_{\sigma'}^{\dagger}(0, 0) \psi_{\sigma'}(0, 0) \rangle_{H_0}. \quad (6.46)$$

Since we are considering here the non-interacting case, the unperturbed Hamiltonian reduces to H_0 , which allows for a trivial application of Wick's theorem: The quantum statistical average of Eq. (6.46) factorizes in the sum of products of all possible averages (dubbed "contractions") of pairs of ψ^{\dagger} and ψ , allowed by the symmetries⁹ of the physical system under investigation. In practice, one becomes:

$$\begin{aligned} &= \underbrace{\sum_{\sigma} \langle \psi_{\sigma}^{\dagger}(r, \tau) \psi_{\sigma}(r, \tau) \rangle_{H_0}}_{\langle n_0 \rangle} \underbrace{\sum_{\sigma'} \langle \psi_{\sigma'}^{\dagger}(0, 0) \psi_{\sigma'}(0, 0) \rangle_{H_0}}_{\langle n_0 \rangle} \\ &\quad - \sum_{\sigma \sigma'} \underbrace{\langle \psi_{\sigma}(r, \tau) \psi_{\sigma'}^{\dagger}(0, 0) \rangle_{H_0}}_{G^{(0)}(r, \tau)} \underbrace{\langle \psi_{\sigma'}(0, 0) \psi_{\sigma}^{\dagger}(r, \tau) \rangle_{H_0}}_{G^{(0)}(-r, -\tau)} \\ &= \langle n_0 \rangle^2 - 2G^{(0)}(r, \tau)G^{(0)}(-r, -\tau) \\ &= \langle n_0 \rangle^2 - 2 \begin{array}{c} (r, \tau) \quad \text{---} \quad (0, 0) \\ \text{---} \quad \text{---} \\ (0, 0) \quad \text{---} \quad (r, \tau) \end{array}, \end{aligned} \quad (6.47)$$

where, in the first term, we have identified the definition of the density of the unperturbed system (i.e., n_0 , constant in space and time) and in the second term the definition of the (non-interacting) one particle Green's function in the imaginary time domain. Note that, since we assume here that H_0 is SU(2)-symmetric (non-magnetic/paramagnetic system), the non interacting one-particle Green's function $G_{\sigma\sigma'}^{(0)}$ are independent of the spin-indexes $G_{\sigma\sigma'}^{(0)} = G^{(0)} \delta_{\sigma'\sigma}$, which eventually leads to the explicit prefactor 2 in front of the second term.

It is worth, now, to briefly examine the result obtained for this basic case, as it already entails the fundamental ingredients for performing and physically understanding more complex calculations. $\chi_{nn}^{(0)}$ appears factorized in two terms: The first one simply encodes the average value of the observable(s) considered in the unperturbed system. As this represents a rather trivial piece of information in the context of the L.R.T., this term (if nonzero) is often subtracted away when analyzing the system response. Instead, the second term, whose Feynman diagrammatic representation looks like a "bubble", is built upon propagators of one electron and one hole (between the same pair of coordinates (r, τ) and $(0, 0)$) and, as such, it encodes pivotal information about the fluctuations occurring in the many-electron system (in this case, obviously: density fluctuation). As we will see in the next chapter, this "bubble" term will play a crucial role in the theoretical description of the electronic *screening* of the Coulomb interaction.

⁹For instance, in the absence of a spontaneous breaking of the U(1) symmetry (which would correspond to consider a superconducting phase) all averages of the kind $\langle \psi\psi \rangle$ or $\langle \psi^{\dagger}\psi^{\dagger} \rangle$ will exactly vanish. For an analogous reason, when the H_0 is SU(2)-symmetric, e.g., when we are considering a non-magnetic/paramagnetic system, the averages of any pair of creation/annihilation operator will be diagonal in the spin space: $\langle \psi_{\sigma}^{\dagger}\psi_{\sigma} \rangle \propto \delta_{\sigma'\sigma}$.

Spin-spin (magnetic) response: Following the structure of Sec. 1.3.1, we proceed by considering the response of our (non-interacting) system to a time and space dependent magnetic field, which is coupled of the spins of the electrons ("Pauli-coupling"). The corresponding magnetic response reads:

$$\chi_{S_\beta S_\alpha}^{(0)}(r, \tau) = G^2 \underbrace{\langle S_\beta(r, \tau) \rangle}_{B(r, \tau)} \underbrace{\langle S_\alpha(0, 0) \rangle}_{A(0, 0)} \quad (6.48)$$

where $S_\beta(r, \tau) = \frac{\hbar}{2} \begin{pmatrix} \psi_\uparrow^\dagger(r, \tau) & \psi_\downarrow^\dagger(r, \tau) \end{pmatrix} (\sigma_\beta) \begin{pmatrix} \psi_\uparrow(r, \tau) \\ \psi_\downarrow(r, \tau) \end{pmatrix}$, $\sigma_{\beta=x,y,z}$ are the Pauli matrices, and $G = -\frac{\mu_B g}{\hbar}$ (with $g \simeq 2$).

For example, if we consider the magnetic response in the z -direction to a magnetic field applied along the same axis, we have:

$$\begin{aligned} \hat{B} = \hat{A} = G S_z(r, \tau) &\Rightarrow \frac{\hbar}{2} G \left(\psi_\uparrow(r, \tau)^\dagger \psi_\uparrow(r, \tau) - \psi_\downarrow(r, \tau)^\dagger \psi_\downarrow(r, \tau) \right) \\ &\Rightarrow \chi_{S_z S_z}^{(0)}(r, \tau) = \mu_B^2 \langle \left(\psi_\uparrow(r, \tau)^\dagger \psi_\uparrow(r, \tau) - \psi_\downarrow(r, \tau)^\dagger \psi_\downarrow(r, \tau) \right) \\ &\quad \cdot \left(\psi_\uparrow(0, 0)^\dagger \psi_\uparrow(0, 0) - \psi_\downarrow(0, 0)^\dagger \psi_\downarrow(0, 0) \right) \rangle_{H_0} \\ &\quad - \sum_{\sigma} \underbrace{\langle \psi_\sigma(r, \tau) \psi_\sigma^\dagger(0, 0) \rangle_{H_0}}_{G^{(0)}(r, \tau)} \underbrace{\langle \psi_\sigma(0, 0) \psi_\sigma^\dagger(r, \tau) \rangle_{H_0}}_{G^{(0)}(-r, -\tau)} \\ &\quad = -2 \mu_B^2 G^{(0)}(r, \tau) G^{(0)}(-r, -\tau) \\ &\quad = -2 \mu_B^2 \begin{matrix} (r, \tau) \end{matrix} \begin{matrix} \circlearrowleft \\ \circlearrowright \end{matrix} \begin{matrix} (0, 0) \end{matrix}, \end{aligned} \quad (6.49)$$

where we have exploited, analogously as in the density case discussed before, the straightforward application of the Wick theorem for the non-interacting SU(2)-symmetric system.

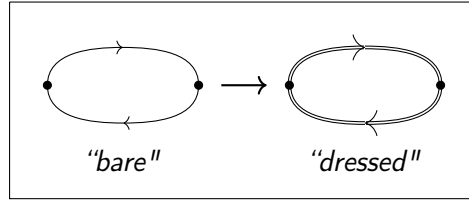
General case: A (rather generic) expression for the observable B is the following:

$$B(r, \tau) = \begin{pmatrix} \psi_\uparrow^\dagger(r, \tau) & \psi_\downarrow^\dagger(r, \tau) \end{pmatrix} (\mathcal{O}_B) \begin{pmatrix} \psi_\uparrow(r, \tau) \\ \psi_\downarrow(r, \tau) \end{pmatrix} \quad (6.50)$$

and the same applies to the observable A (with \mathcal{O}_A instead of \mathcal{O}_B), whereas \mathcal{O} is defined via the matrix elements of the specific observable considered in the Pauli spinor space. When computing $\chi_{BA}(r, \tau)$ in the *non-interacting* case, one has:

$$\chi_{BA}(r, \tau) = \langle B \rangle_0 \langle A \rangle_0 - \begin{matrix} \mathcal{O}_B \end{matrix} \begin{matrix} \circlearrowleft \\ \circlearrowright \end{matrix} \begin{matrix} \mathcal{O}_A \end{matrix}. \quad (6.51)$$

We note that the previously discussed cases of density and magnetic responses are readily recovered as

Figure 6.3: Bubble diagrams with “bare” (G_0) and “dressed” (G) Green’s function lines.

1. **Density-density:** $\chi_{nn} \Rightarrow \mathcal{O}_B = \mathcal{O}_A = \mathbb{1}$
2. **Spin-spin:** $\chi_{S_\beta S_\alpha} \Rightarrow \mathcal{O}_B = \frac{\hbar}{2} \sigma_\beta; \mathcal{O}_A = \frac{\hbar}{2} \sigma_\alpha$

If we now drop the restriction of considering a free electron systems, and we explicitly take into account the electronic interaction within the many-body perturbation theory ($H_V \neq 0$) we get additional Feynman diagrams beyond those appearing in Eq. (6.51). For instance, considering all corrections at the first order in $H_V \neq 0$, one finds:

$$\begin{aligned}
 \chi_{BA}(r, \tau) = & \underbrace{\langle B \rangle_0 \langle A \rangle_0 - \mathcal{O}_B \text{ (bubble) } \mathcal{O}_A}_{\text{0-th order in } H_V} \\
 & + \underbrace{\mathcal{O}_B \text{ (self-energy)} \mathcal{O}_A + \mathcal{O}_B \text{ (self-energy)} \mathcal{O}_A + \mathcal{O}_B \text{ (self-energy)} \mathcal{O}_A + \mathcal{O}_B \text{ (self-energy)} \mathcal{O}_A}_{\text{Self energy corrections}} \\
 & + \underbrace{\mathcal{O}_B \text{ (vertex)} \mathcal{O}_A}_{\text{Vertex corrections}} + O(H_V^2),
 \end{aligned} \tag{6.52}$$

where the first order diagrams have been classified in self-energy- and vertex- corrections w.r.t. the original bare bubble term. While the inclusion both kind of corrections is -in general- necessary to obtain a satisfactory approximation, the self-energy-corrections and vertex-corrections of the response function have an intrinsically different physical nature.

The former ones (i.e., the self-energy correction) describe how the propagation of a single added/removed particle (or hole) is affected by the scattering with the other electrons in the system. More formally, one can observe that the resummation of all self-energy corrections diagrams to the upper or the lower line of the bubble diagram would correspond to “dress” with all possible interaction effects the pair of one-particle Green’s function appearing in the bare bubble term. Such modification of the single particle propagators from the bare G_0 s to the interacting “dressed” G s, via the inclusion of the respective self-energy, is often graphically evidenced by replacing the two thin G_0 -lines of the bare bubble diagram with the thicker (“bold”) or, equivalently, with the double-lined G -lines of the dressed bubble (as illustrated in Fig. 6.3).

The physical picture is quite different, instead, for the vertex-correction terms, as these directly arise from the scattering between the particle and the hole (or between two particles or two holes) added to the system. In fact, the resummation of all these kind of (vertex) corrections reconstructs

the *full scattering amplitude* between the interacting electrons¹⁰. The vertex corrections are a distinctive element of the (interacting) *two*-particle Green's function ($G^{(2)}$), as they cannot be directly obtained from the knowledge of the interacting one-particle Green's function (even if one would know the exact one!), which reflects a typical hallmark of correlation: $G^{(2)} \neq G \times G$. From a more physical point of view, vertex corrections are mostly responsible for the differentiation of the system response w.r.t. different perturbations. For instance, they are known to typically drive a damping of the local charge response of a many-electron system, which occurs simultaneously with an enhancement of the magnetic one for increasing values of the on-site electronic interaction. Evidently, in most of the cases, the calculation of vertex corrections to the response function is more challenging than the evaluation of the "dressed" bubble term. However, if correlation effects are not negligible, the proper inclusion of vertex corrections is of pivotal importance for correctly capturing fundamental physical properties of the system¹¹ such as conservation laws, underlying symmetries or the Pauli exclusion principle, and often also for getting a quantitatively accurate comparison with experiments.

On a practical level, in order to calculate response functions diagrammatically, one should (i) first determine the expressions of \mathcal{O}_B and \mathcal{O}_A corresponding to the observable associated to the desired response (i.e., their matrix elements in the Pauli spinor space¹²) and then (ii) apply the usual Feynman-diagrammatic rules to include, order per order in perturbation theory, the corrections induced

by the electronic interaction $H_V \neq 0$ to the corresponding "bubble" term. The expressions of the specific bubble-term to be considered, starting point of the Feynman diagrammatic of the response functions, are particularly simple -as we have seen- in the case of charge ($\mathcal{O}_B = \mathcal{O}_A = \mathbb{1}$) or spin ($\mathcal{O}_B = \frac{\hbar}{2} \sigma_\beta$; $\mathcal{O}_A = \frac{\hbar}{2} \sigma_\alpha$) operators.

6.5 LRT for the electromagnetic field

A particularly important case of the LRT, for its direct application to a very broad class of spectroscopic experiments, is the calculation of the system response to the application of a electromagnetic (EM) field.

In this context, we will first consider the generic case of an **electrical current** $\vec{J}(r, t)$ induced by an applied (time/frequency and space/momentum dependent) **electric field** $\vec{E}(r, t)$.

¹⁰This has a direct physical interpretation in terms of the conventional scattering theory in the Fermi-liquid regime: The vertex function would corresponds to the scattering amplitude between two coherent quasi-particle excitations.

¹¹"[...]vertex corrections are usually very important and should be assumed to be important until shown otherwise" [G. D. Mahan, "Many Particle Physics", p. 499, Springer (US) 3.Edition (2000)]. A noticeable case in which is actually possible to prove vertex corrections are not relevant is represented by the dynamical mean-field theory (DMFT) calculation of the (thermal or electrical) *current-current* response (χ_{jj}) in the single orbital Hubbard model, cf. corresponding discussion in the last part of this chapter.

¹²Due to a somewhat inconvenient wording, \mathcal{O}_B and \mathcal{O}_A are sometimes referred to, in the literature, as "vertex operators", especially when they correspond to (thermal or electrical) current operators. In spite of the somewhat confusing name, they should not be confused with the vertex corrections described in the following.

Hence, in the LRT framework, we will consider the following expression:

$$\begin{aligned} \langle \vec{J}(r) \rangle_{\vec{E}}(t) - \underbrace{\langle \vec{J}(r) \rangle_{\vec{E}=0}}_{\text{no current wo. appl. field}} &= \int d^d r' \int_{-\infty}^t dt' \overset{\leftrightarrow}{\sigma}(r-r', t-t') \vec{E}(r', t') \\ \langle J_b(r) \rangle_{\vec{E}}(t) &= \int d^d r' \int_{-\infty}^t dt' \sigma_{ba}(r-r', t-t') E_a(r', t'), \end{aligned} \quad (6.53)$$

where the $a, b = x, y, z$ indicate the vector components of the electrical current \vec{J} and the electrical field \vec{E} , as well the ones of the corresponding conductivity tensor $\overset{\leftrightarrow}{\sigma}$. The latter quantity defines the linear response of the many-electron system to the perturbing electric field.

Eq.(6.53) acquires a particularly simplified expression in Fourier space, where convolution integrals become simple products:

$$\langle J_b(\mathbf{q}, \omega) \rangle_{\vec{E}} = \sigma_{ba}(\mathbf{q}, \omega) E_a(\mathbf{q}, \omega). \quad (6.54)$$

Evidently, our goal here will be to compute, Feynman diagrammatically, the explicit expression of the conductivity tensor $\sigma_{ba}(\mathbf{q}, \omega)$ for the many-electron problem under consideration.

In order to apply the Kubo-Nakano formula, introduced in Eq. (6.3) at the beginning of this chapter, one should first identify the operators/observable corresponding \hat{B} , \hat{A} as well the perturbing/external field $a(t)$. However, due to the specific gauge-invariance properties of the EM theory, this task is less trivial than in the simpler cases considered so far.

Intuitively, one would set:

- $\hat{B} = \vec{J}$, as this is our measured observable
- $a(t) = \vec{E}$, as this is our external perturbation
- $\hat{A} = ???$ – here, the corresponding identification is no longer straightforward, because, consistent with the gauge-invariance of the EM-theory, the coupling between the electrons in the system and the external field occurs via the vector potential $\vec{\mathcal{A}}(r, t)$ and *not* via $\vec{E}(r, t)$!

Hence, before we can apply the Kubo-Nakano formula, we should first understand how the EM field is coupled with operators/observables (\hat{A}) of the many-electron systems. As the explicit form of the coupling between electrically charged particles and the EM-field is dictated by the **gauge-invariance** of the electromagnetism, we must consider this important theoretical aspect explicitly, before proceeding with our LRT derivations.

As discussed in previous courses, electric and magnetic fields can be expressed in term of derivatives of the scalar (ϕ) and vector potential ($\vec{\mathcal{A}}$):

- $\vec{E} = -\frac{\partial \vec{\mathcal{A}}}{\partial t} - \vec{\nabla} \phi$
- $\vec{B} = \vec{\nabla} \times \vec{\mathcal{A}}$

(where we put $c = \hbar = 1$).

It should also be well known that no change in the value of physical observables (including the values of \vec{E} and \vec{B}) can occur under the following "gauge" transformation of the EM potential ($\phi, \vec{\mathcal{A}}$):

- $\vec{\mathcal{A}} \Rightarrow \vec{A} + \vec{\nabla} \Lambda$
- $\phi \Rightarrow \phi - \frac{\partial \Lambda}{\partial t}$,

\forall scalar functions $\Lambda(r, t)$.

When considering a system of charged particles (such as the particles of our many-electron problem) in the presence of an EM field, the gauge-invariance of the theory can be guaranteed by defining the coupling of the particles with electric charge $Q = -e$ with external EM field through the so-called “**minimal substitution**” This procedure corresponds -in practice- to replace each momentum operators $\vec{p} = -i\hbar\vec{\nabla}$ appearing in all system observables with

$$\vec{p} = -i\hbar\vec{\nabla} \implies (\vec{p} - Q\vec{\mathcal{A}}) = (-i\hbar\vec{\nabla} - Q\vec{\mathcal{A}}).$$

In particular, by applying the minimal substitution to our many-electron Hamiltonian, we have:

$$\begin{aligned} H = H_0 + H_V &= \sum_i \frac{p_i^2}{2m} + H_V \\ &\Rightarrow \sum_i \frac{(\vec{p}_i - Q\vec{\mathcal{A}}_i)^2}{2m} + \underbrace{Q \sum_i n(r_i) \phi_i}_{\text{neutral system}=0} + H_V \\ &= H_0 + H_V - \frac{Q}{2m} \sum_i (\vec{p}_i \vec{\mathcal{A}}_i + \vec{\mathcal{A}}_i \vec{p}_i), \end{aligned} \quad (6.55)$$

which, in the formalism of second quantization, reads:

$$\begin{aligned} H &= \int d^d r \psi^\dagger(r) \left(\frac{-\hbar^2 \vec{\nabla}_r^2}{2m} \right) \psi(r) + H_V \\ &= \int d^d r \psi^\dagger(r) \left(\frac{-\hbar \vec{\nabla}_r - Q\vec{\mathcal{A}}}{2m} \right)^2 \psi(r) + H_V \\ &= \int d^d r \left\{ \psi^\dagger(r) \left(\frac{-\hbar^2 \vec{\nabla}_r^2}{2m} \right) \psi(r) + \right. \\ &\quad \left. + \frac{i\hbar Q}{2m} \left[\psi^\dagger(r) \vec{\nabla} \cdot (\vec{\mathcal{A}} \psi(r)) + \psi^\dagger(r) \vec{\mathcal{A}} \cdot \vec{\nabla} \psi(r) \right] \right\} + H_V \\ &= H_0 + H_V + \\ &\quad + \frac{i\hbar Q}{2m} \int d^d r \left[-(\vec{\nabla} \psi^\dagger(r)) \cdot \vec{\mathcal{A}} \psi(r) + \psi^\dagger(r) \vec{\mathcal{A}} \cdot \vec{\nabla} \psi(r) \right] + o(\vec{\mathcal{A}}^2) \\ &= H - \int d^d r \left[\vec{j}(r) \cdot \vec{\mathcal{A}}(r) \right] + o(\vec{\mathcal{A}}^2), \end{aligned} \quad (6.56)$$

where we have introduced the so-called “*paramagnetic current*” operator, formally defined as

$$\begin{aligned} \vec{j}(r) &= -\frac{i\hbar Q \hbar q}{2m} [\psi^\dagger(r) \vec{\nabla}_r \psi(r) - \vec{\nabla}_r \psi^\dagger(r) \psi(r)] \\ &= -\frac{i\hbar Q \hbar q}{2m} [\psi^\dagger(r) (\vec{\nabla}_r - \overleftarrow{\nabla}_r) \psi(r)], \end{aligned} \quad (6.57)$$

which describes quantum-mechanically the particle-current operator in the *absence* of an external EM field.

On the basis of the explicit form (6.56) of the EM coupling, we can now readily identify the external perturbing field $a(t) = \vec{\mathcal{A}}(r, t)$ and the system observable coupled to it $\hat{A} = \vec{j}(r)$ within the usual Kubo-Nakano formalims of Eq. (6.3).

As for the measured observable \hat{B} , we have already mentioned this corresponds to the *physical* current operator $\vec{J}(r)$ of the many-electron systems in the *presence* of the external EM field. Consistent to the discussion above, in order to preserve the *gauge invariance* of our problem, the explicit expression of $\vec{J}(r)$ has to be derived applying the *minimal substitution* to the current operator in *absence* of the external field, i.e. to the paramagnetic current operator $\vec{j}(r)$ defined above in Eq. (6.57). Hence, since $\pm i\hbar \vec{\nabla} \Rightarrow \pm i\hbar \vec{\nabla} - Q\vec{\mathcal{A}}$, we get

$$\begin{aligned}\vec{J}(r) &= \frac{Q}{2m} \psi^\dagger(r) \left[-i\hbar(\vec{\nabla} - \overleftarrow{\nabla}) - 2Q\vec{\mathcal{A}} \right] \psi(r) \\ &= \vec{j}(r) - \frac{Q^2}{m} \psi^\dagger(r) \psi(r) \vec{\mathcal{A}}(r).\end{aligned}\quad (6.58)$$

Since the external perturbation $\vec{\mathcal{A}}$ explicitly appears in the second term of (6.58), in the context of the LRT, the corresponding quantum statistical average of the associated coefficient can be directly evaluated for $\vec{\mathcal{A}} = 0$:

$$\vec{J}(r) = \vec{j}(r) - \frac{Q^2}{m} \langle n(r) \rangle_{\vec{\mathcal{A}}=0} \vec{\mathcal{A}}(r). \quad (6.59)$$

Eventually, we see that the LRT expression for the electrical current induced by an external vector potential consists of two terms:

$$\underbrace{\langle \vec{J}(r, t) \rangle_{\vec{\mathcal{A}}}}_{\text{total physical current}} = \underbrace{\langle \vec{j}(r, t) \rangle_{\vec{\mathcal{A}}}}_{\text{paramagnetic term}} - \underbrace{\frac{Q^2}{m} \vec{\mathcal{A}}(r, t)}_{\text{diamagnetic term}}, \quad (6.60)$$

whereas, the second one, which is directly proportional to $\vec{\mathcal{A}}$, describes the “*diamagnetic*” response of the many-electron systems¹³

We can readily notice that all quantities appearing in the diamagnetic term are already explicit, and, therefore, such term does not need any further calculation. The paramagnetic term needs, instead, to be explicitly evaluated, which we can do now by means of a straightforward application of the Kubo-Nakano expression (namely, with $B = A = \vec{j}(r)$, $a(t) = \vec{\mathcal{A}}(r, t)$ and $Q = -e$):

$$H_t = H - \int d^d r \vec{j}(r) \vec{\mathcal{A}}(r, t) \quad (6.61)$$

$$\langle \vec{J}(r, t) \rangle_{\vec{\mathcal{A}}} = \underbrace{\langle \vec{j}(r, t) \rangle_{\vec{\mathcal{A}}}}_{\int d^d r' \int_{-\infty}^t dt' \chi_{jj}(r-r', t-t') \vec{\mathcal{A}}(r', t')} - e^2 \frac{n}{m} \vec{\mathcal{A}}(r, t), \quad (6.62)$$

where the paramagnetic part of the response function will given by $\overset{\leftrightarrow}{\chi}_{jj}(r-r', t-t') = -\frac{1}{i} \Theta(t-t') \langle [\vec{j}(r, t), \vec{j}(r', t')] \rangle_{\vec{\mathcal{A}}=0}$. Hence, by summing up the two contributions to the physical current, we

¹³For instance, it can be shown that this term is the only one, which does *not* vanish in the perfectly diamagnetic ground state of superconducting systems.

find:

$$\langle J_b(r, t) \rangle = \int d^d r' \int_{-\infty}^t dt' \underbrace{[\chi_{jj}^{ba}(r - r', t - t') - e^2 \frac{n}{m} \delta(r - r') \delta(t - t') \delta_{ba}]}_{K^{ba}(r - r', t - t')} A_a(r', t'), \quad (6.63)$$

which, in Fourier space, is simplified in the expression:

$$J_b(q, \omega) = \underbrace{[\chi_{jj}^{ba}(q, \omega) - e^2 \frac{n}{m} \delta_{ba}]}_{K^{ba}(q, \omega)} A_a(q, \omega), \quad (6.64)$$

where the tensor $K^{ba}(q, \omega)$ is known as “*electromagnetic kernel*”.

We must also underline, here, that the standard Kubo-Nakano expression for the paramagnetic-current response, i.e.

$$\chi_{jj}^{ba}(r - r', t - t') = -\frac{1}{i} \Theta(t - t') \langle [j_b(r, t), j_a(r', t')] \rangle_{\vec{A}=0}$$

is typically extracted, in practical calculation, from the associated expression in imaginary times, similarly as in the case of the LRT for the density and the magnetic perturbation discussed in the previous sections:

$$\chi_{jj}^{ba}(r - r', \tau - \tau') = \langle T_\tau j_b(r, \tau) j_a(r', \tau') \rangle_{\vec{A}=0}. \quad (6.65)$$

After deriving Eq.(6.64), an important, final step is needed to make direct contact with the quantities accessible in the spectroscopic experiments. In fact, Eq.(6.64) entails the EM response to the vector potential \vec{A} and *not* to the physical field \vec{E} actually applied in experiments.

This problem can be solved by exploiting the definition of \vec{E} in terms of the EM-potentials in a specific gauge, such as the Coulomb gauge (where $\vec{\nabla} \cdot \vec{A}(r, t) = 0$ and, w.l.o.g., $\phi(r, t)$ can be also set to 0), because the physical results will be eventually *independent* on such choice.

Hence, instead of the general expression

$$\vec{E}(r, t) = -\vec{\nabla} \phi(r, t) - \frac{\partial \vec{A}(r, t)}{\partial t}, \quad (6.66)$$

we will adopt the specific one, valid in the Coulomb gauge:

$$\vec{E}(r, t) = -\frac{\partial \vec{A}(r, t)}{\partial t}. \quad (6.67)$$

Hence, by inserting the corresponding expression of the anti-Fourier transformation $\vec{A}(t) = \int_{-\infty}^{+\infty} d\omega e^{-i\omega t} \vec{A}(\omega)$ (where we omitted the dependence on the spatial/momentum coordinates, for the sake of readability), one gets:

$$\vec{E}(\omega) = i\omega \vec{A}(\omega) \Rightarrow \vec{A}(\omega) = \frac{\vec{E}(\omega)}{i\omega}$$

Hence, by means of a simple substitution of $\vec{\mathcal{A}}$ in the previous expression, one obtains:

$$J_b(\mathbf{q}, \omega) = \frac{K^{ba}(\mathbf{q}, \omega) E_a(\mathbf{q}, \omega)}{i(\omega + i0^+)} = \frac{(\chi_{jj}^{ba}(\mathbf{q}, \omega) - e^2 \frac{n}{m} \delta^{ba}) E_a(\mathbf{q}, \omega)}{i(\omega + i0^+)}, \quad (6.68)$$

where, in order to properly treat the $\omega = 0$ singularity associated to the $1/i\omega$ term, we have included the usual vanishingly (imaginary) shift $\omega \rightarrow \omega + i0^+$, consistent with the *retarded* nature of the Kubo-Nakano response function. Hence, the final expression for the generalized EM conductivity tensor $\sigma_{ba}(\mathbf{q}, \omega)$ reads:

$$J_b(\mathbf{q}, \omega) = \underbrace{\frac{K^{ba}(\mathbf{q}, \omega)}{i(\omega + i0^+)}}_{=\sigma_{ba}(\mathbf{q}, \omega)} E_a(\mathbf{q}, \omega) = \sigma_{ba}(\mathbf{q}, \omega) E_a(\mathbf{q}, \omega), \quad (6.69)$$

where the EM kernel $K^{ba}(\mathbf{q}, \omega) = \chi_{jj}^{ba}(\mathbf{q}, \omega) - e^2 \frac{n}{m} \delta^{ba}$ can be explicitly computed by evaluating the paramagnetic part of the current response, $\chi_{jj}^{ba}(\mathbf{q}, \omega)$, via its standard Kubo-Nakano expression.

Before showing how to evaluate $\chi_{jj}^{ba}(\mathbf{q}, \omega)$ Feynman-diagrammatically, it is worth to discuss, more explicitly, a couple of important aspects related to the underlying gauge-invariance in the context of the many-electron theory.

6.5.1 Considerations on the gauge-invariance

In the previous subsection we have explicitly exploited the *gauge-invariance* of the EM-theory, by choosing a specific gauge (the Coulomb gauge), particularly convenient for making our analytic derivation easier, finally obtaining in Eqs. (6.68)-(6.69) a manifestly gauge-invariant expression (i.e., dependent on physical quantities only). Evidently, if we had chosen another gauge, we might have faced a more cumbersome derivation, but we would have obtained the same expression for the physical quantities, i.e., Eqs. (6.68)-(6.69), at the very end.

At the same time, the underlying gauge-invariance of the theory, as well as the associated electric charge conservation properties, is also directly reflected into specific, but exact relations, which the physical response functions of our many-electron systems to an EM perturbation must obey.

In particular, let us consider the following equations:

- **Continuity equation**

$$\frac{\partial \rho(r, t)}{\partial t} = -\vec{\nabla} \cdot \vec{J}(r, t) \Rightarrow -i\omega \rho(\mathbf{q}, \omega) + i\mathbf{q} \cdot \vec{J}(\mathbf{q}, \omega) = 0 \quad \text{with } \rho = -en \quad (6.70)$$

which ensures the local conservation of the electric charge (i.e., a time variation of the electric charge density at a specific position r is associated to simultaneous onset of a corresponding current \vec{J} flowing from there)

• **Invariance under gauge transformation**

$$\phi \Rightarrow \phi - \frac{\partial \Lambda}{\partial t} \xrightarrow{F.T.} \phi(\mathbf{q}, \omega) + i\omega \Lambda(\mathbf{q}, \omega) \quad (6.71)$$

$$\vec{\mathcal{A}} \Rightarrow \vec{\mathcal{A}} + \vec{\nabla} \Lambda \xrightarrow{F.T.} \vec{\mathcal{A}}(\mathbf{q}, \omega) + i\mathbf{q} \Lambda(\mathbf{q}, \omega) \quad (6.72)$$

These relations, linking the expression of the charge density to that of the current operator, evidently imply that the current and the charge (= density) response function of the many-electron systems cannot be completely independent one from the other. In order to derive the corresponding relations, it is here convenient to adopt (for this scope only) a 4-dimensional "relativistic" notation (with the Greek indices $\alpha, \beta = 0, 1, 2, 3$), defining

$q^\alpha = (\omega, \mathbf{q})$; $\mathcal{A}^\alpha = (\phi, \vec{\mathcal{A}})$; $J^\alpha = (\rho, \vec{J})$; $q_\alpha = (-\omega, \mathbf{q})$; $\mathcal{A}_\alpha = (-\phi, \vec{\mathcal{A}})$; $J_\alpha = (-\rho, \vec{J})$. In this formalism the two relations above yield, respectively:

- $-q_0 J_0 + \vec{q} \cdot \vec{J} = q_\beta J^\beta(\mathbf{q}, \omega) = 0 = q_\beta K^{\beta\alpha}(\mathbf{q}, \omega) \mathcal{A}_\alpha(\mathbf{q}, \omega) \Rightarrow q_\beta K^{\beta\alpha}(\mathbf{q}, \omega) \equiv 0$
- $K^{\beta\alpha}(\mathbf{q}, \omega) q_\alpha \Lambda(\mathbf{q}, \omega) = 0 \Rightarrow K^{\beta\alpha}(\mathbf{q}, \omega) q_\alpha \equiv 0,$

where, in the last steps, we have used the validity of the corresponding equalities $\forall \mathcal{A}_\alpha(\mathbf{q}, \omega)$ and $\forall \Lambda(\mathbf{q}, \omega)$, respectively.

The fulfilment of these specific relations between the charge/density and current response of many-electron systems might be then used to check whether the underlying gauge-invariance of the theory gets violated in the context of a given approximation scheme, or to evaluate the magnitude of such violation. In fact, while the exact solution (and, hence, per default, the non-interacting case) will always be gauge-invariant, once a specific (e.g., diagrammatic) approximation for the interacting problem is made, there isn't *a priori* any guarantee, whether such approximation will preserve the underlying gauge-invariance of the EM theory. Hence, violations of different severity of the exact relations (marked above in green color) between the different response functions might actually occur in approximate calculations. In general, the fulfillment/violation of the gauge-invariance within a given approximation is linked to the fulfillment/violation of specific equalities (known under the name of "*Ward identities*") between the one-particle self-energy and the irreducible two-particle vertex functions of the many-electron systems. Hence, depending on whether the approximation scheme considered does preserve or does alter such identities, the gauge-invariance of the theory will be preserved or violated.

Let us just mention, in this respect, that a well-definite route to construct "*conserving*" approximation schemes, i.e. approximations, which automatically preserve the gauge-invariance of the theory, is based on the so-called Luttinger-Ward functional $\Phi_{LW}[G]$, a functional of the interacting one particle Green's function (G), through which is possible to express the thermodynamic grand-potential of many-electron systems: By performing a (e.g., diagrammatic) approximation for $\Phi_{LW}[G]$, and then computing its first- and second-order functional derivatives allows to obtain expressions for the self-energy ($\Sigma = \frac{\delta \Phi_{LW}}{\delta G}$) and the irreducible vertex functions ($\Gamma = \frac{\delta^2 \Phi_{LW}}{\delta G^2}$), which automatically fulfill the Ward-identities, and hence, the gauge-invariance relations. A famous example, in this respect, is provided by the Hartree-Fock self-energy and the random phase approximation (RPA) expressions for the susceptibilities (see next chapter), which, taken together, build a well-known conserving approximation

scheme.

It should be stressed, however, that choosing the route of deriving a “conserving” approximation will not guarantee that all physical symmetries of the exact solution are correctly preserved. In fact, consistent with the empirical, all-day-life observation that, in general, “*there is no free lunch*”, conserving approximation schemes will typically violate other important physical properties, e.g., the crossing symmetries associated to the Pauli exclusion principle for the many-electron problem. Hence, the choice of the physical properties to be preserved should be carefully considered on the basis of the physical questions, before selecting or deriving the corresponding approximation scheme.

6.5.2 Calculation of the generalized conductivity for the non-interacting case

In order to illustrate how the diagrammatic calculations of the generalized conductivity tensor can be performed in practice, we start by showing, similarly as before, how the procedure works for the non-interacting case.

As discussed in the previous section, the LRT expression to consider for the EM response is:

$$J_b(\mathbf{q}, \omega) = \sigma_{ba}(\mathbf{q}, \omega) E_a(\mathbf{q}, \omega) \quad (6.73)$$

$$\sigma_{ba}(\mathbf{q}, \omega) = \frac{(\chi_{jj}^{ba}(\mathbf{q}, \omega) - e^2 \frac{n}{m} \delta^{ba})}{\underbrace{i(\omega + i0^+)}_{\frac{1}{2} \left(\mathcal{P} \frac{1}{\omega} - i\pi \delta(\omega) \right)}} \quad (6.74)$$

which can be separately written for the real and the imaginary part of the conductivity tensor as:

$$\text{Re } \sigma_{ba}(\mathbf{q}, \omega) = -\pi \left(\text{Re } \chi_{jj}^{ba}(\mathbf{q}, \omega) - e^2 \frac{n}{m} \delta^{ba} \right) \delta(\omega) + \frac{\text{Im } \chi_{jj}^{ba}(\mathbf{q}, \omega)}{\omega} \quad (6.75)$$

$$\text{Im } \sigma_{ba}(\mathbf{q}, \omega) = -\pi \text{Im } \chi_{jj}^{ba}(\mathbf{q}, \omega) \delta(\omega) - \frac{\text{Re } \chi_{jj}^{ba}(\mathbf{q}, \omega) - e^2 \frac{n}{m} \delta^{ba}}{\omega}.$$

As mentioned before, the only missing piece, which we still need to calculate here is the paramagnetic-current response, $\chi_{jj}^{ba}(\mathbf{q}, \omega)$. Since this can be expressed in term of a conventional Kubo-Nakano formula, for its evaluation we can follow essentially the same steps previously illustrated for the density and the magnetic response:

$$\begin{aligned} \chi_{jj}^{ba}(r - r', \tau - \tau') &= \langle T_\tau j_b(r, \tau) j_a(r', \tau') \rangle_{\vec{A}=0} = \\ &= -\frac{e^2}{4m^2} \langle T_\tau \psi^\dagger(r, \tau) (\vec{\nabla}_r - \overleftarrow{\nabla}_r)_b \psi(r, \tau) \psi^\dagger(r', \tau') (\vec{\nabla}_{r'} - \overleftarrow{\nabla}_{r'})_a \psi(r', \tau') \rangle, \end{aligned} \quad (6.76)$$

where one can define $\mathcal{O}_B = (\vec{\nabla}_r - \overleftarrow{\nabla}_r)_b$ and $\mathcal{O}_A = (\vec{\nabla}_{r'} - \overleftarrow{\nabla}_{r'})_a$ as the explicit expressions in real (coordinate) space corresponding to the b and a components of the paramagnetic current operator. Applying the Wick theorem, which is an exact procedure for the non-interacting case considered here,

yields the following contractions:

$$= -\frac{e^2}{4m^2} \langle T_\tau \psi^\dagger(r, \tau) (\vec{\nabla}_r - \overleftarrow{\nabla}_r)_b \psi(r, \tau) \psi^\dagger(r', \tau') (\vec{\nabla}_{r'} - \overleftarrow{\nabla}_{r'})_a \psi(r', \tau') \rangle = \quad (6.77)$$

$$= \underbrace{\langle \vec{J}(r, \tau) \rangle_{\vec{A}=0}}_{=0} \langle \vec{J}(r', \tau') \rangle_{\vec{A}=0} - \mathcal{O}_B(r, \tau) \circ \mathcal{O}_A(r', \tau') \quad (6.78)$$

where we have (reasonably) assumed that in absence of any external EM perturbation no electrical current is flowing. As a consequence, the calculation of $\chi_{jj}^{ba}(\mathbf{q}, \omega)$ reduces, for the non-interacting case, to the evaluation of a non-interacting ("bare") bubble term, which entails the two extra gradients associated to the paramagnetic current operator w.r.t. the bare-bubble term of the density/magnetic response discussed previously.

The explicit evaluation of this term can be most easily performed in Fourier space, as illustrated here below:

$$\xrightarrow{F.T.} \sim \nabla_b \begin{array}{c} \curvearrowright^k \\ \curvearrowleft^{k'} \end{array} \nabla_a \sim = \left| \begin{array}{c} k \Rightarrow k + \frac{q}{2} \\ k' \Rightarrow k - \frac{q}{2} \end{array} \right| = \sim \nabla_b \begin{array}{c} \curvearrowright^{k + \frac{q}{2}} \\ \curvearrowleft^{k - \frac{q}{2}} \end{array} \nabla_a \sim \quad (6.79)$$

$$= -\frac{e^2}{\beta} \sum_n \int \frac{d^d k}{(2\pi)^d} \frac{k_b k_a}{m^2} G^0(k + q/2, i\omega_n + i\Omega_m) G^0(k - q/2, i\omega_n) \quad (6.80)$$

$$= -\frac{e^2}{m^2} \int \frac{d^d k}{(2\pi)^d} k_b k_a \left[\frac{f(\epsilon_{k+q/2}) - f(\epsilon_{k-q/2})}{-i\Omega_m + \epsilon_{k+q/2} - \epsilon_{k-q/2}} \right], \quad (6.81)$$

where a change of momentum variable was made in Eq.(6.79), in order to make the dependence on the transfer momentum \mathbf{q} more transparent. Then, we have explicitly evaluated the summation over the fermionic Matsubara frequencies $i\nu_n$ in Eq. (6.80), obtaining the final expression (6.81). In Eq. (6.81), one can easily recognize between the square brackets the *Lindhardt function* expression (which defines the bare/non-interacting bubble term of the density/magnetic response) as well the additional momentum-dependent tensorial prefactor $k_b k_a$ which reflects the momentum structure of the (paramagnetic) current operator \vec{j} .

6.6 Optical Conductivity

The "optical" conductivity can be defined as the (absorption) spectrum associated to the response of our many-electron system to an applied EM-field with a frequency ranging from the far infrared-(FIR) to the near ultraviolet-range (UVR), which is typically measured by means of reflectivity or ellipsometry experiments¹⁴. The corresponding wavelengths are thus of the order $\lambda \approx 10^3 - 10^4 \text{\AA}$, i.e., several order of magnitude larger¹⁵ than the typical lattice spacing $a \sim 5 \text{\AA}$ of the materials we consider. Hence, one can quite safely neglect the space variation of the applied electric field:

$$E(\mathbf{r}, t) \cong \vec{E}(t) \xrightarrow{F.T.} \vec{E}(0, \omega) \delta_{\mathbf{q}, 0}.$$

¹⁴See the additional handwritten extra-notes for further details.

¹⁵And even larger values in the FIR!

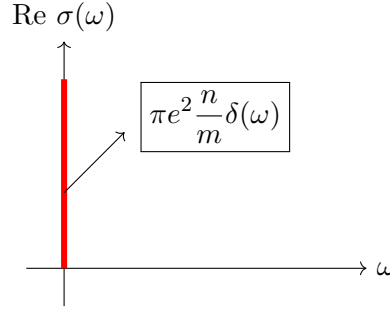


Figure 6.4: Sketch of the optical conductivity spectrum for the non-interacting case.

In practice, this means that we have to compute the corresponding conductivity tensor, e.g. from Eqs.(6.75) directly setting $\mathbf{q} = 0$. Further, one should note that, when considering the absorption part of the optical spectrum, this will be essentially encoded in $\text{Re}\sigma_{ba}$ (as its regular part explicitly depends on $\text{Im}\chi_{jj}$):

$$\text{Re}\sigma_{ba}(\mathbf{q} = 0, \omega) = \sigma_{ba}(\omega) = \underbrace{-\pi \left(\text{Re}\chi_{jj}^{ba}(0) - e^2 \frac{n}{m} \delta_{ba} \right) \delta(\omega)}_{\text{singular part} \propto \delta(\omega)} + \underbrace{\frac{\text{Im}\chi_{jj}^{ba}(\omega)}{\omega}}_{\text{regular part } \sigma_{\text{reg}}(\omega)} \quad (6.82)$$

By considering first, as usual, $H = H_0$ (i.e., the non-interacting case) we get:

$$\lim_{\mathbf{q} \rightarrow 0} \chi_{jj}(\mathbf{q}, \omega) = \lim_{\mathbf{q} \rightarrow 0} e^2 \int \frac{d^d k}{(2\pi)^d} \frac{k_\beta k_\alpha}{m^2} \left[\frac{f(\epsilon_{k+q/2}) - f(\epsilon_{k-q/2})}{-(\omega + i0^+) + \epsilon_{k+q/2} - \epsilon_{k-q/2}} \right] \equiv 0, \quad (6.83)$$

where we have directly performed the analytic continuation on the real frequency axis $i\Omega_m \rightarrow \omega + i0^+$. This results demonstrates that for the non-interacting cases, the regular part of the part of the optical conductivity exactly vanishes for all frequencies. Consequently, the optical conductivity of the non-interacting case reduces to its diamagnetic/singular part:

$$\text{Re}\sigma_{ba}(\omega) = \pi e^2 \frac{n}{m} \delta_{ba} \delta(\omega) \quad (6.84)$$

as also schematically depicted in Fig. 6.4 This apparently peculiar result has actually a clear physical origin: In the non-interacting systems -per definition- no electronic scattering process will occur and each electron will retain its initial momentum for ever¹⁶. This corresponds physically to the case of an ideal metal with zero DC resistivity $\rho_{DC} = 0$, or, equivalently, infinite DC conductivity $\sigma_{DC} = \frac{1}{\rho_{DC}} = +\infty$, the latter being directly marked by the singular δ -peak contribution at $\omega = 0$. The academic case of an “ideal/perfect metal” should not be confused, however, with the case of a superconductor. In fact, while superconductivity evidently implies $\rho_{DC} = 0$, this zero-resistivity condition occurs *in the presence* of electronic scattering processes. More specifically, $\rho_{DC} = 0$ is

¹⁶Formally, this reflects the fact that the paramagnetic current operator is a *constant of motion* for the non-interacting system. As such, \vec{j} will not depend on the time, making its commutator appearing in the Kubo-Nakano formula for χ_{jj} (and hence the entire paramagnetic part of the optical conductivity) exactly vanish.

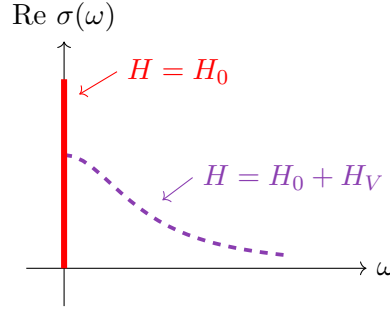


Figure 6.5: Sketch of the Drude expression of the optical conductivity as a result of Eq.(6.85) (purple), compared with the non-interacting result (red).

driven here by the *Meissner* effect (perfect diamagnetism) which characterizes the superconducting order and is not present in the perfect metal case.

Evidently, as soon as a scattering source (electron-phonon, electron-impurity or electron-electron) is introduced for a realistic description of the many-electron system, one can expect to observe a finite-life time τ for the propagation of coherent excitations in the material, which will immediately make $\chi_{jj} \neq 0$, depleting the singular term at $\omega = 0$. In general, these modifications w.r.t. the bare-bubble/perfect metal case will be encoded in the corresponding self-energy- and the vertex corrections to χ_{jj} , analogously as previously discussed in the case of the density and magnetic response for the interacting case. While we are not discussing here specific calculations of these quantities, we will try to heuristically understand -on the basis of general and intuitive arguments- which are the main effects of the inclusion of the electronic interaction on the optical conductivity results.

Even without further calculations, we know already that the interaction, via the $\text{Im } \Sigma(k_F, \omega \approx 0)$ can induce a finite life time $\frac{1}{\tau} \approx \text{Im } \Sigma(k_F, \omega \approx 0)$ of the electronic excitations. Hence, if we assume that a similar¹⁷ time-scale $\tau_{tr} \sim \tau$ will also control the coherent behavior of the electrons moving under the action of an electric field, possibly yielding a Drude-like behavior:

$$\sigma(\omega) = \frac{ne^2\tau}{m} \frac{1}{1-i\omega\tau} \Rightarrow \text{Re } \sigma(\omega) = \frac{ne^2\tau}{m} \frac{1}{1+\omega^2\tau^2}, \quad (6.85)$$

as schematically depicted in Fig. 6.5. Such Drude-like behavior often represents a fairly accurate approximation in the regime of weak-coupling electronic interactions.

More general, we note that the stronger interaction values are, the larger will be the shift of the optical spectral weight from low- to high-frequencies. We are intentionally using here the definition of "spectral weight *shift*", because as a consequence of the underlying gauge-invariance and of the associated conservation of the electric charge, the following sum-rule for the optical spectral weight holds:

$$\int_{-\infty}^{+\infty} d\omega \text{Re } \sigma(\omega) = -\pi(\chi'_{jj}(0) - e^2 \frac{n}{m}) + \int d\omega \frac{\chi''_{jj}(\omega)}{\omega} = \quad (6.86)$$

$$= \cancel{-\pi\chi'_{jj}(0)} + \pi e^2 \frac{n}{m} + \cancel{\pi\chi'_{jj}(0)} = \pi e^2 \frac{n}{m}, \quad (6.87)$$

¹⁷Of course, vertex corrections may significantly modify the value of such time-scale w.r.t. to the value estimated by the self-energy only, see, e.g., [1]

where, in the first line, we used the corresponding Kramers-Kronig relation for the (retarded) response function $\chi_{jj}(\omega)$. Eq.(6.87) is known under the name of Ferrell-Glover-Tinkham sum-rule or, more often, referred to as "f-sum-rule". Evidently, as a consequence of Eq. (6.87), whenever the electronic density n is fixed (which is most often the case), the optical spectral weight can be only shifted between different frequency region e.g., when the electronic interaction is varied in the calculations and/or when external parameters are changed in the experiments.

In order to illustrate the effect of an progressively increasing electronic interaction in a more concrete fashion we consider the case of Hubbard-Model, i.e., of one of the most fundamental lattice models used to describe the effects of electronic correlations in condensed matter physics[11, 3], whose Hamiltonian reads:

$$H = -t \sum_{\langle i,j \rangle, \sigma=\uparrow, \downarrow} (c_{i\sigma}^\dagger c_{j\sigma} + h.c.) + U \sum_i n_{i\uparrow} n_{i\downarrow} - \mu \sum_{i,\sigma} n_{i\sigma}, \quad (6.88)$$

where i and j indicate the positions on the specific lattice considered¹⁸, $\sigma = \uparrow, \downarrow$ the spin-configuration of the electrons, t the probability amplitude for an electron to "hop" between neighboring sites i and $j = i \pm 1$, U the local Coulomb electrostatic repulsion ("Hubbard interaction") between two electrons with opposite spin occupying the same site i , and μ the chemical potential.

Further, as the Hubbard Hamiltonian in Eq. (6.88), in spite of its apparently formal simplicity, cannot be exactly solved for the general three or two-dimensional case, we will consider in the following its non-perturbative description provided by the *Dynamical Mean-Field Theory* (DMFT) [6]. While a focused lecture about the DMFT will be given at the end of the QFT-VO, we can anticipate here that DMFT represents a powerful many-body approach in which the *purely local* part of the irreducible diagrams (i.e., the self-energy at the one-particle level and the two-particle irreducible vertex functions) is retained, *non-perturbatively*, at *all* order in the Hubbard interaction U , while, on the other hand, all non-local spatial dependencies of these quantities are fully neglected. For the purposes of our discussion of the optical conductivity response, this means that the self-energy and the irreducible vertex functions will not depend on momenta but only on frequencies [e.g., $\Sigma(\mathbf{k}, i\nu_n) \xrightarrow{\text{DMFT}} \Sigma(i\nu_n)$].

In this (DMFT-based) framework, we expect the following evolution when progressively increasing the local ("Hubbard") interaction U in Eq.(6.88). We start, once again, from the non-interacting case, which here means $U = 0$. In such case, schematically illustrated in Fig. 6.6, the electronic self-energy will be identically zero, the one-particle spectral function will coincide to the D.O.S. of the model (e.g., for a Bethe lattice in the limit of high-coordination/dimensions it will be semi-circularly shaped), the bare bubble term of χ_{jj} will exactly vanish, and, thus, we will find the expected (singular) behavior of the optical response for a perfect metal, analogous to that already shown in Fig. 6.4.

By turning on the interaction U , one obviously gets finite results for both the self-energy and the irreducible vertex functions. However, as we already mentioned, these quantities are purely local (i.e., momentum-independent) in the DMFT approximation, which allows for an important simplification of the calculation of the optical conductivity in the interacting case. In fact, it can be rigorously shown that the inclusion of a momentum-independent irreducible vertex functions Γ in the paramagnetic current response function, makes all possible vertex correction vanish for all one-band lattice model (such

¹⁸For example, a three dimensional simple cubic lattice, or, as it is sometime assumed for the sake of mathematical simplicit, a Bethe-lattice, whose DOS acquires a particularly easy semi-circular shape in the limit of large coordination/dimensions)

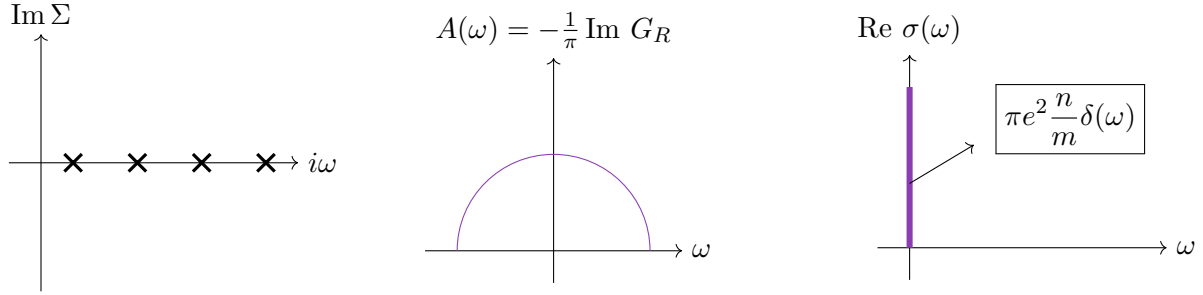


Figure 6.6: Sketch of the Hubbard model results in the non-interacting case, $U \equiv 0$. Left panel: self-energy; Middle panel: local spectral function (e.g., for the Bethe-lattice case); right: optical conductivity.

as the Hubbard model in Eq.(6.88)), due to the odd-symmetry of the gradient/current operator under the internal momentum k and/or k' summations. Hence, for computing the optical conductivity at the DMFT level, we just need to consider the self-energy corrections to $\chi_{jj}(\mathbf{q}=0, i\Omega_n)$, i.e., the “dressed” bubble-term, where the two non-interacting Green’s functions G_0 are replaced with the corresponding interacting ones (and in this case, with the DMFT ones, i.e., $G(k, i\nu_n) = [G_0^{-1}((k, i\nu_n) - \Sigma(i\nu_n))]^{-1}$), as schematically illustrated below:

$$\begin{aligned}
 & \text{Diagram: A bubble diagram with two vertices labeled } \nabla_b \text{ and } \nabla_a. \text{ The top arc is labeled } k + \frac{q}{2}, i\nu + i\Omega \text{ and the bottom arc is labeled } k - \frac{q}{2}, i\nu. \\
 & \propto \frac{1}{\beta} \sum_n \sum_k k_b k_a \underbrace{G(k + \frac{q}{2}, i\nu_n + i\Omega)}_{\int d\omega_1 \frac{A_{k+\frac{q}{2}}(\omega_1)}{i\nu_n + i\Omega - \omega_1}} \underbrace{G(k - \frac{q}{2}, i\nu_n)}_{\int d\omega_2 \frac{A_{k-\frac{q}{2}}(\omega_2)}{i\nu_n - \omega_2}},
 \end{aligned}$$

where we used the spectral representation of the (interacting) DMFT Green’s function G , in order to make it easier to perform the Matsubara summation¹⁹ over $i\nu_n$ in the dressed bubble-term. After having performed the Matsubara summation, having set $\mathbf{q} = 0$ and having made the analytic continuation of the bosonic Matsubara frequency ($i\Omega_m \rightarrow \omega + i0^+$), we get the following expression for the *regular* part of the optical conductivity [cf. Eq. (6.82)]:

$$\Rightarrow \sigma_{ba}(\omega) \propto \sum_k k_b k_a \int d\omega_1 A_k(\omega_1) A_k(\omega_1 + \omega) \left[\frac{f(\omega_1) - f(\omega_1 + \omega)}{\omega} \right]. \quad (6.89)$$

This expression suggests that one should expect significant contributions to $\sigma_{ba}(\omega)$ when the product

¹⁹In fact, differently from the non-interacting case, we do not know, in general, an analytic expression for $G(k, i\nu_n)$. In this case, resorting to its spectral representation formally allows to make explicit its analytic dependence on the Matsubara frequencies, and hence to more easily perform the corresponding summation. Clearly, the “actual” hurdle of the calculation remains posed by the evaluation of the *interacting* one-particle spectral function $A_k(\omega) = -\frac{1}{\pi} G_R(k, \omega)$ on the real frequency axis.

of $A_k(\omega_1) A_k(\omega_1 + \omega)$ is sizable, i.e., when for a given frequency ω both $A_k(\omega_1)$ and $A_k(\omega_1 + \omega)$ are large enough.

In the following, for the sake of simplicity, we will discard the k -dependence in all the quantities of Eq. (6.89), and focus on the frequency-domain only.

In the weak-to-intermediate coupling domain, the DMFT calculations often yield a self-energy similar to that shown in the left panel of Fig. 6.7. One can easily recognize that its behavior as a function of the Matsubara frequency $i\omega_n$ corresponds to the one expected in the Fermi-liquid regime, yielding a sizable mass renormalization (via its slope in the limit of $i\omega_n \rightarrow 0$) and a finite life-time (via its finite intercept for $i\omega_n \rightarrow 0$) of the quasi-particle excitations. As a result, the corresponding spectral function $A(\omega)$ will display a renormalized low-energy quasi-particle peak (of spectral weight $Z = \frac{m}{m^*}$, marked in violet color in the central panel of Fig. 6.7) and an incoherent background of spectral weight $1 - Z$, marked in red) at larger positive/negative frequencies. The latter spectral feature, if U is comparable with the bandwidth of the non-interacting problem, becomes clearly separated by the central quasi-particle peak, heralding the emergence of the so-called “Hubbard-bands”, located approximatively at $\omega = \pm \frac{U}{2}$.

This characteristic shape of the spectral function $A(\omega)$, which is a typical hallmark of how the physics of correlated metal is captured by DMFT, is directly reflected in the corresponding shape of $\sigma(\omega)$ (we assume here to treat a homogeneous and isotropic case, i.e., $\sigma_{ba}(\omega) = \delta_{ab} \sigma(\omega)$). Specifically, in the low-frequency regime a large value of $\sigma(\omega)$ will be found, due to the relatively large quasi-particle-peak contributions of both $A(\omega_1)$ and $A(\omega_1 + \omega) \sim A(\omega_1)$ at low-frequency. The corresponding optical transitions between coherent quasi-particle excitations at small ω yield the typical Drude-peak in $\sigma(\omega)$ discussed already before.

At the same time, for intermediate values of ω one gets possible optical transitions between the low-energy quasi-particle peak and the emerging Hubbard-bands. These optical transitions, marked by the corresponding blue arrows in Fig. 6.7 feature a rather featureless bump in $\sigma(\omega)$, which is sometimes labelled with MIR²⁰, due to a loose analogy of its intermediate frequency location with similar spectral features actually observed in IR/optical experiments of correlated materials. Finally, for larger frequencies of order U , optical transitions between the incoherent states of the two Hubbard-bands will become possible, yielding a further (but way smaller in magnitude) increase of $\sigma(\omega)$ in the high-frequency regime of $\omega \sim U$.

The last case to be examined is the strongly-correlated regime, where the Hubbard interaction U is larger than all other energy scales of the problem (i.e., temperature, bandwidth, etc.). In such situation, the potential-energy cost to be paid by the electrons for double-occupying any lattice site of the system might become so large to completely hinder any coherent electronic motion: This situation corresponds to a so-called *Mott-insulating phase*, to be clearly distinguished from a conventional band-insulator, in that the physical origin of the Mott insulating behavior is the large value of the local electrostatic/Coulomb repulsion U and *not* the Pauli-principle as in a band-insulator.

The hallmark of the major role played by the electronic interaction in this case is immediately recognizable in the self-energy behavior (s. left panel of Fig. 6.8), which looks exactly the opposite of the correlated Fermi-liquid/metallic regime considered above: $\text{Im}\Sigma(i\omega_n)$ now strongly *increases* in absolute value for $i\omega_n \rightarrow 0$, and it can even *diverge* in the low-temperature limit. As the self-energy appears in the denominator of the Green’s function, such behavior corresponds to a significant

²⁰MIR = Mid-Infrared

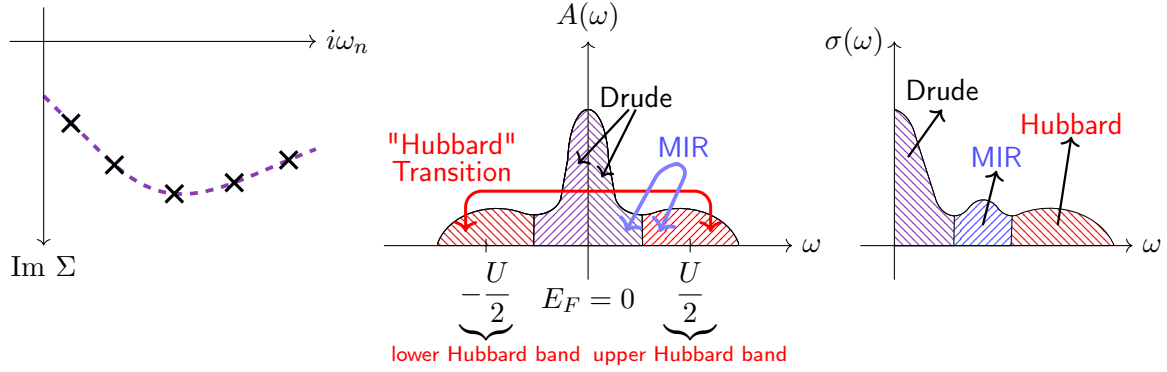


Figure 6.7: Sketch of the DMFT results for the Hubbard model in the correlated Fermi-liquid/metallic regime, of low-to-intermediate U values. Left panel: imaginary part of self-energy as a function of the Matsubara frequency; Middle panel: local spectral function (e.g., its k -integrated value); right: optical conductivity.

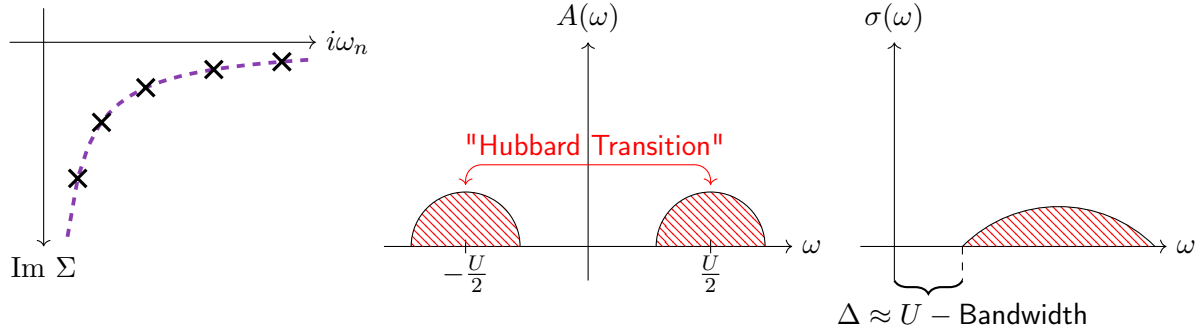


Figure 6.8: Sketch of the DMFT results for the Hubbard model in the Mott insulating regime, of large values of U . Left panel: imaginary part of self-energy as a function of the Matsubara frequency; Middle panel: local spectral function (e.g., its k -integrated value); right: optical conductivity.

suppression of the low-frequency spectral weight in $A(\omega)$. In fact, by looking at the $A(\omega)$ computed by means of DMFT in the Mott insulating regime (cf. the central panel of Fig. 6.8), one notes the complete disappearance of the coherent quasi-particle peak, which leaves a large spectral ("Mott insulating") gap between the two remaining incoherent Hubbard-bands.

Following the same reasoning as above, it is clear that now only high-frequency optical transitions will be allowed, preventing the formation of both the Drude-peak as well as of the MIR contribution: The resulting $\sigma(\omega)$ will display a large spectral gap, whose size scales with U , perfectly consistent with the insulating nature of the Mott regime.

Chapter 7

Random phase approximation (RPA)

The RPA is a technique to approximately calculate susceptibilities χ for *interacting* systems. Among others, RPA can describe *collective* excitations and many-body renormalizations beyond Hartree-Fock.

7.1 Derivation of the RPA in the context of screening

Imagine we subject our system, described by the Hamiltonian H , to an external and time-dependent perturbation V_t .

$$H_t = H + V_t \quad (7.1)$$

where $V_t = -\int d^3r \rho(\mathbf{r}, t) V(\mathbf{r}, t)$ is an explicitly time-dependent potential that shall describe the coupling of the system's charge density ρ to the (instantaneous) Coulomb interaction

$$V(\mathbf{r}, t) = \int d^3r' \frac{e^2}{|\mathbf{r} - \mathbf{r}'|} \rho_{ext}(\mathbf{r}') \delta(t) \quad (7.2)$$

arising from an additional, external electron density $\rho_{ext}(\mathbf{r})$. For example, $\rho_{ext}(\mathbf{r}') = \delta(\mathbf{r}')$ could describe a single test charge at position \mathbf{r}' , see Fig. 7.1 for an illustration. This perturbation will

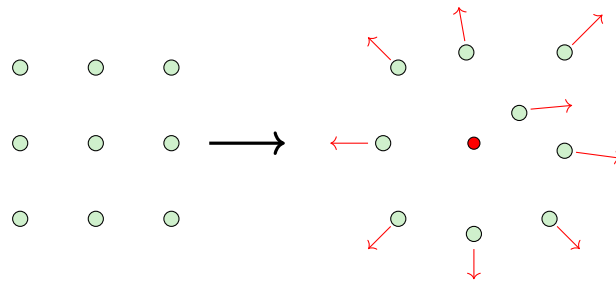


Figure 7.1: Coulomb repulsion in an electron gas $\circ \circ \circ$ in presence of a (negative) test charge \bullet . The perturbation is mitigated (*screened*) as the system's density reacts to it.

induce a change in the charge distribution of the original system. When Fourier-transforming to \mathbf{q} and ω , this change is given by

$$\langle \delta\rho(\mathbf{q}, \omega) \rangle = \langle \rho(\mathbf{q}, \omega) \rangle - \langle \rho(\mathbf{q}, \omega) \rangle_{V=0} = \frac{4\pi e^2}{q^2} \chi(\mathbf{q}, \omega) \rho_{ext}(\mathbf{q}, \omega) \quad (7.3)$$

where we used $\int d^3r \int d^3r' e^{i\mathbf{q}(\mathbf{r}-\mathbf{r}')}/|\mathbf{r}-\mathbf{r}'| = 4\pi/q^2$ for the Coulomb interaction. The response, or change in density, *screens* the perturbation: The extra charge density is accommodated by a rearrangement of the system's charge carriers, a process that effectively weakens the perturbation. The crucial idea now is to describe the external perturbation in a way that already accounts (to an extent) for the system's reaction. The following Ansatz suggests itself:

$$\langle \delta\rho(\mathbf{q}, \omega) \rangle = \frac{4\pi e^2}{q^2} \tilde{\chi}(\mathbf{q}, \omega) (\rho_{ext}(\mathbf{q}, \omega) - \langle \delta\rho(\mathbf{q}, \omega) \rangle) \quad (7.4)$$

In other words, we compute the response to a perturbation given by a modified “*screened*” external density, i.e., the original external density ρ_{ext} , *minus* the portion $\langle \delta\rho(\mathbf{q}, \omega) \rangle$ of the system's charge that redistributes because of the initial “*bare*” perturbation. Since the perturbation has changed, also the response function is different from the one described by Eq. (7.3); we called it $\tilde{\chi}$. Combining Eqs. (7.3) and (7.4), we obtain a relation between (a) the response χ to the *bare* perturbation and (b) the response $\tilde{\chi}$ to the *screened* perturbation:

$$\chi(\mathbf{q}, \omega) = \frac{\tilde{\chi}(\mathbf{q}, \omega)}{1 + \frac{4\pi e^2}{q^2} \tilde{\chi}(\mathbf{q}, \omega)} \quad (7.5)$$

or, generalizing to an arbitrary interaction $V(\mathbf{q})$

$$\chi(\mathbf{q}, \omega) = \frac{\tilde{\chi}(\mathbf{q}, \omega)}{1 + V(\mathbf{q}) \tilde{\chi}(\mathbf{q}, \omega)} \quad (7.6)$$

So far, we haven't actually computed any susceptibility. The point now is that it stands to reason that approximating $\tilde{\chi}$ instead of χ is better, since the perturbation at its origin is, in a sense, weaker. That the perturbation is indeed effectively smaller can be seen as follows. We have

$$\langle \delta\rho(\mathbf{q}, \omega) \rangle \stackrel{(7.4)}{=} V(\mathbf{q}) \tilde{\chi}(\mathbf{q}, \omega) (\rho_{ext}(\mathbf{q}, \omega) - \langle \delta\rho(\mathbf{q}, \omega) \rangle) \stackrel{(7.3)}{=} V(\mathbf{q}) \chi(\mathbf{q}, \omega) \rho_{ext}(\mathbf{q}, \omega) \quad (7.7)$$

$$\equiv V^{\text{eff}}(\mathbf{q}, \omega) \tilde{\chi}(\mathbf{q}, \omega) \rho_{ext}(\mathbf{q}, \omega) \quad (7.8)$$

where we defined an effective interaction V^{eff} , for which holds

$$V^{\text{eff}}(\mathbf{q}, \omega) = \frac{V(\mathbf{q}) \chi(\mathbf{q}, \omega)}{\tilde{\chi}(\mathbf{q}, \omega)} \stackrel{(7.6)}{=} \frac{V(\mathbf{q})}{1 + V(\mathbf{q}) \tilde{\chi}(\mathbf{q}, \omega)} = \varepsilon^{-1}(\mathbf{q}, \omega) V(\mathbf{q}) \leq V(\mathbf{q}) \quad (7.9)$$

where $\varepsilon(\mathbf{q}, \omega)$ is the dielectric function and the last inequality holds in the limit ($\mathbf{q} \rightarrow 0, \omega = 0$), since (as we will later show, see Eq. (7.47)) $\tilde{\chi}(\mathbf{q} \rightarrow 0, \omega = 0) \geq 0$.

In the RPA, one uses the simplest possible approximation to the *screened* susceptibility: $\tilde{\chi} = \chi^0$. In other words, the screened response is approximated by the susceptibility of the *non-interacting* system. Consequently

$$\chi^{\text{RPA}}(\mathbf{q}, \omega) = \frac{\chi^0(\mathbf{q}, \omega)}{1 + V(\mathbf{q})\chi^0(\mathbf{q}, \omega)} \quad (7.10)$$

$$V^{\text{RPA}}(\mathbf{q}, \omega) = \frac{V(\mathbf{q})}{1 + V(\mathbf{q})\chi^0(\mathbf{q}, \omega)} \quad (7.11)$$

While the screened response is by construction independent of the interaction, the RPA susceptibility depends on $V(\mathbf{q})$. However, this dependence is merely *explicit*. Indeed, complicated expectation values for the interacting system are obviated. All that is needed is the evaluation of the susceptibility, χ^0 , of the system in the non-interacting limit.

For the following it will be useful to recall the geometric series, $\sum_{n=0}^{\infty} x^n = \frac{1}{1-x}$ for $|x| < 1$. Indeed, assuming convergence, we can rewrite the above RPA equations as a series expansion

$$\chi^{\text{RPA}}(\mathbf{q}, \omega) = \frac{\chi^0(\mathbf{q}, \omega)}{1 + V(\mathbf{q})\chi^0(\mathbf{q}, \omega)} = \chi^0 + \chi^0(-V)\chi^0 + \dots \quad (7.12)$$

$$-V^{\text{RPA}}(\mathbf{q}, \omega) = \underbrace{[1 + V(\mathbf{q})\chi^0(\mathbf{q}, \omega)]^{-1}}_{\varepsilon(\mathbf{q}, \omega)} (-V(\mathbf{q})) = [1 + (-V)\chi^0 + \dots](-V) \quad (7.13)$$

7.2 Diagrammatic representation

We will now make the connection to the description in terms of Feynman diagrams. From linear response, see chapter 6, we know that

$$\chi^0(r, r', t) = -\frac{1}{i\hbar} \Theta(t) \langle [\rho(r, t), \rho(r', 0)] \rangle_{H_0} \quad (7.14)$$

where H_0 is the non-interacting part of the system's Hamiltonian. We could evaluate the commutator explicitly. Here, instead, we will express χ_0 in terms of Green's functions via Wick's theorem (cf. section 5.2). Using

$$\rho(r) = \sum_{\sigma} \psi_{\sigma}^{\dagger}(r) \psi_{\sigma}(r) = \sum_{kk'} c_{k\sigma}^{\dagger} c_{k'\sigma} e^{i(k'-k)r} = \sum_{kq\sigma} c_{k\sigma}^{\dagger} c_{(k+q)\sigma} e^{iqr} \quad (7.15)$$

and writing χ in the Matsubara imaginary time τ formalism

$$\chi^0(r, r', \tau) = \sum_{kq\sigma} \sum_{k'q'\sigma'} \langle \mathcal{T}_{\tau} c_{k\sigma}^{\dagger}(\tau) c_{(k+q)\sigma}(\tau) c_{k'\sigma'}^{\dagger}(0) c_{(k'+q')\sigma'}(0) \rangle_{H_0} e^{iqr} e^{iq'r'} \quad (7.16)$$

$$= \sum_{kk'\sigma\sigma'q} e^{iq(r-r')} \langle \mathcal{T}_{\tau} c_{k\sigma}^{\dagger}(\tau) c_{(k+q)\sigma}(\tau) c_{k'\sigma'}^{\dagger}(0) c_{(k'-q)\sigma'}(0) \rangle_{H_0} . \quad (7.17)$$

Where we exploited momentum conservation, i.e., $k + k' = k + q + k' + q' \Leftrightarrow q' = -q$. Then, Wick's theorem gives

$$\chi^0(q, \tau) = \sum_{kk'\sigma\sigma'} \langle \mathcal{T}_\tau c_{k\sigma}^\dagger(\tau) c_{(k+q)\sigma}(\tau) c_{k'\sigma'}^\dagger(0) c_{(k'-q)\sigma'}(0) \rangle_{H_0} \quad (7.18)$$

$$= \sum_{kk'\sigma\sigma'} \underbrace{\langle \mathcal{T}_\tau c_{k\sigma}^\dagger(\tau) c_{(k+q)\sigma}(\tau) \rangle}_{\delta_{q0} n_{k\sigma}} \underbrace{\langle \mathcal{T}_\tau c_{k'\sigma'}^\dagger(0) c_{(k'-q)\sigma'}(0) \rangle}_{\delta_{q0} n_{k'\sigma'}} \quad (7.19)$$

$$+ \sum_{kk'\sigma\sigma'} \underbrace{\langle \mathcal{T}_\tau c_{k\sigma}^\dagger(\tau) c_{(k'-q)\sigma'}(0) \rangle}_{G_{k\sigma}(-\tau)} \underbrace{\langle \mathcal{T}_\tau c_{(k+q)\sigma}(\tau) c_{k'\sigma'}^\dagger(0) \rangle}_{-G_{k+q}(\tau) \delta_{k+q, k'} \delta_{\sigma\sigma'}}$$

$$= - \sum_{k, \sigma} G_{k\sigma}^{(0)}(-\tau) G_{(k+q)\sigma}^{(0)}(\tau) = 0 \quad \begin{array}{c} k+q, \sigma \\ \circlearrowleft \\ k, \sigma \end{array} \quad \tau \quad (7.20)$$

The first term in Eq.(7.19) only contributes for $q = 0$, i.e., it is uniform in space, $f(q = 0) = \int d^3r f(r)$. Further, it is τ -independent, i.e., static. Thus corresponding to a mere global shift, we will neglect this term. With only the bubble diagram remaining, and using Eq. (7.12), we see that the RPA consists of the following subset of 2-particle diagrams:

$$\underbrace{\text{bubble}}_{\chi^{\text{RPA}}} = \underbrace{\text{bubble}}_{\chi^0} + \underbrace{\text{bubble with wavy line}}_{\chi^0(-V)\chi^0} + \underbrace{\text{bubble with two wavy lines}}_{\mathcal{O}(V^2)} + \dots \quad (7.21)$$

Where the minus sign in front of V comes from the corresponding Feynman rule: one minus sign per power of the interaction. In turn, the screened interaction can be represented as

$$\underbrace{\text{wavy line}}_{-V_{\text{eff}}} = \underbrace{\text{wavy line}}_{-V} + \underbrace{\text{wavy line with bubble}}_{(-V)\chi^0(-V)} + \underbrace{\text{wavy line with two bubbles}}_{(-V)(\chi^0(-V))^2} + \dots \quad (7.22)$$

This (two-particle) series is similar to the (one-particle) Dyson equation for the Green's function

$$\Rightarrow \Rightarrow = \Rightarrow \Rightarrow + \Rightarrow \Rightarrow (\Sigma) \Rightarrow \Rightarrow. \quad (7.23)$$

Indeed, in complete analogy, we can visualize Eq. (7.11) by

$$\underbrace{\text{wavy line}}_{-V_{\text{eff}}} = \underbrace{\text{wavy line}}_{-V} + \underbrace{\text{wavy line with bubble}}_{-V\chi^0(-V_{\text{eff}})} \quad (7.24)$$

which is a so called Bethe-Salpeter-equation (BSE).

The RPA is an approximation that contains a subset of two-particle diagrams. The general expression of the screened interaction can be visualized by

$$\text{wavy line} \text{---} \boxed{P} \text{---} \text{wavy line}$$

where P is a place-holder for all possible, so-called polarization diagrams:

$$\begin{aligned}
 \boxed{P} = & \underbrace{\text{RPA}} + \underbrace{\text{renormalized propagators}} + \underbrace{\text{vertex correction}} \\
 & \Rightarrow \text{...} + \text{...} + \dots
 \end{aligned} \tag{7.25}$$

First, we note that the polarization only contains diagrams that are “V-irreducible”. Indeed, diagrams that can be disconnected into two parts by cutting an interaction line (see, e.g., the stroked out diagram above) are recursively generated in the BSE and have thus to be excluded in the polarization. This is in complete analogy to the irreducibility of the self-energy. There, the recursion in Dyson’s equation generates diagrams that can be separated into two part when cutting a Green’s function line. Second, the RPA is the lowest order approximation of the V-irreducible polarization. Higher order terms can be classified into two categories (cf. the discussion in Sec. 6.4.3): (1) diagrams where individual Green’s function lines are dressed with self-energy insertions. These diagrams can be accounted for in so-called “bold” theories, where the free propagators G_0 (single line) are replaced with interacting Green’s functions (double line), see Fig. 6.3. More complicated are (2) diagrams in which interactions couple different propagators. These terms are called “vertex corrections”.

The RPA is non-perturbative in the sense that in the susceptibility, terms to all order in the interaction are generated. Still, as is evident from the above diagrams, there are contributions, again, at all orders, that are not included in the RPA. Therefore, the RPA is in practice still an approach best suited for weak coupling.

7.3 RPA for the electron-gas

We will now apply the RPA to the (interacting) electron gas.

7.3.1 Evaluation of χ^0

For the evaluation of χ^0 in the Matsubara formalism we start with

$$\chi^0(q, i\nu_n) = -2 \sum_k \sum_{i\omega_m} \frac{1}{\beta} G_0(k+q, i\omega_m + i\nu_n) G_0(k, i\omega_m) \quad (7.26)$$

$$= -\frac{2}{\beta} \sum_k \sum_{i\omega_m} \frac{1}{i\omega_m + i\nu_n - \epsilon_{k+q}} \frac{1}{i\omega_m - \epsilon_k} \quad (7.27)$$

$$= -2 \sum_k \frac{1}{2\pi i} \oint dz \frac{f(z)}{(z + i\nu_n - \epsilon_{k+q})(z - \epsilon_k)} \quad (7.28)$$

$$\left(\begin{array}{l} \text{partial fraction} \\ \text{decomposition} \end{array} \right) \rightarrow = -2 \sum_k \frac{1}{2\pi i} \oint dz \left(\frac{f(z)}{z - \epsilon_k} - \frac{f(z)}{z + i\nu_n - \epsilon_{k+q}} \right) \frac{1}{i\nu_n - (\epsilon_{k+q} - \epsilon_k)} \quad (7.29)$$

$$= -2 \sum_k [f(\epsilon_k) - f(\epsilon_{k+q} - i\nu_n)] \frac{1}{i\nu_n - (\epsilon_{k+q} - \epsilon_k)} \quad (7.30)$$

$$= -2 \sum_k \frac{f(\epsilon_k) - f(\epsilon_{k+q})}{i\nu_n - (\epsilon_{k+q} - \epsilon_k)}, \quad (7.31)$$

where we used $\nu_n = \frac{2n\pi}{\beta} \rightarrow e^{i\beta\nu_n} = 1 \Rightarrow f(\epsilon_{k+q} - i\nu) = f(\epsilon_{k+q})$ to get from the fourth to the fifth line.¹ Analytical continuation to real frequencies $i\nu \rightarrow \omega + i0^+$ leads to

the **LINDHARD** Function

$$\chi^0(q, \omega) = 2 \sum_k \frac{f(\epsilon_{k+q}) - f(\epsilon_k)}{\omega - (\epsilon_{k+q} - \epsilon_k) + i0^+} \quad (7.32)$$

Quite generally, poles in propagators or susceptibilities describe eigenmodes of the system. $\text{Re } \chi^0(q, \omega)$ diverges for $\omega = \epsilon_{k+q} - \epsilon_k > 0$ if ϵ_k is an occupied and ϵ_{k+q} an empty state. One speaks of particle-hole excitations, see Fig. 7.2.

7.3.2 Eigenmodes encoded in χ^{RPA} excitations

What are the excitations encoded in the RPA susceptibility? For this, we perform in Fig. 7.3 a graphical analysis of

$$\chi^{\text{RPA}}(q, \omega) = \frac{\chi_0(q, \omega)}{1 + V(q)\chi_0(q, \omega)}. \quad (7.33)$$

at fixed momentum q . The (real-part of the) RPA susceptibility diverges when the denominator cancels, i.e., $V(q)\chi_0(q, 0) = -1$. First, we see that the poles of χ_0 translate into poles of χ^{RPA} . While

¹We have made the partial fraction decomposition for the contour integral for clarity and rigor. When performing the decomposition directly for the Matsubara sum, complications in the necessary convergence factors arise.

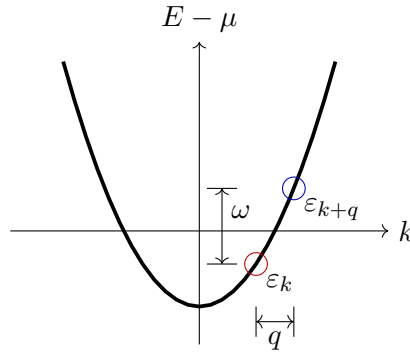


Figure 7.2: Poles ω of the Lindhard function connect occupied states ϵ_k with unoccupied states ϵ_{k+q} .

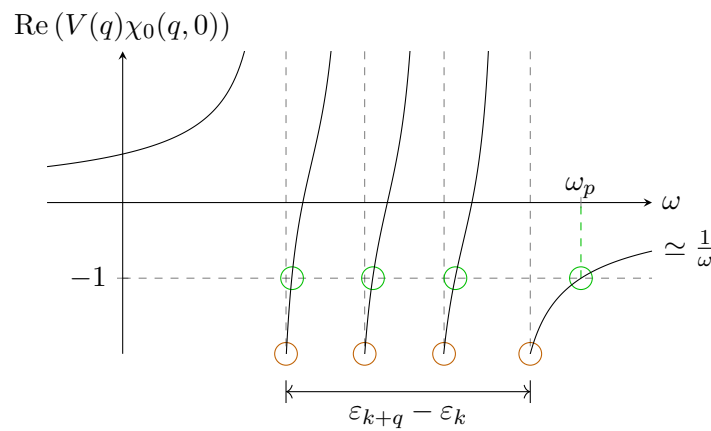


Figure 7.3: Eigenmodes

individual poles are shifted, a dense continuum emerges in the thermodynamic limit that is shared between χ_0 and χ^{RPA} . This particle-hole continuum is confined by the possible values of $\epsilon_{k+q} - \epsilon_k$. The *one-particle* spectrum available determines the energy/frequency range of these eigenmodes. The crucial observation now is that the $1/\omega$ decay in $\text{Re } \chi^{\text{RPA}}$ causes an additional pole at $\omega = \omega_p$ above the one-particle continuum, whose existence hinges on the presence of the interaction V . This mode is called the *plasmon*. It corresponds to a quantum of *collective* plasma oscillations.

Classically, plasma oscillation can be understood as follows: Consider a positively charged rigid and periodic ionic background, populated by negatively charged electrons. When electrons are displaced with respect to the ions, the Coulomb force tries to restore their equilibrium positions, acting as a “spring” causing the electrons to oscillate. Assuming an oscillating charge density $\rho(\omega) = \rho_0 \exp(-i\omega t)$, the continuity equation becomes $\nabla \cdot \mathbf{j} = -\partial \rho / \partial t = i\omega \rho(\omega)$. Combining with Gauss’ law $\nabla \cdot \mathbf{E}(\omega) = 4\pi \rho(\omega)$ and Ohm’s law $\mathbf{j}(\omega) = \sigma(\omega) \mathbf{E}(\omega)$, one finds $i\omega \rho(\omega) = 4\pi \sigma(\omega) \rho(\omega)$. For this equation to hold for an arbitrary $\rho(\omega)$ requires $\epsilon(\omega) = 1 + \frac{4\pi i \sigma(\omega)}{\omega} \stackrel{!}{=} 0$. According to Eq. (7.9), this is the same as demanding $1 + V(\mathbf{q})\chi^0(\mathbf{q}, \omega) = 0$, which precisely holds for $\omega = \omega_p$, the plasmon! Above ω_p , absorption can no longer take place, and the system is transparent at those frequencies.

7.3.3 Properties of the plasmon

Consider $\chi(q, \omega)$ in the limit $q \rightarrow 0$ at finite ω

$$\text{Re } \chi_0(q, \omega) = -2 \sum_k \frac{f(\varepsilon_k) - f(\varepsilon_{k+q})}{\omega - (\varepsilon_{k+q} - \varepsilon_k)} \quad (7.34)$$

$$= -2 \sum_k \left(\frac{f(\varepsilon_k)}{\omega - (\varepsilon_{k+q} - \varepsilon_k)} - \frac{f(\overbrace{\varepsilon_{-k}}^{\varepsilon_k})}{\omega - (\varepsilon_{-k} - \varepsilon_{-k-q})} \right) \quad (7.35)$$

$$= -4 \sum_k f(\varepsilon_k) \frac{(\varepsilon_{k+q} - \varepsilon_k)}{\omega^2 - (\varepsilon_{k+q} - \varepsilon_k)^2} \quad (7.36)$$

$$\stackrel{q \rightarrow 0}{=} -\frac{2}{m\omega^2} \int \frac{d^3k}{(2\pi)^3} f(\varepsilon_k) \left(\underbrace{2|k||q|\cos\theta}_{=0 \text{ by angular integration}} + q^2 + \dots \right) \quad (7.37)$$

$$= -\frac{nq^2}{m\omega^2}, \quad (7.38)$$

where we made the replacement $k + q \rightarrow -k$ in the second term of Eq. (7.35), used the (even) symmetry of the dispersion $\varepsilon_k = \frac{\hbar^2 k^2}{2m} = \varepsilon_{-k}$,² and

$$n = 2 \int \frac{d^3k}{(2\pi)^3} f(\varepsilon_k) \quad (7.39)$$

is the number density of electrons. In Eq. (7.10), this leads to

$$\chi^{\text{RPA}}(q \rightarrow 0, \omega) = -\frac{nq^2/m}{\omega^2 - \omega_p^2} \quad (7.40)$$

where we defined the plasma frequency $\omega_p = \sqrt{\frac{ne^2}{\varepsilon_0 m}} > 0$, with the permittivity of the vacuum ε_0 .³ This limiting form of the RPA susceptibility clearly exposes the plasmon as an extra mode in the system. Typically, $\omega_p = \mathcal{O}(10\text{eV})$. For example, in solid sodium, $\omega_p \approx 6\text{eV}$ [14]. Having a finite energy in the long wavelength limit, the plasmon is not a Goldstone boson. It is not associated with the remaining freedom in a symmetry-broken state. Applying the RPA formalism to the spin-flip susceptibility in a ferromagnet, one finds collective spin-excitation called the *magnon*. This Goldstone boson is associated with the all-up-or-all-down freedom of the spontaneous order and its energy indeed vanishes in the $q \rightarrow 0$ limit.

7.3.4 The excitation spectrum of the electron-gas within RPA

The excitations corresponding to transitions between one-particle energies occur at

$$\omega = \varepsilon_{k+q} - \varepsilon_k = \frac{\hbar q^2}{2m} + \frac{\hbar}{m} |k| |q| \cos \theta. \quad (7.41)$$

²In the one-orbital case, $\varepsilon_k = \varepsilon_{-k}$ also holds (by virtue of Bloch's theorem) for dispersions on a lattice. For multi-orbital Hamiltonians, instead, inversion symmetry is required.

³In cgs units (used above): $\omega_p = \sqrt{4\pi ne^2/m}$.

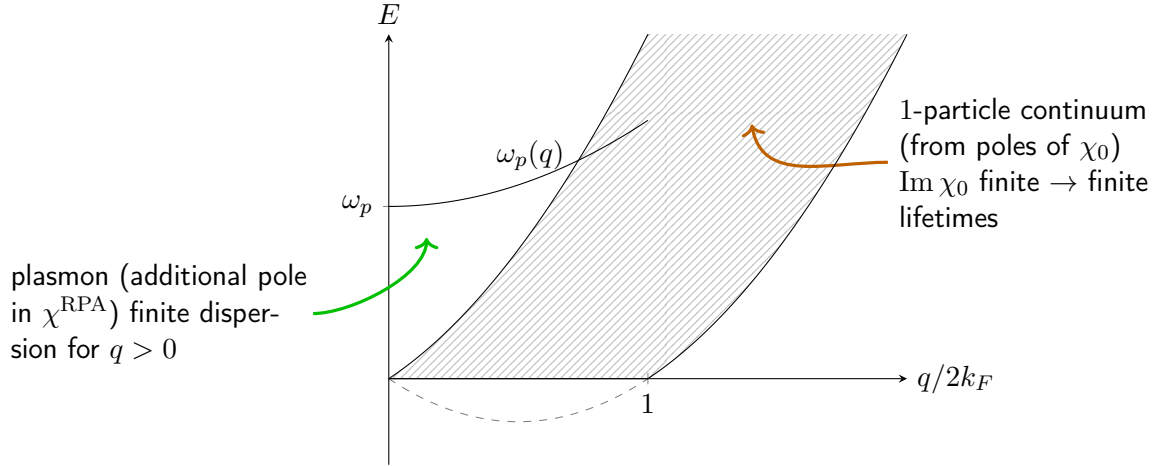


Figure 7.4: Excitation spectrum of the electron gas (in dimensions $d > 1$) within RPA.

When we are in two or more dimensions, this yields a particle-hole continuum delimited by

$$\max(0, \frac{\hbar^2 q^2}{2m} - \frac{\hbar^2 k_F}{m} q) \leq \omega \leq \frac{\hbar^2 q^2}{2m} + \frac{\hbar^2 k_F}{m} q \quad (7.42)$$

as visualized in Fig. 7.4. For small momenta q , the extra plasmon excitation lies above this one-particle continuum. Fig. 7.5 displays an experimental measurement of the plasmon excitation in solid sodium.

7.3.5 Static screening ($\omega = 0$) in the long wavelength limit ($q \rightarrow 0$)

We return to the initial motivation and study, how the polarization screens the interaction within RPA. First, we specialize to the static case in the long wavelength limit. There,

$$\text{Re } \chi_0(q, \omega = 0) = -2 \sum_k \frac{f(\varepsilon_k) - f(\varepsilon_{k+q})}{-(\varepsilon_{k+q} - \varepsilon_k)} \quad (7.43)$$

$$\stackrel{q \rightarrow 0}{=} -2 \sum_k \frac{\partial f(\varepsilon_k)}{\partial \varepsilon_k} \stackrel{T=0}{=} N(0) \quad (7.44)$$

where we further assumed low temperatures and $N(0)$ is the non-interacting system's density of states at the Fermi level. From this follows

$$V_{\text{eff}}(q \ll 1, \omega = 0) = \frac{V(q)}{1 + V(q)\chi_0(q, \omega = 0)} \quad (7.45)$$

$$= \frac{\frac{e^2}{\varepsilon_0 q^2}}{1 + \frac{e^2}{\varepsilon_0 q^2} 2N(0)} = \frac{e^2}{\varepsilon_0} \frac{1}{q^2 + q_{\text{TF}}^2}, \quad (7.46)$$

where $q_{\text{TF}} = \sqrt{\frac{e^2}{\varepsilon_0} N(0)}$ is the (inverse) Thomas-Fermi screening length. Fourier transforming this interaction to real-space, while assuming $V_{\text{eff}}(q \ll 1, \omega = 0)$ to be valid for all q , gives the Yukawa

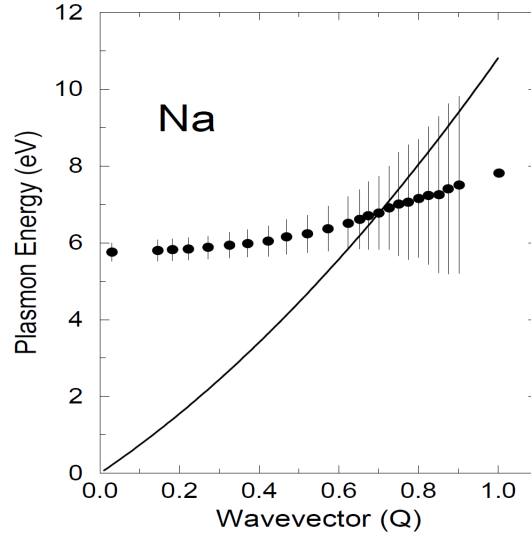


Figure 7.5: Plasmon dispersion in solid sodium obtained from electron energy loss spectroscopy (EELS) by vom Felde *et al* [14]. Vertical bars indicate the peak widths (linked to the imaginary part of the susceptibility); momentum Q is measured in units \AA^{-1} . The solid line indicates the onset of the electron-hole continuum. Figure of Ref. [2] reproduced from [open access version](#).

potential

$$V_{\text{eff}}(r) = \frac{e^2}{4\pi\epsilon_0 r} e^{-q_{\text{TF}} r}. \quad (7.47)$$

Screening reduces the magnitude and range of interactions, making them more local. This can be seen as a motivation for the Hubbard model.

7.3.6 Beyond the long wavelength limit: Friedel oscillation

Above, we evaluated the screened interaction for small q , but still integrated the ensuing potential over all q in the Fourier transform. Now, let us do a better job. Consider again the static susceptibility

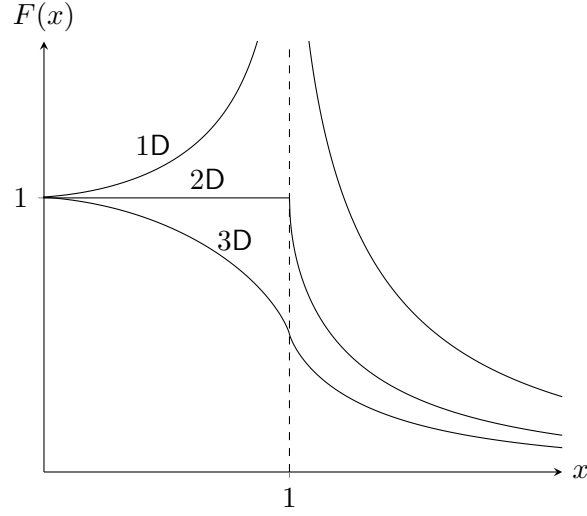


Figure 7.6: Function $F(x)$ that determines, via Eq. (7.53), the real-part of Lindhard function, for different dimensions: In 1D F diverges for $x = 1$, in 2D there is a discontinuity, in 3D the derivative diverges.

of free electrons

$$\text{Re } \chi_0(q, \omega = 0) = -2 \sum_k \frac{f(\varepsilon_k) - f(\varepsilon_{k+q})}{\varepsilon_k - \varepsilon_{k+q}} \quad (7.48)$$

$$\stackrel{3D}{=} +2 \int \frac{d^3k}{(2\pi)^3} \frac{f(\varepsilon_k) - f(\varepsilon_{k+q})}{\frac{\hbar^2}{2m}(q^2 + 2kq)} \quad (7.49)$$

$$\stackrel{T=0}{=} \frac{m}{\hbar^2} \int_0^{k_F} \frac{dk}{\pi^2} k^2 \int_{-1}^1 dx \frac{1}{q^2 + 2kqx} \quad (7.50)$$

$$= \frac{m}{\pi^2 \hbar^2} \frac{1}{2q} \int_0^{k_F} dk k \ln \left| \frac{q + 2k}{q - 2k} \right| \quad (7.51)$$

$$= \frac{1}{2} \frac{m}{\pi^2 \hbar^2} k_F F\left(\frac{q}{2k_F}\right) \quad (7.52)$$

Where we used the short-hand

$$F(x) \stackrel{3D}{=} \frac{1}{2} \left[1 + \frac{1}{2x} (1 - x^2) \ln \left| \frac{1+x}{1-x} \right| \right] \quad \text{for which} \quad F(1) = \frac{1}{2}. \quad (7.53)$$

Within RPA, this yields the following screened interaction

$$V^{\text{RPA}}(q, \omega = 0) = \frac{V(q)}{1 + V(q) \chi_0(q, \omega = 0)} \quad (7.54)$$

$$= \frac{V(q)}{1 + \frac{q_{\text{TF}}^2}{q^2} F(q/2k_F)} \xrightarrow{q/k_F \rightarrow 0} \frac{e^2}{\varepsilon_0} \frac{1}{q^2 + q_{\text{TF}}^2}, \quad (7.55)$$

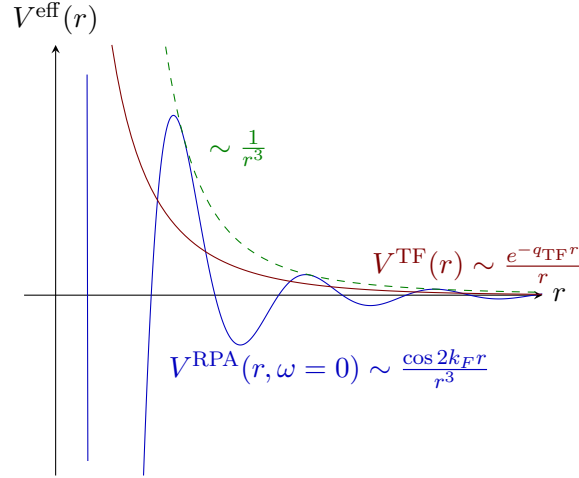



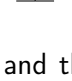
Figure 7.7: The screened Coulomb interactions within RPA. V^{TF} indicates the Yukawa potential from Thomas-Fermi theory, while the full V^{RPA} exhibits a slower overall decay with Friedel oscillations of period $2k_F$. Note that the RPA-screened interaction has minima that are below zero: There are distances at which the screened interaction is *attractive*!

Naturally, our solution contains the Thomas-Fermi result as the long-wavelength limit. Now disposing of the full q -dependence, a more decent Fourier transform can be performed. In 3D, while at *short* distances the interaction still falls off rapidly, the divergence of the derivative of $F(x)$ in momentum-space (see Fig. 7.6) can be shown to lead to a slowly decaying oscillatory behavior in real-space for *large* distances:

$$V^{\text{RPA}}(r, \omega = 0) \sim \frac{\cos(2k_F r)}{r^3} \quad (\text{for large } r) \quad (7.56)$$

Contrary to the (Thomas-Fermi) Yukawa potential, Eq. (7.47), the full $V^{\text{RPA}}(r)$ is long-ranged: the screened interaction only decays polynomial with distance. Inside the $1/r^3$ envelop, $V^{\text{RPA}}(r)$ oscillates. These “Friedel oscillations” are in fact observable, e.g., with **Scanning Tunneling Microscopy** (STM). Fig. 7.8 from Ref. [8] shows the example of an STM measurement of point defects on a (111) surface of silver.⁴

7.4 The GW approach

The lowest order Feynman diagrams for the self-energy Σ are the Hartree  and Fock terms . These diagrams are build from the *free* Green's function G_0 and the *bare* Coulomb

⁴Note that this is a 2D system. Accounting for effects of an asymmetric Fermi surface, one finds for the investigated system an interaction falloff $\propto \cos(2k_F r)/r^2$ [8].

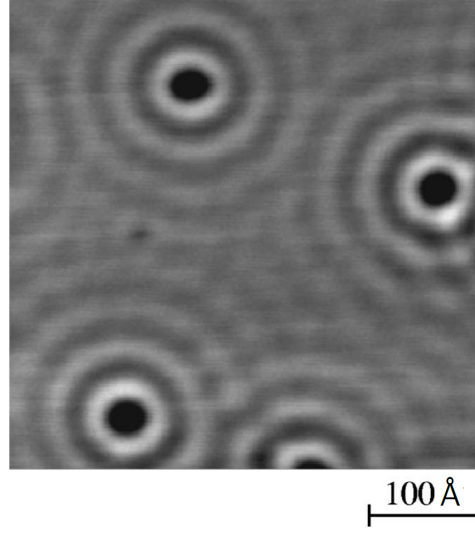
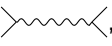



Figure 7.8: Scanning tunneling microscopy image of a Ag(111) surface with four point defects from Knorr *et al* [8]. Reprinted figure with permission from Knorr *et al*, [Phys. Rev. B 65, 115420 \(2002\)](#). Copyright (2002) by the American Physical Society.

interaction $V(r) = \frac{e^2}{4\pi\epsilon_0} \frac{1}{r}$. The idea now is to incorporate the screening of the interaction also on the level of the self-energy: quasi-particles only feel a reduced (screened) interaction V^{eff} , that in this context is often denoted by W . So instead of expanding Σ in V , we will expand it in W . If we take into account all orders, both expansions are equivalent. The hope is, that the series in W (the 'smaller' perturbation) converges faster and low-order approximations are more justified. Basically, we will replace $-V$ lines, , with $-W$ lines, .

7.4.1 Screened Hartree term

$$\Sigma_{H\sigma}^{\text{screened}}(k, i\omega) = \text{diagram} = 2 \frac{1}{\beta} \sum_{i\omega_m, k'} G(k', i\omega_m) W(q=0, i\omega=0) \quad (7.57)$$

$$= 2 \underbrace{W(0,0)}_{<V} n \quad (7.58)$$

Screening reduces the Hartree self-energy Σ_H . Qualitatively, however, nothing has happened: Σ_H is still static (frequency-independent) and local (momentum-independent).

7.4.2 Screened Fock term

The Fock term is much more interesting.

$$\Sigma_{\sigma}^{GW}(k, i\omega_n) = \text{diagram} = -\frac{1}{\beta} \sum_{i\omega_{n'}, k'} \underbrace{G(k', i\omega_{n'}) W(k - k', i\omega_n - i\omega_{n'})}_{\text{hence the name "GW"}} \quad (7.59)$$

$$= \text{diagram} + \text{diagram} + \text{diagram} + \dots \quad (7.60)$$

By using the screened interaction W , we effectively evaluate an infinite number of irreducible self-energy diagrams. The approach that consists in evaluation the first order diagram in W is called the GW approximation and is due to Hedin[7]. It is our goal to evaluate the GW diagram for an illustrative case.

The screened interaction W

Instead of computing the screened interaction W , we will motivate how it typically looks like in solids. A phenomenological form is

$$W(\omega) = V + (V - U) \frac{\omega_p}{2} \left(\frac{1}{\omega - \omega_p + i0^+} - \frac{1}{\omega + \omega_p + i0^+} \right) \quad (7.61)$$

$$= V + W_c(\omega) \quad (7.62)$$

that is illustrated in Fig. 7.9: At large frequencies, screening is ineffective and the screened interaction approaches the bare Coulomb repulsion, $\text{Re} W(\omega \rightarrow \infty) \rightarrow V$. This can be understood from an electrodynamics point of view: For frequencies above the plasma frequency ω_p , the system's electrons can no longer keep up with the fast pace of the external perturbation. The charges thus cease to mitigate the perturbation and the system becomes transparent. At the plasma frequency ω_p , which is a resonance (corresponds to an eigenmode) of the system, the interaction has a pole. Below ω_p , $\text{Re} W(\omega)$ is smaller than V and approaches the limit $U < V$ in the static limit, as motivated by Thomas-Fermi theory above.

On the Matsubara axis, the dynamical part $W_c(\omega)$ of the interaction reads

$$W(i\nu) = \int d\omega \frac{-\frac{1}{\pi} \text{Im} W(\omega)}{i\nu - \omega} = g^2 \left(\frac{1}{i\nu - \omega_p} - \frac{1}{i\nu + \omega_p} \right) \quad (7.63)$$

Evaluation of the GW self-energy

Forgoing any complications of momentum-dependencies, let us further assume a simplistic non-interacting electronic structure of a single level

$$H_0 = \epsilon \sum_{\sigma} c_{\sigma}^{\dagger} c_{\sigma} \quad (7.64)$$

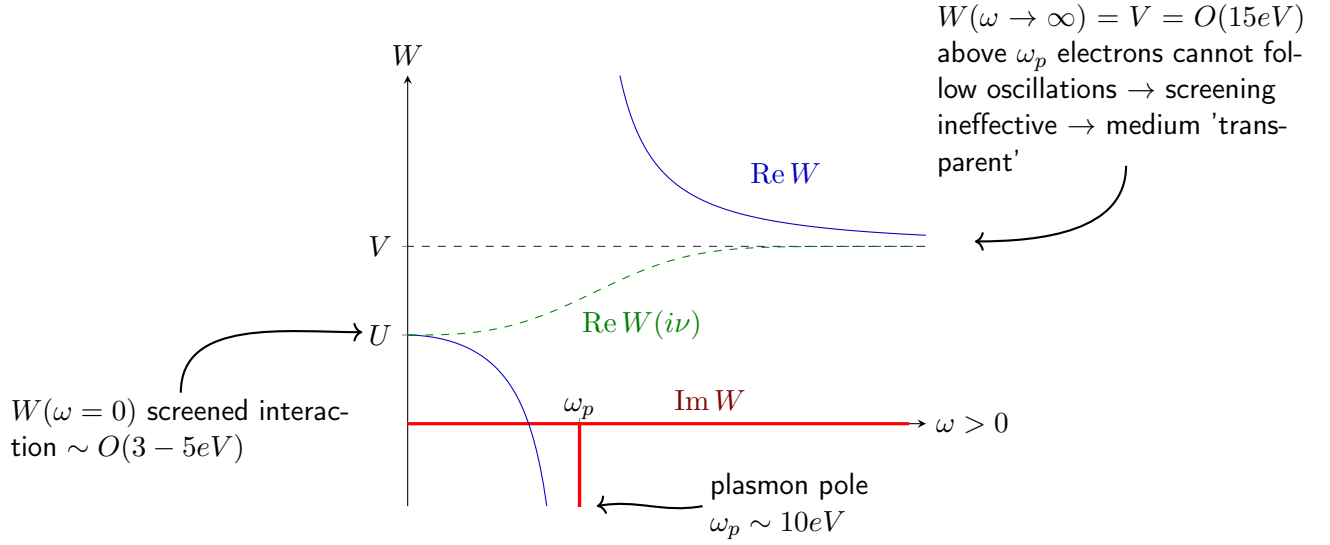


Figure 7.9: Phenomenological form of the frequency dependence of the screened interaction $W(\omega)$.

Now, we have all the ingredients necessary to evaluate the GW diagram. We limit the calculation to the dynamical part of the interaction $W_c(\omega)$. Note also that, despite the name GW, the used propagator is the one of the non-interacting system, $G^0(i\omega_n)$.

$$\Sigma(i\omega_n) = -\frac{1}{\beta} \sum_{n'} G^0(i\omega_{n'}) W_c(i\omega_n - i\omega_{n'}) \quad (7.65)$$

$$= -g^2 \oint dz \frac{f(z)}{z - \varepsilon} \left(\frac{1}{i\omega_n - z - \omega_p} - \frac{1}{i\omega_n - z + \omega_p} \right) \quad (7.66)$$

$$= -g^2 \oint dz f(z) \left[\left(\frac{1}{z - \varepsilon} + \frac{1}{i\omega_n - z - \omega_p} \right) \frac{1}{i\omega_n - \varepsilon - \omega_p} - \left(\frac{1}{z - \varepsilon} + \frac{1}{i\omega_n - z + \omega_p} \right) \frac{1}{i\omega_n - \varepsilon + \omega_p} \right] \quad (7.67)$$

$$= -g^2 \left(\frac{f(\varepsilon) - \overbrace{f(-\omega_p + i\omega_n)}^{-n_B(-\omega_p) \approx 1}}{i\omega_n - \varepsilon + \omega_p} - \frac{f(\varepsilon) + \overbrace{f(\omega_p + i\omega_n)}^{-n_B(+\omega_p) \approx 0}}{i\omega_n - \varepsilon + \omega_p} \right) \quad (7.68)$$

$$= -g^2 \left(\frac{f(\varepsilon) - 1}{i\omega_n - \varepsilon + \omega_p} - \frac{f(\varepsilon)}{i\omega_n - \varepsilon + \omega_p} \right). \quad (7.69)$$

Where we assumed $\omega_p \gg k_B T$. Let us further consider $\varepsilon \ll -\frac{1}{\beta}$, i.e., the state shall be occupied, $f(\varepsilon) = 1$.

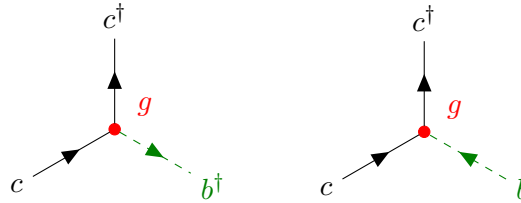
$$\Sigma(i\omega) = g^2 \frac{1}{i\omega - \varepsilon + \omega_p} \xrightarrow{i\omega \rightarrow \omega + i0^+} \Sigma(\omega) = g^2 \frac{1}{\omega - \varepsilon + \omega_p + i0^+} \quad (7.70)$$

Fermion-boson model

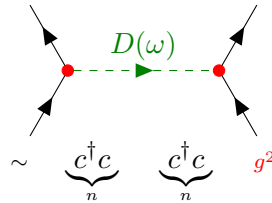
Interestingly, there is a toy model that has the same non-interacting Hamiltonian H_0 , and a coupling to a bosonic mode that, as we shall see, generates the interaction W_c from above. This Hamiltonian is simple enough to allow for an exact solution. We thus have a way to see how good our *GW* approximation really is. The Hamiltonian of said model reads [9]

$$H = \underbrace{\varepsilon c^\dagger c}_{\text{spinless fermion (non-interacting)}} + \underbrace{\omega_p b^\dagger b}_{\text{plasmon (boson)}} + \underbrace{g c c^\dagger (b^\dagger + b)}_{\text{electron-plasmon coupling}} \quad (7.71)$$

where the “ c ” operators refer to spin-less fermions (i.e., we neglect the spin, but fermionic anticommutation rules are obeyed), and “ b ” operators describe bosons. The first two terms are the non-interacting fermionic and bosonic contributions, respectively. The third term couples the fermions and the bosons. Manifestly, this interaction term conserves the number of fermions, whereas the number of bosons increases or decreases by one. In terms of Feynman diagrams, the interaction term encodes the following scattering processes:



Combining both contributions, we see that the fermion-boson coupling can mediate an electron-electron interaction:



In fact using the path integral formalism, one can easily see that the electron part of the electron-boson Hamiltonian is equivalent to an action with “ $\varepsilon c^\dagger c + W_c(\omega)nn$ ” where, using the causal bosonic

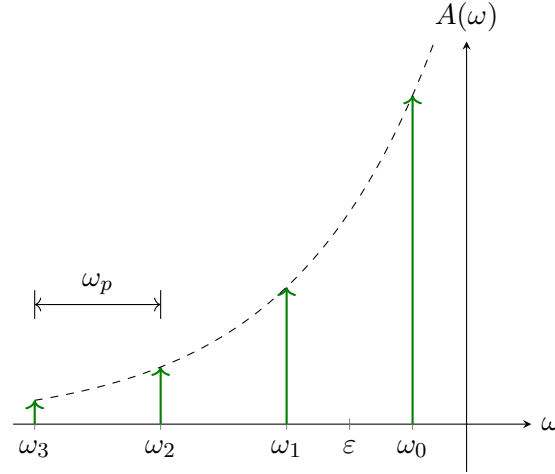


Figure 7.10: Exact spectral function $A(\omega)$ of the fermions, Eq. (7.73), of the fermion-boson Hamiltonian from Eq. (7.71).

Green's function $D(\omega)$,

$$W_c(\omega) = g^2 \underbrace{\left(\frac{1}{\omega - \omega_p + i0^+} - \frac{1}{\omega + \omega_p + i0^+} \right)}_{D(\omega)}, \quad (7.72)$$

which is of the form discussed previously. Note that $\text{Re } W_c(\omega = 0) = -\frac{2g^2}{\omega_p} < 0$ i.e. at low energies, the mediated interaction is *attractive*. This is a harbinger for conventional superconductivity, where the boson modes that induce an effectively attractive electron-electron interactions are phonons.

The exact solution [9] of the Hamiltonian given in Eq. (7.71) provides the following spectral function for the fermions

$$A(\omega) = \underbrace{e^{-(g/\omega_p)^2}}_{\substack{\text{weight} \\ (\int d\omega A(\omega)=1)}} \sum_{n=0}^{\infty} \frac{1}{n!} \left(\frac{g}{\omega_p} \right)^{2n} \underbrace{\delta\left(\omega - \epsilon - \frac{g^2}{\omega_p} + n\omega_p\right)}_{\substack{\text{infinte number of excitations} \\ \omega_n = \epsilon + \frac{g^2}{\omega_p} - n\omega_p}}, \quad (7.73)$$

which is the sum of an infinite number of equally spaced peaks, with consecutively suppressed weights, see Fig. 7.10.

Comparison of the exact solution and the *GW* approximation

We will compare the peaks in the spectral functions, their energetic position and the weight that they carry. In the exact solution, the *excitation energies* are easily read off as

$$\omega_n^{\text{exact}} = \epsilon + \frac{g^2}{\omega_p} - n \times \omega_p \quad (7.74)$$

The weight factor in front of Eq. (7.73) gives the integrated weight of the main ($n = 0$) peak of the series, which we associate with the quasi-particle weight Z :

$$Z^{\text{exact}} = e^{-(g/\omega_p)^2} = 1 - \frac{g^2}{\omega_p^2} + \frac{g^4}{2\omega_p^4} - \dots \quad (7.75)$$

which we have further expanded in powers of the coupling constant g .

Turning to the *GW* approximation, we can obtain the excitation energies from the poles in the Green's function $G(\omega) = [\omega - \epsilon - \Sigma(\omega)]^{-1}$, i.e.,

$$\omega - \epsilon - \text{Re } \Sigma(\omega) \stackrel{!}{=} 0 \quad (7.76)$$

$$\Leftrightarrow \omega - \epsilon - \frac{g^2}{\omega - \epsilon + \omega_p} = 0 \quad (7.77)$$

$$\Leftrightarrow (\omega - \epsilon)^2 + (\omega - \epsilon)\omega_p - g^2 = 0 \quad (7.78)$$

$$\Leftrightarrow \omega^2 + \epsilon^2 - 2\omega\epsilon + \omega\omega_p - \epsilon\omega_p - g^2 = 0 \quad (7.79)$$

$$\Leftrightarrow \omega^2 + \omega(\omega_p - 2\epsilon) + \epsilon^2 - g^2 - \epsilon\omega = 0 \quad (7.80)$$

$$\rightarrow \omega_{0/1} = \epsilon - \frac{\omega_p}{2} \pm \sqrt{\left(\epsilon - \frac{\omega_p}{2}\right)^2 - \epsilon^2 + \epsilon\omega_p + g^2} \quad (7.81)$$

$$= \epsilon - \frac{\omega_p}{2} \pm \frac{\omega_p}{2} \sqrt{1 + \left(\frac{2g}{\omega_p}\right)^2} \quad (7.82)$$

$$= \epsilon - \frac{\omega_p}{2} \pm \left(\frac{\omega_p}{2} + \frac{g^2}{\omega_p} - \frac{g^4}{\omega_p^3} \dots\right) \quad (7.83)$$

In other words, there are *two* peaks in the *GW* spectral function instead of the infinitely many in the exact solution. Expanding in orders of g , we see that

$$\omega_0 = \overbrace{\epsilon + \frac{g^2}{\omega_p}}^{=\omega_0^{\text{exact}} \text{ to order } g^2/\omega_p} - \frac{g^4}{\omega_p^3} + \dots \quad (7.84)$$

$$\omega_1 = \underbrace{\epsilon - \omega_p - \frac{g^2}{\omega_p}}_{\neq \omega_1^{\text{exact}}} + \frac{g^4}{\omega_p^3} - \dots \quad (7.85)$$

Comparing to Eq. (7.74), we see that in *GW* the quasi-particle peak's position ω_0 is correct to order g^2/ω_p , while the first satellite ω_1 does not agree in that order; it is off by $2g^2/\omega_p$.

Remembering from Fermi liquid theory that $\Sigma(\omega) = \text{Re}\Sigma(\omega = 0) + (1 - \frac{1}{Z})\omega \rightarrow G(\omega) = \frac{1}{\omega - \epsilon - \Sigma(\omega)} = \frac{Z}{\omega - Z\epsilon}$, we see that the quasi-particle weight can be obtained from the derivative of the *GW* self-energy. Here, instead of at the Fermi level, we evaluate the derivative at the bare position ϵ of the energy level:

$$Z = \left(1 - \frac{\partial \text{Re}\Sigma}{\partial \omega}\right)^{-1}_{\omega=\epsilon} \quad (7.86)$$

yielding

$$Z = \left(1 + \frac{g^2}{\omega_p^2}\right)^{-1} = \underbrace{1 - \frac{g^2}{\omega_p^2}}_{=Z^{\text{exact}} \text{ to order } g^2} + \frac{g^4}{\omega_p^4} - \dots \quad (7.87)$$

In all, the main spectral feature in the *GW* approximation agrees well with the exact solution, provided that $|g| \ll \omega_p$. The properties of satellite features and their number are less accurate.

In the example discussed above, we focused on signatures arising from the *dynamics* in the screened interaction, which leads to spectral-weight transfers and satellite features. A second merit of the *GW* approximation is the treatment of momentum-dependent effects in the self-energy. Most notably, the gaps in semiconductors, such as Si or GaAs come out far too small in simpler, so-called density-functional based electronic structure methods. The numerically more expensive *GW* approximation, instead, yields notably more accurate gaps. For reviews of the *GW* approach, see, e.g., Refs. [4, 13].

Appendix A

Time-evolution of perturbed states

We remember the equation of state for the interaction picture and its connection to the Heisenberg picture

$$i\hbar \frac{\partial}{\partial t} |\psi_I(t)\rangle = V_I(t) |\psi_I(t)\rangle \quad (\text{A.1})$$

$$A_H(t) = U_I^\dagger(t) A_I(t) U_I(t) \quad (\text{A.2})$$

so that

$$U_I(t) = \mathbb{1} + \frac{1}{i} \int_0^t dt' V_I(t') U_I(t') = \mathbb{1} + i \int_0^t dt' a(t') A_I(t') U_I(t') \quad (\text{A.3})$$

using $U_I(0) = \mathbb{1}$ we iteratively expand this to

$$U_I(t) = \mathbb{1} + i \int_0^t dt' a(t') A_I(t') \left(\mathbb{1} + i \int_0^{t'} dt'' a(t'') A_I(t'') U_I(t'') \right) \quad (\text{A.4})$$

since we are only interested in linear terms in $V_I(t)$, we cancel this series at first order:

$$\Rightarrow U_I^{(1)}(t) = \mathbb{1} + i \int_0^t dt' a(t') A_I(t') \quad (\text{A.5})$$

analogous:

$$\Rightarrow U_I^{\dagger(1)}(t) = \mathbb{1} - i \int_0^t dt' a(t') A_I(t') \quad (\text{A.6})$$

We apply that result to (A.2):

$$\begin{aligned} A_H(t) &= \left(\mathbb{1} - i \int_0^t dt' a(t') A_I(t') \right) A_I(t) \left(\mathbb{1} + i \int_0^t dt' a(t') A_I(t') \right) \\ &= A_I(t) + i \int_0^t dt' a(t') [A_I(t), A_I(t')] + O(V_I(t)^2) \end{aligned} \quad (\text{A.7})$$

where $[.,.]$ denotes the commutator. Again higher order terms in $V_I(t)$ are neglected, since we are only interested in linear terms.

If we take the expectationvalue of expression (A.7), it then can be written as:

$$\langle A_H(t) \rangle = \langle A_I(t) \rangle + \int_{-\infty}^{\infty} dt' \chi(t-t') a(t') \quad (\text{A.8})$$

with

$$\chi(t-t') = i \langle [A_I(t), A_I(t')] \rangle \theta(t-t') \quad (\text{A.9})$$

which is known as the Kubo-Nakano formula.

A more general form is written as

$$\chi_{BA}(t-t') = i \langle [B_I(t), A_I(t')] \rangle \theta(t-t'). \quad (\text{A.10})$$

Appendix B

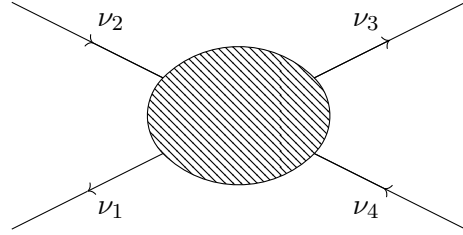
Explicit relation between 2P-Greens' functions and linear response functions

$$G^{II}(\nu_1, \nu_2, \nu_3, \nu_4) = \int_0^\beta d\tau_1 d\tau_2 d\tau_3 d\tau_4 e^{i\nu_1\tau_1} e^{-i\nu_2\tau_2} e^{i\nu_3\tau_3} e^{-i\nu_4\tau_4} \langle \mathcal{T}_2 c(\tau_1) c^\dagger(\tau_2) c(\tau_3) c^\dagger(\tau_4) \rangle \quad (\text{B.1})$$

$$\Rightarrow G^{II}(\tau_1, \tau_2, \tau_3, \tau_4)$$

$\nu_1, \nu_2, \nu_3, \nu_4 \Rightarrow$ Fermionic Matsubara Frequencies

$$\nu_i^n = \frac{\pi}{\beta} (2n + 1)$$



Time translation invariance: $G^{II}(\tau_1, \tau_2, \tau_3, \tau_4) = G^{II}(\tau_1 - \tau_4, \tau_2 - \tau_4, \tau_3 - \tau_4, 0)$

$$G^{II}(\nu_1, \nu_2, \nu_3, \nu_4) = \int_0^\beta d\tau_1 d\tau_2 d\tau_3 d\tau_4 e^{i\nu_1\tau_1} e^{-i\nu_2\tau_2} e^{i\nu_3\tau_3} e^{-i\nu_4\tau_4} G^{II}(\tau_1 - \tau_4, \tau_2 - \tau_4, \tau_3 - \tau_4, 0) \quad (\text{B.2})$$

$$= \int_0^\beta d\tau_4 \int_{-\tau_4}^{\beta-\tau_4} d\tilde{\tau}_1 d\tilde{\tau}_2 d\tilde{\tau}_3 e^{i\nu_1(\tilde{\tau}_1+\tau_4)} e^{-i\nu_2(\tilde{\tau}_2+\tau_4)} e^{i\nu_3(\tilde{\tau}_3+\tau_4)} e^{-i\nu_4\tau_4} G^{II}(\tilde{\tau}_1, \tilde{\tau}_2, \tilde{\tau}_3, 0) \quad (\text{B.3})$$

$$= \int_0^\beta d\tau_4 e^{i(\nu_1-\nu_2+\nu_3-\nu_4)\tau_4} \int_0^\beta d\tilde{\tau}_1 d\tilde{\tau}_2 d\tilde{\tau}_3 e^{i\nu_1\tilde{\tau}_1} e^{-i\nu_2\tilde{\tau}_2} e^{i\nu_3\tilde{\tau}_3} G^{II}(\tilde{\tau}_1, \tilde{\tau}_2, \tilde{\tau}_3, 0) \quad (\text{B.4})$$

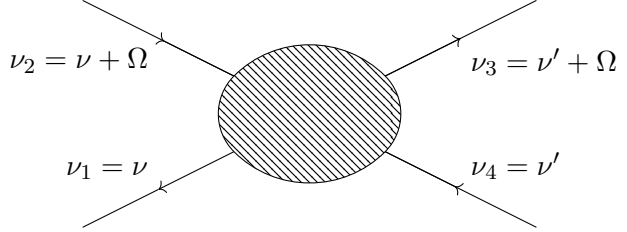
$$G^{II}(\nu_1, \nu_2, \nu_3, \nu_4) = \beta \delta(\nu_4 = \nu_1 - \nu_2 + \nu_3) \int_0^\beta d\tau_1 d\tau_2 d\tau_3 e^{i\nu_1\tau_1} e^{-i\nu_2\tau_2} e^{i\nu_3\tau_3} G^{II}(\tau_1, \tau_2, \tau_3, 0) \quad (\text{B.5})$$

$$G^{II}(\nu_1, \nu_2, \nu_3, \nu_4 = \nu_1 - \nu_2 + \nu_3) = \beta \int_0^\beta d\tau_1 d\tau_2 d\tau_3 e^{i\nu_1 \tau_1} e^{-i\nu_2 \tau_2} e^{i\nu_3 \tau_3} \langle \mathcal{T}_\tau c(\tau_1) c^\dagger(\tau_2) c(\tau_3) c^\dagger(0) \rangle \quad (\text{B.6})$$

$$\nu_2 - \nu_1 = \nu_3 - \nu_4 = \Omega$$

$$\Omega = \text{Bosonic!}$$

$$\Omega_n = \frac{2\pi}{\beta} n$$



$$G^{II}(\nu, \nu', \Omega) \propto \int_0^\beta d\tau_1 d\tau_2 d\tau_3 e^{i\nu \tau_1} e^{-i(\nu + \Omega) \tau_2} G^{II}(\tau_1, \tau_2, \tau_3) \quad (\text{B.7})$$

$$\frac{1}{\beta^2} \sum_{\nu \nu'} G(\nu, \nu', \Omega) = \int d\tau_1 d\tau_2 d\tau_3 \left[\frac{1}{\beta} \sum_{\nu} e^{i\nu(\tau_1 - \tau_2)} \right] \left[\frac{1}{\beta} \sum_{\nu'} e^{i\nu' \tau_3} \right] e^{-i\Omega \tau_2} e^{i\Omega \tau_3} G^{II}(\tau_1, \tau_2, \tau_3) \quad (\text{B.8})$$

$$\left| \tau_1 = \tau_2 = \tau; \tau_3 = 0 \right| \Rightarrow \int d\tau e^{-i\Omega \tau} \langle \mathcal{T}_\tau c(\tau) c^\dagger(\tau) c(0) c^\dagger(0) \rangle \Rightarrow \langle \mathcal{T}_\tau n(\tau) n(0) \rangle \quad (\text{B.9})$$

Bibliography

- [1] A. A. Abrikosov, I. Dzyaloshinskii, L. P. Gorkov, and R. A. Silverman. *Methods of quantum field theory in statistical physics*. Dover, New York, NY, 1975.
- [2] P. B. Allen. Single particle versus collective electronic excitations. In Z. Petru, J. Przystawa, and K. Rapcewicz, editors, *From Quantum Mechanics to Technology*, pages 125–141, Berlin, Heidelberg, 1996. Springer Berlin Heidelberg.
- [3] A. Altland and B. D. Simons. *Condensed Matter Field Theory*. Cambridge University Press, 2 edition, 2010.
- [4] F. Aryasetiawan and O. Gunnarsson. The GW method. 61(3):237–312, 1998.
- [5] P. Coleman. *Introduction to Many-Body Physics*. Cambridge University Press, 2015.
- [6] A. Georges, G. Kotliar, W. Krauth, and M. J. Rozenberg. Dynamical mean-field theory of strongly correlated fermion systems and the limit of infinite dimensions. *Rev. Mod. Phys.*, 68:13–125, Jan 1996.
- [7] L. Hedin. New method for calculating the one-particle green's function with application to the electron-gas problem. *Phys. Rev.*, 139:A796–A823, Aug 1965.
- [8] N. Knorr, H. Brune, M. Eppe, A. Hirstein, M. A. Schneider, and K. Kern. Long-range adsorbate interactions mediated by a two-dimensional electron gas. *Phys. Rev. B*, 65:115420, Mar 2002.
- [9] D. C. Langreth. Singularities in the x-ray spectra of metals. *Phys. Rev. B*, 1:471–477, Jan 1970.
- [10] A. G. Laura Leber, Stefan Danner. Quantentheorie 2 skriptum zur vorlesung von professor karsten held, 2019.
- [11] G. D. Mahan. *Many Particle Physics, Third Edition*. Plenum, New York, 2000.
- [12] P. Nozieres. *Theory Of Interacting Fermi Systems*. CRC Press, 1st edition, 1988.
- [13] G. Onida, L. Reining, and A. Rubio. Electronic excitations: density-functional versus many-body Green's-function approaches. *Rev. Mod. Phys.*, 74(2):601–659, Jun 2002.
- [14] A. vom Felde, J. Sprösser-Prou, and J. Fink. Valence-electron excitations in the alkali metals. *Phys. Rev. B*, 40:10181–10193, Nov 1989.

- [15] C. Watzenböck, M. Feller, K. Held, and A. Toschi. Long-term memory magnetic correlations in the hubbard model: A dynamical mean-field theory analysis, 2021.
- [16] R. M. Wilcox. Bounds for the isothermal, adiabatic, and isolated static susceptibility tensors. *Phys. Rev.*, 174:624–629, Oct 1968.